Precambrian Research 321 (2019) 303–327

Contents lists available at ScienceDirect

Precambrian Research

journal homepage: www.elsevier.com/locate/precamres

Building up the first continents: Mesoarchean to Paleoproterozoic crustal evolution in West Troms, Norway, inferred from granitoid petrology, geochemistry and zircon U-Pb/Lu-Hf isotopes

Oscar Laurent[a,b,*], Jacqueline Vander Auwera[a], Bernard Bingen[c], Olivier Bolle[a], Axel Gerdes[d]

[a] Université de Liège, Département de Géologie B20, Quartier Agora, allée du six-Août 12, B-4000 Liège, Belgium
[b] ETH Zürich, Institute for Geochemistry and Petrology, Clausiusstrasse 25, CH-8092 Zürich, Switzerland
[c] Geological Survey of Norway, PO Box 6312 Sluppen, 7491 Trondheim, Norway
[d] J.W. Goethe Universität, Institut für Geowissenschaften, Altenhöferallee 1, D-60438 Frankfurt am Main, Germany

ARTICLE INFO

Keywords:
Granitoids
Continental crust
Precambrian
Zircon U-Pb geochronology
Zircon Lu-Hf isotopes
Fennoscandian Shield

ABSTRACT

Combining geological, petrographic, geochemical and zircon U-Pb and Lu-Hf isotopic data on granitoids provides powerful insights into the architecture, growth and geodynamic setting of Precambrian continents. Using such a dataset, we explore ca. 1.3 Ga of continent construction in the West Troms Basement Complex (WTBC), northern Norway, between the Mesoarchean and Paleoproterozoic. The new data show that the WTBC consists of two Archean lithotectonic segments: (1) a northeastern (NE) segment made up by juvenile ($\varepsilon Hf_{(t)} = +2$ to $+3$) TTGs, formed between 2.92 and 2.83 Ga by increasingly deeper melting (Sr/Y from < 50 to > 90) of a young mafic crust; (2) a southwestern (SW) segment dominated by 2.71–2.67 Ga, sanukitoid-like (qz-)diorite-granodiorite-granite, derived from mantle-TTGs interactions and unrelated to the NE segment, as shown by positive $\varepsilon Hf_{(t)}$ ($+1$ to $+2$). The intervening domain comprises 2.74–2.69 Ga sanukitoids and granites with minor 2.96 Ga remnants, and may correspond to either reworked NE segment ($\varepsilon Hf_{(t)} = -1$) or a third segment. The Archean crust was intruded at 1.87–1.86 and 1.80–1.75 Ga by qz-monzonite, monzodiorite and monzo-/syenogranite plutons belonging to the Transscandinavian Igneous Belt (TIB). These show negative $\varepsilon Hf_{(t)}$ (-7 to -13) pointing to melting of Archean mafic-intermediate lower crust and enriched lithospheric mantle.

These observations are explained by a geodynamic model involving: (i) stabilization of the NE segment as a 3.0–2.8 Ga proto-cratonic nucleus, by formation and repeated melting of a progressively thickening mafic plateau; and (ii) drifting of this proto-craton towards the SW at 2.75–2.65 Ga, leading to "passive" subduction at its leading edge and formation of the SW segment as an arc-like complex. The subsequent Svecofennian accretionary orogeny (1.97–1.81 Ga) led to over-thickening and delamination of the lower crust and lithospheric mantle, forming the 1.87–1.75 Ga granitoids. A similar transition from intraplate to horizontal tectonics has been recorded in other cratonic domains, yet at different times ranging from Paleoarchean to Paleoproterozoic. This suggests that the onset of plate tectonics is not a globally synchronous event and depends on the regional lithospheric evolution.

1. Introduction

The continental crust represents one of the best archives of Earth's geological history (Hawkesworth et al., 2010; Roberts and Spencer, 2015). In Phanerozoic times, the continental crust dominantly formed either by accretion of oceanic arcs to pre-existing continental masses (Bouilhol et al., 2013; Cawood et al., 2013; Condie and Kröner, 2013; Dhuime et al., 2012; Jagoutz and Kelemen, 2015) or mantle-derived magmatism in continental arc and collision zones (Couzinié et al., 2016; Moyen et al., 2017; Niu et al., 2013). However, such mechanisms require the existence of a significant volume of pre-existing stable continental lithosphere, raising the question of how the first continents were formed. The characteristics and even the existence of Precambrian plate tectonics are highly debated (Bédard, 2006, 2013; Bédard et al., 2013; Cawood et al., 2006; Gerya, 2014; Moyen and Laurent, 2018; Wyman, 2013), especially since the physical modalities of subduction are expected to be different in the context of a hotter Archean mantle (Fischer and Gerya, 2016; Gerya, 2014; Sizova et al., 2015; van Hunen

* Corresponding author at: ETH Zürich, Institute for Geochemistry and Petrology, Clausiusstrasse 25, CH-8092 Zürich, Switzerland.
E-mail address: oscar.laurent@erdw.ethz.ch (O. Laurent).

https://doi.org/10.1016/j.precamres.2018.12.020
Received 8 August 2018; Received in revised form 10 December 2018; Accepted 17 December 2018
Available online 20 December 2018
0301-9268/

and van den Berg, 2008). Existing models for Precambrian geodynamics fall in two end-member families: those considering formation of the early continents through magmatism at convergent plate boundaries and accretion of island arcs (Arndt 2013; Martin et al. 2014; Nagel et al. 2012; Polat 2012), opposed to non-actualistic scenarios of continental nucleation in intraplate or stagnant lid settings (Bédard 2006; Johnson et al. 2013, 2017; Reimnik et al. 2014; van Kranendonk et al. 2015). In fact, both types of processes likely operated simultaneously at the global scale and in succession to one another in a given segment of continental lithosphere (Moyen and Laurent, 2018; Næraa et al., 2012; Reimnik et al., 2016; van Kranendonk, 2010).

Over the past decade, the issue of continental growth has been addressed using *in-situ* isotopic analyses in zircon. Zircon is a widespread and refractory accessory mineral of continental rocks and contains a wealth of temporal (U-(Th-)Pb geochronometer) and isotopic (Lu-Hf, O) information about the magma in which it crystallized (Hawkesworth and Kemp, 2006). Consequently, large databases of zircon isotopic data, either from detrital grains or global compilations, have been used extensively to constrain the timing and mechanisms of continental formation over geological timescales (Belousova et al., 2010; Condie et al., 2011; Dhuime et al., 2012, 2017; Iizuka et al., 2013; Lancaster et al., 2011). However, this approach considers zircon as disconnected from the rock in which it crystallized and from its geological context, while zircon isotopic signatures cannot be accurately interpreted without information about the nature and petrogenesis of their host igneous rock (Couzinié et al., 2016; Nebel et al., 2011; Roberts et al., 2012). Moreover, the calculation of Hf model ages, on which most zircon-based global crust evolution models rely, is equivocal if the parameters are not constrained by geological information (Nebel et al., 2007; Payne et al., 2016; Roberts and Spencer, 2015; Vervoort and Kemp, 2016). Those issues are even more acute in the Precambrian context, in which the geodynamic setting is ambiguous and cannot be inferred only from zircon U-Pb and Lu-Hf data (Laurent and Zeh, 2015).

It follows from the above discussion that addressing the evolution of the early continental lithosphere on a regional perspective is essential to understand it globally. In fact, recent studies showed that integrating U-Pb and Lu-Hf isotopic data from zircons with geological, petrological and geochemical information on their host granitoids is a powerful tool to investigate Precambrian crustal evolution and geodynamics (Block et al., 2016; Laurent and Zeh, 2015). Here, we apply this approach on the West Troms Basement Complex (WTBC) of northern Norway (Fig. 1), a key domain to investigate Precambrian continent formation. Indeed, it witnesses more than one billion years of continental evolution, characterized by major geological activity in the Meso-/Neoarchean (2.9–2.6 Ga) and Paleoproterozoic (1.9–1.7 Ga) (Bergh et al., 2010, 2012, 2014; Myhre et al., 2013), correlating to the two most prominent peaks of zircon ages at the global scale (Condie and Aster, 2010). The Precambrian rocks of the WTBC show exceptional exposure and limited overprint by younger events, despite their position as a tectonic window within the Norwegian Caledonides (Bergh et al., 2014 and references therein). Although considerable structural, petrological and geochronological work has already been carried out on the WTBC greenstone belts (Armitage and Bergh, 2005; Bergh et al., 2007b, 2010, 2015; Kullerud et al., 2006a,b; Motuza et al., 2001a,b; Myhre et al., 2011; Opheim and Andresen, 1989), little is known about the petrogenesis of the volumetrically dominant granitoids (Krill and Fareth, 1984; Zwaan et al., 1998; Zwaan and Tucker, 1996; Corfu et al., 2003; Myhre et al., 2013).

The aim of this work is therefore to determine the mechanisms and tectonic settings of crustal evolution in the WTBC, as a case study to better constrain Precambrian continent formation. For this purpose, we present a new database of field, petrographic observations, whole-rock major- and trace-element geochemistry and zircon U-Pb and Lu-Hf isotopic measurements from the Archean and Paleoproterozoic granitoids. The samples were selected as to representatively document the geographic extent, lithological and age diversity of granitoid lithologies in this crustal domain (Fig. 1). The combined dataset is used to discuss: (i) the crustal architecture of the WTBC; (ii) the petrogenesis of the granitoid rocks; and (iii) the mechanisms and tectonic setting of crust formation and evolution in the WTBC.

2. Geological setting

The WTBC is exposed over ca. 3300 km^2 as an elongated set of islands flanking the Norwegian coastline from 69° to 70°N, the largest being Senja, Kvaløya, Ringvassøya and Vanna (Fig. 1). Together with the Lofoten-Vesterålen islands further SW, the WTBC corresponds to a Precambrian basement inlier uplifted within the Norwegian passive margin (Bergh et al., 2007a; Indreværet al., 2013; Mjelde et al., 1993; Olesen et al., 1997; Opheim and Andresen, 1989; Roberts and Lippard, 2005). The WTBC and the Lofoten-Vesterålen province likely belong to the Fennoscandian Shield (Fig. 1) and represent the autochtonous Precambrian basement of Caledonian nappes (Bergh et al., 2007a, 2014; Corfu, 2004; Gaál and Gorbatschev, 1987; Griffin et al., 1978; Henkel, 1991; Indreværet al., 2013; Olesen et al., 1997). This is supported by: (i) the presence of similar Precambrian rocks as tectonic windows in the Norwegian Caledonides (Gorbatschev, 1985; Skår, 2002; Stephens et al., 1985); and (ii) the continuity of Precambrian geological structures and geophysical anomalies underneath the Caledonian nappes (Bergh et al., 2014; Henkel, 1991; Olesen et al., 1997; Zwaan, 1995).

The geology of the WTBC has already been described in detail (see Bergh et al., 2010, 2012, 2014; Myhre et al., 2013 and references therein); only the main features are summarized here. The WTBC consists of Meso- to Neoarchean crust (ca. 2.9–2.6 Ga) affected by the Paleoproterozoic Svecofennian orogeny (ca. 2.0–1.7 Ga) (Bergh et al., 2010, 2012). The two most common lithologies are the focus of the present study. First, Meso- to Neoarchean (2.92–2.61 Ga) orthogneisses and plutons are largely made of felsic, tonalitic-trondhjemitic to granodioritic-granitic rocks, with minor mafic phases (Bergh et al., 2007b, 2014; Corfu et al., 2003; Myhre et al., 2013; Zwaan et al., 1998; Zwaan and Tucker, 1996). They carry a weak to penetrative, steeply dipping N-S to NW-SE trending foliation, and commonly are migmatitic and heterogeneous at the outcrop scale (Armitage and Bergh, 2005; Bergh et al., 2010; Myhre et al., 2013; Zwaan et al., 1998). The orthogneisses are relatively homogeneous, low-grade and weakly deformed (except along shear zones) in the northeast of the WTBC (Ringvassøya and Vanna), whereas they are more heterogeneous, tectonized and higher-grade in the southwest (Kvaløya and Senja) (Bergh et al., 2010, 2014; Myhre et al., 2013). Second, weakly foliated to non-foliated, Paleoproterozoic (1.87–1.75 Ga) plutonic rocks are mostly felsic (granites) with subordinate mafic facies (gabbros, diorites) (Bergh et al., 2010, 2012; Corfu et al., 2003; Krill and Fareth, 1984; Zwaan et al., 1998) (Fig. 1).

The Meso- to Neoarchean orthogneisses are subdivided in contrasting units framed by narrow greenstone belts and/or shear zones associated with them (Fig. 1) (Bergh et al., 2010, 2014; Myhre et al., 2013; Zwaan, 1995; Zwaan and Tucker, 1996; Zwaan et al., 1998). The greenstone belts are made up of (ultra-)mafic rocks, felsic volcanic rocks, siliciclastic rocks, calc-silicates and BIFs, all metamorphosed in greenschist to lower amphibolite facies conditions (Armitage and Bergh, 2005; Bergh et al., 2007b, 2010; Motuza et al., 2001a,b; Myhre et al., 2011; Zwaan, 1995; Zwaan et al., 1998). The low-grade Vanna-Ringvassøya block consists of the 2.92–2.80 Ga Dåfjord tonalitic gneisses and ca. 2.85 Ga Ringvassøya greenstone belt (Bergh et al., 2007b, 2014; Kullerud et al., 2006a; Motuza et al., 2001a,b; Myhre et al., 2013; Zwaan and Tucker, 1996), cross-cut by the ca. 2.69 Ga Mikkelvik alkaline stock (Zozulya et al., 2009), a 2.40 Ga mafic dyke swarm (Kullerud et al., 2006b) and overlain by the ≥2.20 Ga Vanna group sediments (Bergh et al., 2007b). The higher-grade Kvaløya-Senja block comprises more heterogeneous (mafic to felsic) and younger (2.75–2.67 Ga) gneisses (Corfu et al., 2003; Myhre et al., 2013) as well

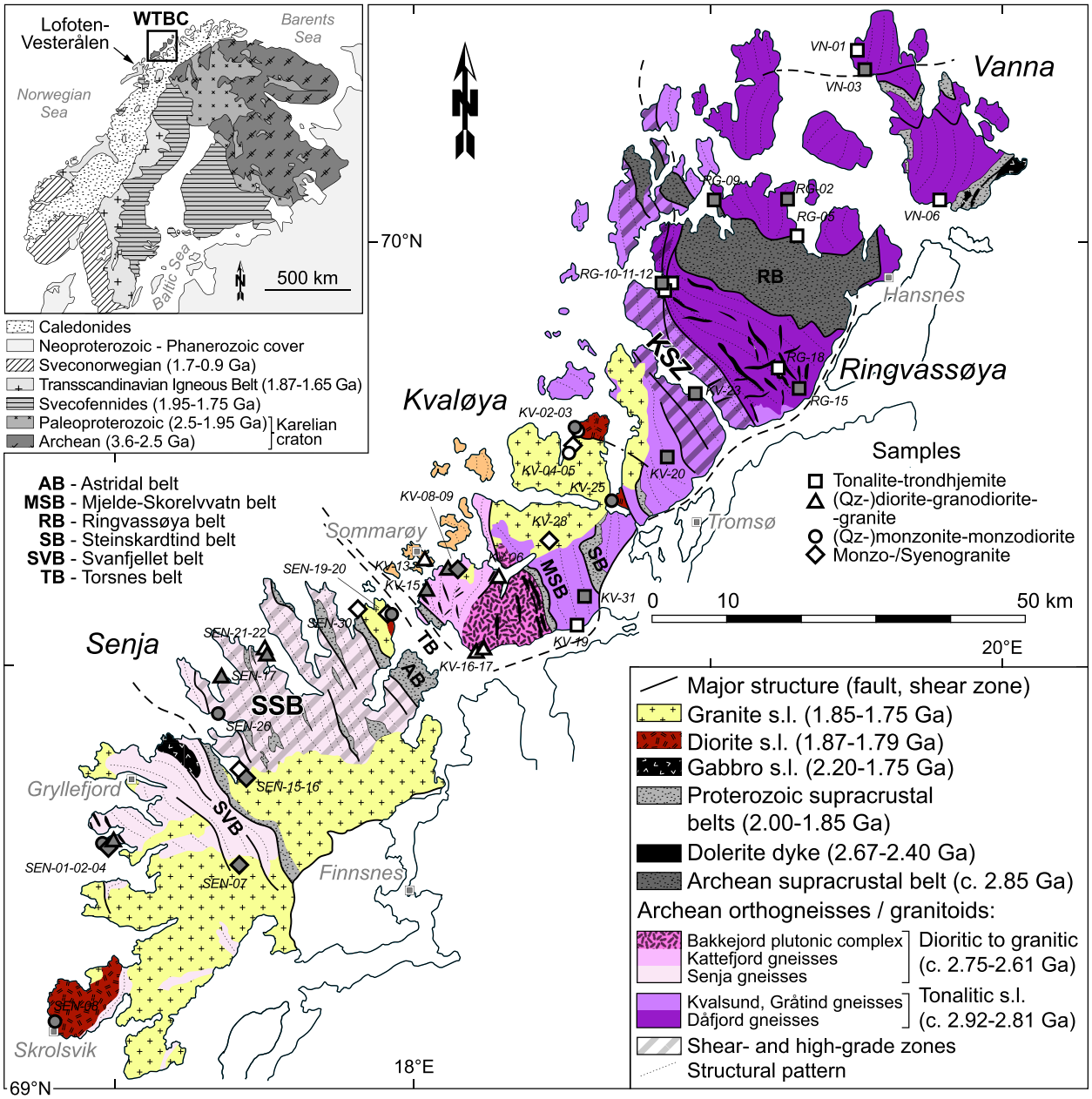

Fig. 1. Sketch geological map of the West Troms Basement Complex (WTBC), after Bergh et al. (2010, 2014), Myhre et al. (2013) and results from this study. KSZ = Kvalsund Shear Zone; SSB = Senja Shear Belt. The inset shows the position of the WTBC within the Fennoscandian shield. Samples in gray correspond to those investigated for zircon U-Pb/Lu-Hf isotopes.

as narrow 2.00–1.95 Ga supracrustal belts such as the Mjelde-Skorelvvatn, Torsnes and Astridal belts (Armitage and Bergh, 2005; Bergh et al., 2010, 2015; Myhre et al., 2011). These rocks are affected by Svecofennian deformation, metamorphism and voluminous 1.80–1.77 Ga magmatism.

Two major NW-trending networks of such shear zones are associated with high-grade (amphibolite- to granulite-facies) metamorphism and migmatization (Bergh et al., 2010, 2014) (Fig. 1). These are: (i) the Kvalsund Shear Zone in SW Ringvassøya and NE Kvaløya (Bergh et al., 2014, 2015; Myhre et al., 2013) and (ii) the 30 km-wide Senja Shear Belt in NE Senja, comprising an anastomosing network of shear zones and supracrustal belts separating blocks of presumably Neoarchean, high-grade gneisses (Bergh et al., 2010; Zwaan 1995; Zwaan et al., 1998). The significance of those structures is still uncertain. According to Bergh et al. (2014), the Kvalsund shear zone represents a major boundary between the Vanna-Ringvassøya block and the Kvaløya-Senja block. In contrast, Zwaan and Tucker (1996) propose that the Senja Shar Belt represents the main delimitation between two crustal segments.

3. Granitoid rocks in the WTBC

Representative examples of the field appearance and petrography of the WTBC granitoids are presented in Fig. 2. More field pictures and microphotographs are presented in the Electronic Supplementary Material for the samples investigated for zircon U-Pb and Lu-Hf isotopes.

According to our observations and existing data (Bergh et al., 2007b; Myhre et al., 2013; Zwaan and Tucker, 1996; Zwaan et al., 1998), the granitoids can be classified in four types, largely based on the different proportions of quartz (Qz), plagioclase (Pl) and K-feldspar (Kfs); and the nature of mafic minerals.

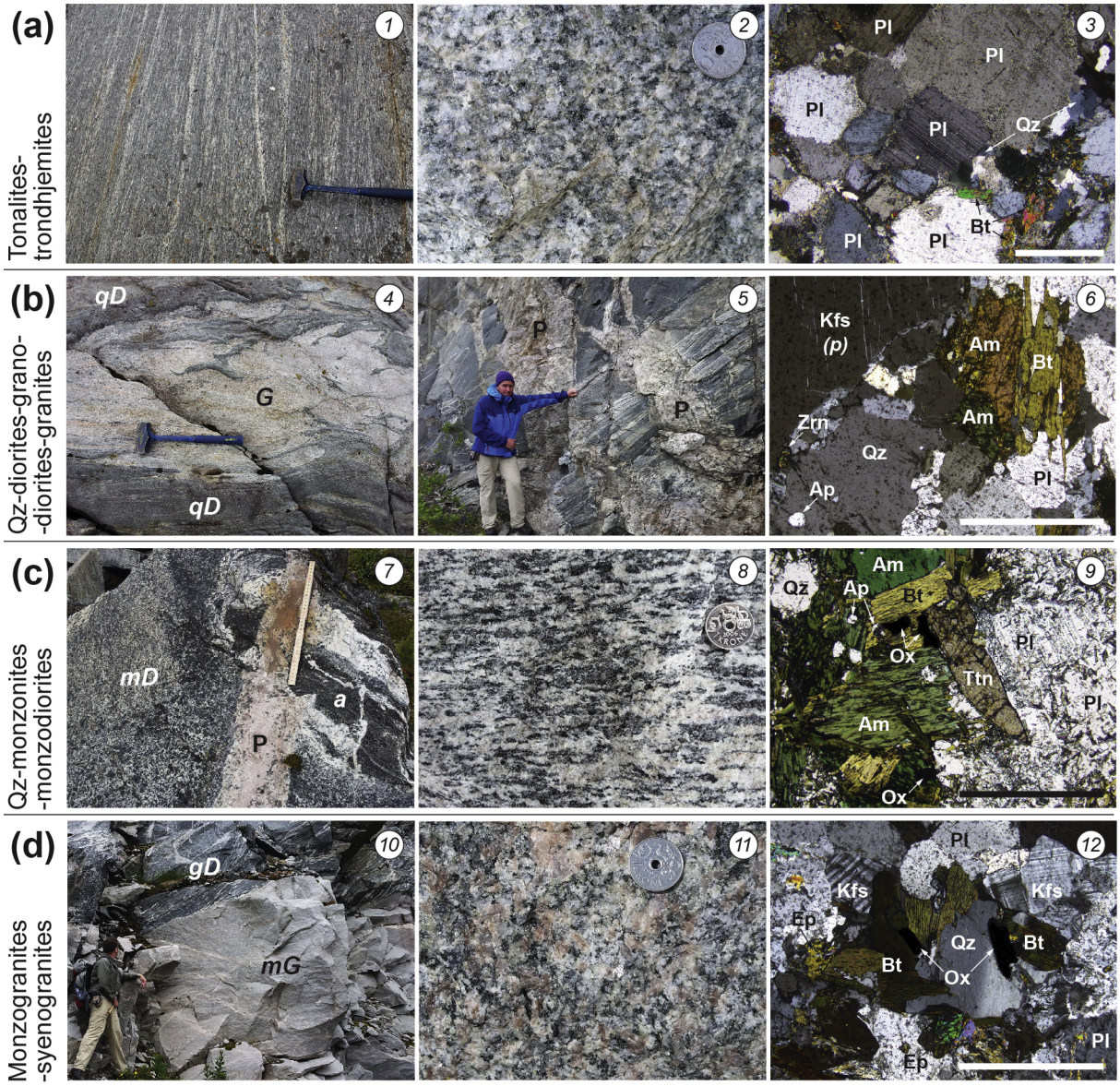

Fig. 2. Representative geological and petrographic features of the four types of granitoids identified in the WTBC: tonalite-trondhjemite (a), (qz-)diorite-granodiorite-granite (b), qz-monzonite-monzodiorite (c) and monzo-/syenogranite (d). (1) Strongly foliated trondhjemitic gneiss in the Kvalsund Shear Zone in W Ringvassøya (RG-10); (2) Coarse-grained, undeformed tonalite in S Vanna (VN-06); (3) Photomicrograph of trondhjemite RG-15; (4) Closely associated qz-dioritic (qD) and granitic (G) gneisses in N Senja (SEN-21/-22); (5) Strongly deformed and layered, granodioritic to granitic gneisses in SW Kvaløya (KV-08) cross-cut by pegmatitic dykes (P) related to the Ersfjord granite; (6) Photomicrograph of granite SEN-17; (7) Monzodiorite (mD) of the Skrolsvik pluton in SW Senja (SEN-08) containing a raft of migmatitic amphibolite (a) and cut by a pegmatitic dyke (P); (8) Deformed qz-monzonite in NW Senja (SEN-26); (9) Photomicrograph of monzodiorite KV-25; (10) dyke of monzogranite (mG) (SEN-02) cutting migmatitic granodiorite gneiss (gD) in W Senja; (11) Coarse-grained, undeformed and porphyritic Ersfjord granite in NW Kvaløya (KV-04); (12) Photomicrograph of monzogranite sample SEN-02. Mineral abbreviations are after Whitney and Evans (2010). Scale bar in photomicrographs is 1 mm; hammer is ca. 40 cm long; ruler is 35 cm long; coin is ca. 1.5 cm in diameter; O. Bolle is 1.85 m tall.

(1) **Tonalites** and **trondhjemites** are characterized by Pl ≥ Qz ≫ Kfs. They contain biotite and locally amphibole ± primary epidote as mafic minerals (Fig. 2a). Pl form euhedral crystals (altered to secondary epidote, sericite and albite) wrapped by anhedral Qtz and very subordinate Kfs (Fig. 2a). Accessory minerals are apatite, zircon and more rarely Fe-Ti oxides, titanite and allanite. Those rocks are medium- to fine-grained, moderately to strongly deformed gneisses (Fig. 2a), locally migmatitic (especially in the Kvalsund Shear Zone). They represent the largely dominant component of the Archean orthogneisses on Vanna, Ringvassøya and NE- to central Kvaløya (Fig. 1).

(2) **Quartz-diorites**, **granodiorites** and **granites** show higher proportions of Kfs than the latter, i.e. Pl ≥ Qz ~ Kfs, and are characterized by biotite and amphibole as dominant mafic minerals (Fig. 2b). The diorites are occasionally clinopyroxene-bearing while the granites locally contain muscovite. Euhedral epidote with allanite cores may also be present. Apatite, zircon, titanite and Fe-Ti oxides are accessory minerals (Fig. 2b). These rocks are medium- to coarse-grained and form the dominant phase of composite Archean gneiss units of SW Kvaløya and Senja (Fig. 1), in which they are complexly associated with amphibolites, pegmatitic bodies and rare meta-sedimentary rocks (Fig. 2b). These gneisses are moderately to strongly deformed, apart from some low-strain areas of the Bakkejord plutonic complex (Fig. 1) and some Kfs-porphyritic granodiorites and granites on Senja.

(3) **Quartz-monzonites** and **monzodiorites** have Pl > Kfs ~ Qtz and

contain amphibole, biotite, euhedral epidote with allanite cores and occasionally clinopyroxene as mafic phases (Fig. 2c). Titanite, Fe-Ti oxides (particularly magnetite) and epidote are more abundant than in the previous two types (Fig. 2c). Accessory minerals are zircon and apatite. These rocks are weakly to moderately deformed (except along shear zones), medium- to coarse-grained, equigranular to Kfs-porphyritic in texture and locally associated with pegmatites (Fig. 2c). They locally form circumscribed plutons intrusive in the Archean orthogneisses of the previous two types (e.g. Bakkan stock, Kvaløya; Skrolsvik pluton, Senja; Fig. 1), in which case they often contain enclaves thereof (Fig. 2c).

(4) **Monzo-** and **syenogranites** are characterized by Kfs ≥ Qtz ~ Pl. Kfs is found as perthitic or microcline crystals and porphyroblasts (Fig. 2d). These rocks contain biotite, primary epidote and occasionally muscovite. Epidote forms euhedral crystals, locally with allanite cores and is as abundant as biotite, in contrast with other groups in which biotite and/or amphibole are dominant. Both minerals form mafic clusters in association with abundant titanite and Fe-Ti oxides (mostly magnetite). Apatite and zircon are accessory phases. These rocks are generally not deformed (except along shear zones), medium- to coarse-grained and equigranular to Kfs-porphyritic (Fig. 2d). They form either the dominant phase of the large Paleoproterozoic plutons (Ersfjord and Senja granites; Fig. 1) or small bodies and dykes cross-cutting the Archean orthogneisses (Fig. 2d), especially in SW Kvaløya and Senja.

4. Whole-rock geochemistry

Representative whole-rock major- and trace-element compositions of the four groups of WTBC granitoids are presented in Table 1 and illustrated in Figs. 3–5. The detailed analytical methods are available in the Electronic Supplementary Material, together with the whole dataset (Table S1).

4.1. Major elements

The **tonalites-trondhjemites** display a moderate range of SiO_2 contents (63–76 wt%) together with higher CaO (1.5–5.7 wt%) and Al_2O_3 (14.7–17.4 wt%) than other rock types at a given SiO_2 content (Fig. 3). They typically show low K_2O (0.7–2.3 wt%) and high Na_2O contents (3.8–6.1 wt%) (Fig. 3), leading to low K_2O/Na_2O ratios (0.1–0.7) (Fig. 4a). They classify as metaluminous to slightly peraluminous with A/CNK (molar $Al_2O_3/[CaO + Na_2O + K_2O]$ ratio) in the range 0.85–1.10 (Fig. 4a), and show dominantly calcic and magnesian affinities (Fig. 4b-c). Besides three samples with < 67 wt% SiO_2, tonalites-trondhjemites also show low FeO_t (≤3.3 wt%) and MgO (≤1.4 wt%), as well as variable Mg# (molar Fe/[Fe + Mg] ratio) ranging from 0.25 to 0.50 (Fig. 4d).

The **qz-diorites**, **granodiorites** and **granites** are characterized by lower and more scattered SiO_2 contents (54–71 wt%) than tonalite-trondhjemites (Fig. 3). They show variable concentrations of Al_2O_3 (15.1–18.0 wt%), CaO (1.9–5.7 wt%), FeO_t (1.3–7.4 wt%) and MgO (0.5–4.2 wt%) that are negatively correlated with SiO_2 (Fig. 3). Besides one outlier, Na_2O concentrations are fairly constant (3.7–4.5 wt%) whereas K_2O (1.1–4.4 wt%) is positively correlated with SiO_2 and higher than in tonalite-trondhjemites at a given SiO_2 content (Fig. 3), with K_2O/Na_2O ratios in the range 0.5–1.0 (Fig. 4a). These characteristics correspond to metaluminous to slightly peraluminous (A/CNK = 0.80–1.05), magnesian and calc-alkalic to alkali-calcic affinities (Fig. 4). These rocks also show a relatively restricted range of Mg# from 0.35 to 0.51 (Fig. 4f).

The **qz-monzonites** and **monzodiorites** have relatively lower SiO_2 (51–63 wt%) and higher FeO_t contents (4.6–14.3 wt%) than qz-diorites, granodiorites and granites, but show comparable ranges of Al_2O_3 (14.0–17.9 wt%), CaO (2.6–7.0 wt%), MgO (0.9–3.3 wt%) and Na_2O (3.4–4.8 wt%) contents (Fig. 3). Their K_2O concentrations are, however, distinctively higher (1.4–6.3 wt%, up to the shoshonitic field) and increase with SiO_2 (Fig. 5), K_2O/Na_2O ratios ranging from 0.4 to 1.6 (Fig. 4a). The qz-monzonites and (monzo)diorites are strictly metaluminous (A/CNK = 0.68–099), ferroan to magnesian and alkali-calcic to alkalic rocks with a comparable range of Mg# (0.29–0.52) as qz-diorites-granodiorites-granites (Fig. 4).

The **monzo-** and **syenogranites** form a tight compositional cluster at high SiO_2 (69–76 wt%) and K_2O contents (3.9–5.4 wt%), showing low Al_2O_3 (13.1–15.0 wt%), CaO (0.9–2.3 wt%), MgO (0.1–0.7 wt%) and Na_2O (2.9–4.1 wt%), all negatively correlated with silica (Fig. 3). FeO_t concentrations (1.3–3.6 wt%) are notably higher than for other rock types at the same SiO_2 content (Fig. 3). These granites have very high K_2O/Na_2O ratios (≥0.9 and up to 1.9), peraluminous (A/CNK = 1.0–1.1) and ferroan signatures, alkali-calcic to calc-alkaline compositions and lower Mg# (0.05–0.28) than any other rock type (Fig. 4).

4.2. Trace elements

Chondrite-normalized REE patterns and primitive mantle-normalized multi element patterns are presented in Fig. 5. Despite strong variations in absolute concentrations (one to two orders of magnitude), samples from all granitoid groups are characterized by fractionated trace element profiles with enrichment in LILE and LREE relative to the primitive mantle and chondrite, together with systematic negative anomalies in HFSE (Nb-Ta, Ti), P and positive Pb anomalies (Fig. 5).

The **tonalites-trondhjemites** (Fig. 5a) show moderate and relatively homogeneous LREE contents (La = 5.5–39.9 ppm), while HREE and Y contents span over two orders of magnitude (Yb = 0.18–17.8 ppm; Y = 1.7–160 ppm), leading to strongly variable fractionation of chondrite-normalized REE patterns (La_N/Yb_N = 2–59; Dy_N/Yb_N = 0.7–5.0). The Eu anomalies range from slightly positive to strongly negative (Eu_N/Eu^* = 0.4–1.5, correlated to La_N/Yb_N; $Eu^* = [Sm_N \cdot Gd_N]^{1/2}$). These rocks show moderate concentrations in Rb (22–88 ppm), Cs (0.3–6.4 ppm) (except sample KV-31 with 269 and 11 ppm respectively) and Pb (3.0–17.1 ppm), as well as Ba (299–682 ppm) and Sr (241–693 ppm) that do not show any anomaly. Similar to HREE, HFSE concentrations vary by at least an order of magnitude (Th = 0.1–8.8 ppm; U = 0.17–1.40 ppm; Nb = 1.5–23.6 ppm; Zr = 60–572 ppm). With the exception of samples with ≤67 wt% SiO_2, transition element contents are low (V < 35 ppm; Cr < 10 ppm; Ni < 10 ppm).

The **qz-diorites**, **granodiorites** and **granites** (Fig. 5b) have higher LREE contents than tonalites-trondhjemites (La = 18.4–108.1 ppm) and more homogeneous, moderate HREE–Y contents (Yb = 0.46–2.35 ppm; Y = 6.0–29.6 ppm). This corresponds to moderately to strongly fractionated REE patterns (La_N/Yb_N = 8–89) with no or slightly negative Eu anomalies (Eu_N/Eu^* = 0.5–1.1). LILE concentrations are generally higher than in tonalites-trondhjemites (Rb = 58–262 ppm; Ba = 634–1929 ppm; Sr = 435–1292 ppm; Pb = 5.4–39.3 ppm), while HFSE contents are in the same range (Th = 1.0–14.3 ppm; U = 0.12–2.90 ppm; Nb = 2.7–19.7 ppm; Zr = 113–518 ppm). Transition element concentrations are negatively correlated with SiO_2 (V = 14–121 ppm; Cr = 1.8–53.9 ppm; Ni = 3.5–30.5 ppm).

The **qz-monzonites** and **monzodiorites** (Fig. 5c) show homogeneous trace element compositions compared with the two previous groups. REE contents are comparable to those of qz-diorites, granodiorites and granites (La = 29.6–108.9 ppm; Yb = 0.73–2.42 ppm; Y = 10.5–31.4 ppm), with moderately fractionated patterns (La_N/Yb_N = 17–32) and generally no Eu anomaly (Eu_N/Eu^* = 0.9–1.0, except sample SEN-26 that has Eu_N/Eu^* = 2.2). These rocks are notably rich in Ba (640–5570 ppm) and Sr (687–1457 ppm) that show positive anomalies, whereas other LILE concentrations are comparable to those of other groups (Rb = 41–151 ppm; Cs = 0.4–2.5 ppm; Pb = 11.8–22.4 ppm). Nb and Ta contents are also higher than in other rock types (5.8–29.7 and 0.43–1.37 ppm respectively), but other HFSE concentrations are in the same range (Th = 2.9–7.4 ppm;

Table 1
Selected whole-rock major- and trace-element compositions of granitoids in the WTBC, representative of the four groups discussed in text.

Granitoid group	Tonalite-trondhjemite		(Qz-)diorite-granodiorite-granite		Qz-monzonite-monzodiorite		Monzo-/Syenogranite	
Sample	RG-09	RG-15	SEN-17	SEN-22	KV-25	SEN-26	KV-04	SEN-07
Rock	Tonalite	Trondhjemite	Granite	Qz-diorite	Monzodiorite	Qz-monzonite	Monzogranite	Syenogranite
Major elements (wt.%)								
SiO_2	62.83	70.13	71.14	53.93	59.49	62.45	71.21	73.91
TiO_2	0.64	0.14	0.16	1.17	0.65	0.60	0.51	0.21
Al_2O_3	16.05	17.37	15.42	17.97	16.52	17.44	13.57	13.88
$Fe_2O_{3\ (T)}$[a]	6.13	1.27	1.47	8.19	6.06	5.08	2.97	2.02
MnO	0.10	0.01	0.03	0.14	0.10	0.07	0.04	0.03
MgO	2.54	0.62	0.53	4.20	2.98	0.86	0.60	0.14
CaO	5.49	3.32	2.11	5.68	4.99	2.62	1.58	1.18
Na_2O	4.14	5.95	4.10	5.31	4.79	3.69	3.39	3.15
K_2O	1.64	0.71	4.44	2.94	3.24	6.30	4.70	5.31
P_2O_5	0.15	0.04	0.03	0.78	0.33	0.33	0.13	0.02
LOI[b]	0.86	0.77	0.47	0.83	0.97	0.97	1.11	0.41
Sum	100.58	100.32	99.92	101.13	100.12	100.40	99.80	100.27
Trace elements (ppm)								
Sc	18.0	8.4	9.9	16.9	21.5	14.2	10.4	10.9
V	91	9	14	115	118	27	29	11
Cr	35	3	5	51	40	1	3	1
Co	17.1	2.0	3.7	20.7	15.9	5.6	4.0	1.6
Ni	34.2	3.0	6.4	30.5	14.8	0.7	1.0	< l.o.d.[c]
Ga	20	14	17	27	24	22	23	22
Rb	88	22	96	193	82	119	173	254
Sr	319	499	718	1292	1457	687	431	170
Y	16	2	7	18	21	18	28	13
Zr	161	77	113	187	198	231	378	266
Nb	13.9	1.5	2.7	10.2	11.1	5.8	24.1	13.9
Cs	6.4	0.6	0.2	3.2	2.5	0.4	0.4	1.7
Ba	440	394	1357	1029	2682	5570	1125	723
La	22.3	5.5	52.7	66.0	51.4	37.2	100.6	83.2
Ce	47.3	11.6	102.9	144.5	107.9	77.9	197.8	172.1
Pr	5.7	1.5	10.5	18.2	13.4	9.7	21.7	18.9
Nd	21.2	5.4	32.1	67.5	49.6	36.3	71.2	60.4
Sm	4.0	1.0	3.9	10.2	8.4	6.2	10.7	8.6
Eu	1.10	0.40	1.11	2.78	2.27	4.02	1.78	0.97
Gd	3.5	0.7	2.7	7.2	6.2	4.9	8.0	5.9
Dy	2.8	0.4	1.4	3.5	3.7	3.2	5.1	2.7
Ho	0.56	0.07	0.25	0.64	0.71	0.64	0.98	0.46
Er	1.52	0.17	0.65	1.57	1.76	1.66	2.55	1.19
Yb	1.57	0.22	0.60	1.26	1.61	1.52	2.38	0.90
Lu	0.23	0.02	0.09	0.19	0.25	0.23	0.33	0.15
Hf	3.9	2.0	2.6	3.8	4.4	4.7	8.4	6.7
Ta	0.58	0.05	0.06	0.42	0.46	0.19	2.15	0.67
Pb	12.0	7.1	22.4	17.8	13.3	18.3	19.9	32.7
Th	5.8	0.4	9.7	2.3	5.3	2.9	18.4	43.1
U	1.2	0.2	0.2	1.5	1.4	0.4	2.0	3.3

[a] All iron expressed as Fe_2O_3.
[b] Loss Of Ignition.
[c] Below the limit of detection.

U = 0.40–3.42 ppm; Zr = 133–340 ppm). Qz-monzonites and monzodiorites show higher V contents (27–285 ppm) than qz-diorites, granodiorites and granites, but lower Cr (1.1–39.8 ppm) and Ni (0.6–15.6 ppm) contents.

The **monzo-** and **syenogranites** (Fig. 5d) have slightly higher LREE (43.5–148.3 ppm) and lower HREE–Y contents (0.54–2.38 and 5.8–28.3 ppm respectively) than qz-monzonites and monzodiorites, leading to more fractionated REE patterns (La_N/Yb_N = 29–63 and up to 188). They also show a strong negative anomaly, not only in Eu (Eu_N/Eu^* = 0.4–0.7) but also in Sr and Ba, despite moderate to high concentrations (170–431 ppm and 488–1235 ppm respectively). Monzo- and syenogranites are particularly richer in Rb (153–254 ppm), Pb (19.9–38.3 ppm), Th (18.4–48.6 ppm) and U (1.09–5.23 ppm) than any other granitoid type. Other HFSE contents are similar to other groups (Nb = 3.7–37.3 ppm; Zr = 159–535 ppm). Monzo- and syenogranites are also the poorest in transition elements (V = 6–29 ppm; Cr = 1.1–8.7 ppm; Ni = 0.7–2.0 ppm).

5. Zircon U-Pb and Lu-Hf analyses

5.1. Sample selection and methods

Zircon U-Pb and Lu-Hf isotope analyses were performed on a selection of 23 samples representative of the petrographic and chemical diversity of the granitoids and distributed over the whole surface of the WTBC (Fig. 1). Samples (2–5 kg) were crushed using a jaw crusher and disc mill, and subsequently sieved to < 280 µm using disposable Nylon sieves. Zircon was concentrated using panning, magnetic separation and heavy liquids (methylene iodide). About 50 to 100 grains were hand-picked for each sample, set in 1-inch Epoxy mounts and polished.

Prior to analyses, zircon images were acquired using a Jeol JSM-6490 Scanning Electron Microscope (SEM) equipped with cathodoluminescence (CL) and back-scattered electron (BSE) detectors, at Goethe Universität Frankfurt (GUF). Zircon isotopic analyses were performed by laser ablation–(multi-collection)–inductively coupled

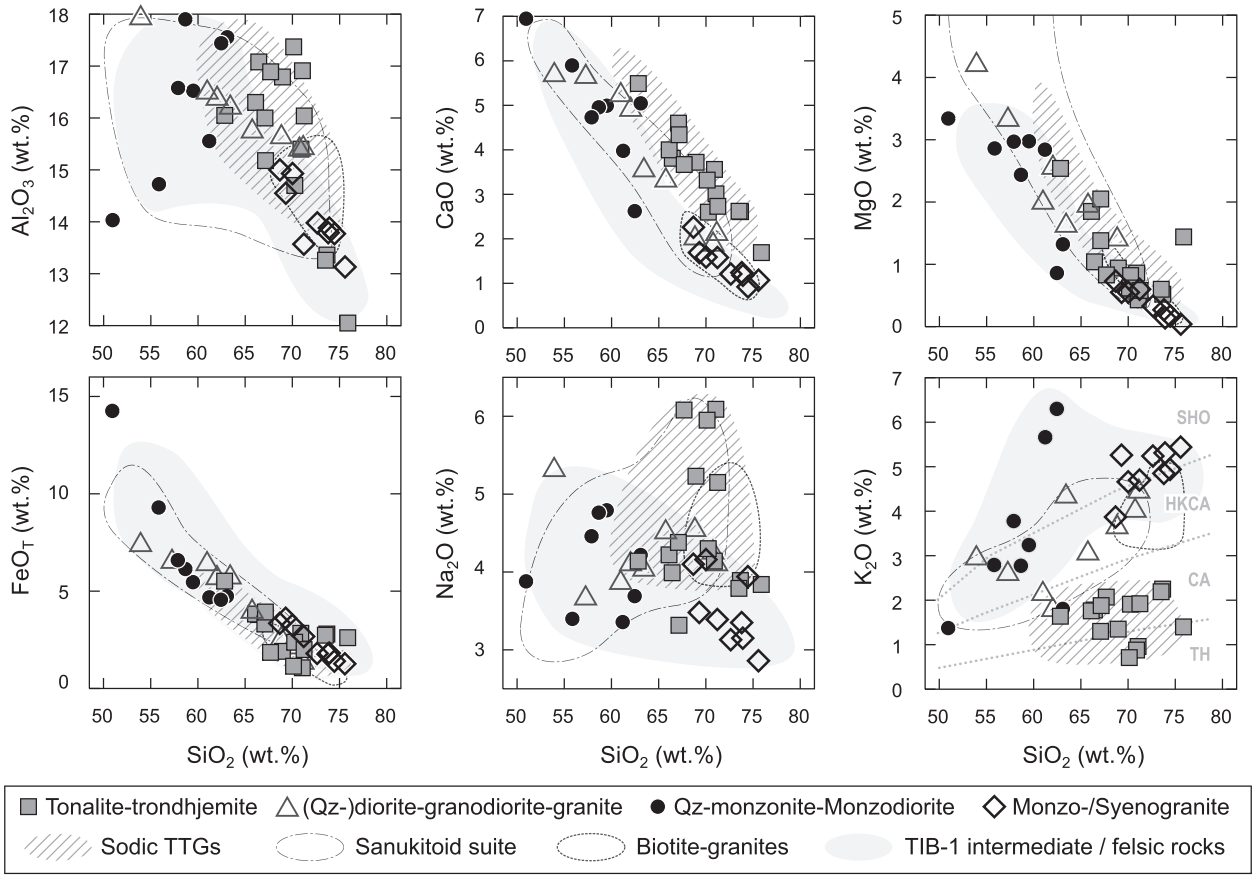

Fig. 3. Selected Harker plots showing the major element compositions of the WTBC granitoids. The compositions of TTGs, the sanukitoid suite and biotite granites are from Laurent et al. (2014) and Moyen (2011). The composition of 1.81–1.76 Ga granitoids from the Transscandinavian Igneous Belt (TIB-1), including mangerite and charnockite from the Lofoten-Vesterålen province, are also reported (data from Ahl et al., 1999; Andersson, 1997; Kornfält et al., 1997; Malm and Ormaasen, 1978; Markl, 2001; Markl and Höhndorf, 2003; Skår, 2002). Fields in the K_2O vs. SiO_2 diagram are after Peccerillo and Taylor (1976): TH = tholeiitic, CA = calc-alkaline; HKCA = high-K calc-alkaline; SHO = shoshonitic.

plasma–mass spectrometry (LA-(MC-)ICP-MS) at GUF using a RESOlution (ASI) M-50E 193 nm ArF Excimer laser system coupled to a ThermoFinnigan Element 2 sector-field mass spectrometer for U-Pb dating; and to a ThermoFinnigan Neptune multi-collector mass spectrometer for Lu-Hf analyses. The Electronic Supplementary Material contains details about the analytical methods and setup, together with the whole dataset of U-Pb (Table S2) and Lu-Hf analyses (Table S3) on samples and zircon reference materials GJ-1, OG-1, Plešovice, Temora-2 and 91500.

5.2. Results

A detailed description of zircon textures, U-Pb dates, Lu-Hf isotopic results, together with the interpretation of the combined data, are provided for each sample in the Electronic Supplementary Material. The results are summarized in Table 2 and Figs. 6 and 7. According to the combined dataset, the samples can be classified in three groups (Fig. 6, Table 2):

(1) **Group 1** represents samples containing zircon crystals with simple CL zoning (no core-rim relationship; simple oscillatory, patchy or sector zoning) and characterized by a single population of dominantly concordant U-Pb dates and homogeneous $^{176}Hf/^{177}Hf_{(t)}$ ratios (Fig. 6a). These are interpreted as reflecting the age and Hf isotopic composition of the original magma. This group includes tonalite-trondhjemite samples VN-03, RG-09 and RG-15; quartz-monzonite-monzodiorite samples KV-03, SEN-20 and SEN-26; and monzo-/syenogranite sample SEN-15.

(2) **Group 2** samples are characterized by a single zircon population similar to group 1, yet showing concordant to strongly discordant U-Pb data with variable $^{207}Pb/^{206}Pb$ dates (Fig. 6b). However, these samples show identical $^{176}Hf/^{177}Hf_{(t)}$ ratios within uncertainty, resulting in sub-horizontal arrays in $^{176}Hf/^{177}Hf_{(t)}$ vs. apparent $^{207}Pb/^{206}Pb$ date diagrams (Fig. 6b). This corresponds to a single generation of igneous zircon that underwent multiple Pb loss without disturbing the Hf isotopic composition (e.g. Amelin et al., 1999; Gerdes and Zeh, 2009; Guitreau et al., 2012; Laurent and Zeh, 2015; Zeh et al., 2009). The latter is thus considered as representative of the original magma. In this case, the U-Pb emplacement age was obtained from the concordant analyses or upper intercept of the discordant spots. This group comprises tonalite-trondhjemite samples RG-10 and KV-31; quartz-diorite-granodiorite-granite samples KV-15, SEN-01 and SEN-17; quartz-monzonite-monzodiorite sample SEN-04; and monzo-/syenogranite samples KV-09 and SEN-02.

(3) **Group 3** includes samples characterized by multiple zircon crystallization events. The crystals show either core-rim relationships or several zircon populations with contrasted morphologies and CL features, the different domains/crystals having significantly distinct $^{207}Pb/^{206}Pb$ dates and/or $^{176}Hf/^{177}Hf_{(t)}$ ratios (Fig. 6c). Depending on the characteristics of the different domains/crystals, the data were interpreted in two ways. First, inherited/xenocrystic zircon grains or cores (oldest dates) coexist with igneous rims or grains (youngest dates) in tonalite-trondhjemite samples RG-02, KV-23, quartz-monzonite-monzodiorite samples KV-25, SEN-08a and monzo-/syenogranite sample SEN-07. Second, igneous zircons

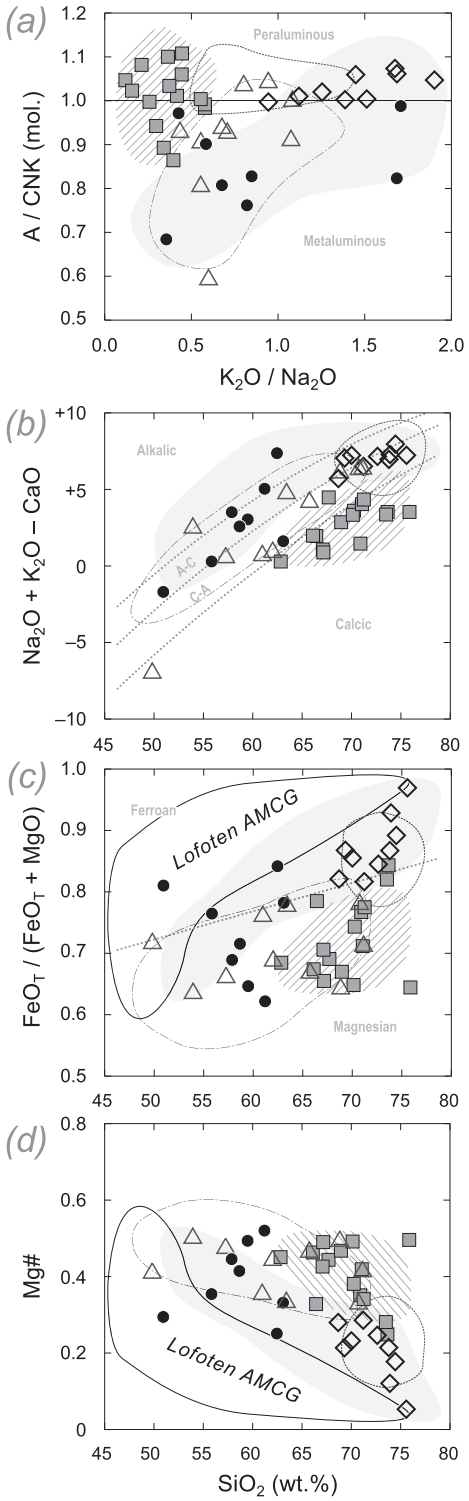

Fig. 4. Classification diagrams for the WTBC granitoids, based on major element geochemistry. (a) A/CNK (molar Al_2O_3/[CaO + Na_2O + K_2O]) vs. K_2O/Na_2O (Laurent et al., 2014); limit between peraluminous and metaluminous field after Shand (1943); (b–d) diagrams of Frost et al. (2001), showing the MALI index (Na_2O + K_2O–CaO), Fe* (FeO_T/[FeO_T + MgO]) and Mg# (molar Mg/Mg + Fe) against SiO_2. Fields in (b–d) are after Frost et al. (2001); A–C = alkali-calcic, C-A = calc-alkalic. Fields and symbols are as in Fig. 3; except in (c) and (d) where the Lofoten-Vesterålen anorthosite-mangerite-charnockite-granite suite (Malm and Ormaasen, 1978; Markl, 2001; Markl and Höhndorf, 2003) is separated from other TIB-1 granitoids.

(oldest dates) are overgrown by rims or post-dated by a different zircon generation (youngest dates) corresponding to post-emplacement events (migmatitization; fluid and/or melt-rock interaction). This includes tonalite-trondhjemite sample KV-20 and quartz-diorite-granodiorite-granite samples KV-08 and SEN-22.

Unless explicitly mentioned otherwise, all the ages quoted below are crystallization ages and Hf isotopic compositions correspond to the average calculated at this age from all igneous zircon analyses (see Table 2). The uncertainties are quoted at 95% confidence level and, for $^{176}Hf/^{177}Hf_{(t)}$ ratios, are on the last significant digit.

With the exception of KV-23 that shows a Neoarchean age of 2685 ± 8 Ma and a sub-chondritic zircon Hf isotopic composition ($^{176}Hf/^{177}Hf_{(t)}$ = 0.28103 ± 4; $\varepsilon Hf_{(t)}$ = −0.9 ± 1.4), all samples of the tonalite-trondhjemite group show Mesoarchean emplacement ages and supra-chondritic $\varepsilon Hf_{(t)}$ (Fig. 7). In details, three episodes of tonalite-trondhjemite emplacement can be identified: (i) ca. 2920 Ma (represented by sample RG-10 at 2920 ± 7 Ma); (ii) ca. 2865 Ma (emplacement age of tonalitic gneisses VN-03 at 2865 ± 8 Ma and RG-09 at 2866 ± 7 Ma); and (iii) ca. 2840–2830 Ma (mostly trondhjemitic samples, i.e. RG-02 at 2840 ± 9 Ma; KV-31 at 2835 ± 8 Ma; RG-15 at 2831 ± 7 Ma; and KV-20 at 2828 ± 8 Ma) (Table 2). Although their ages span ca. 100 Ma, all samples have identical zircon $^{176}Hf/^{177}Hf_{(t)}$ ratio within uncertainty (0.28097 ± 3 to 0.28104 ± 6) corresponding to positive $\varepsilon Hf_{(t)}$ (+2.5 ± 0.9 to + 3.0 ± 2.1) (Fig. 7). Zircon from sample KV-20 is characterized by prominent, bright-CL and unzoned rims having a crystallization age of 2681 ± 10 Ma (see Electronic Supplementary Material), interpreted as reflecting a metamorphic/migmatitic event and showing a homogeneous Hf isotopic composition ($^{176}Hf/^{177}Hf_{(t)}$ = 0.28099 ± 1) corresponding to a sub-chondritic value ($\varepsilon Hf_{(t)}$ = −2.4 ± 0.4) (Fig. 7). Samples KV-23 and KV-31 contain inherited zircon cores having U-Pb and Lu-Hf isotopic data overlapping with those from other tonalite-trondhjemite samples, i.e. dates between 2920 and 2810 Ma, and $\varepsilon Hf_{(t)}$ between 0 and +3 (Fig. 7).

The zircon data from qz-diorite-granodiorite-granite samples are more disparate than those from tonalites-trondhjemites, albeit also showing exclusively Archean crystallization ages. The quartz-diorite KV-15 shows the oldest age of all the investigated samples (2957 ± 9 Ma) and a low zircon $^{176}Hf/^{177}Hf_{(t)}$ of 0.28077 ± 4 corresponding to sub-chondritic $\varepsilon Hf_{(t)}$ (−3.8 ± 1.5) (Fig. 7). The granitic gneiss sample KV-08 displays two populations of zircon: (i) bright-CL, oscillatory zoned igneous zircons yielded an emplacement age of 2744 ± 11 Ma and a slightly sub-chondritic $\varepsilon Hf_{(t)}$ (−1.0 ± 1.1); (ii) dark-CL zircons have an upper intercept age of 1702 ± 49 Ma and a strongly sub-chondritic average $^{176}Hf/^{177}Hf_{(t)}$ of 0.28138 ± 3 ($\varepsilon Hf_{(t)}$ = −11.8 ± 1.1) (Fig. 7). The latter are interpreted as neocrystals formed in response to the injection of nearby pegmatites (see Electronic Supplementary Material). All other samples (granitic gneisses SEN-01, SEN-17 and quartz-diorite SEN-22) have nearly identical zircon U-Pb ages (granitic gneiss SEN-01 at 2665 ± 8; granite SEN-17 at 2678 ± 9 Ma; quartz-diorite SEN-22 at 2673 ± 7 Ma) and overlapping Hf isotopic composition ($^{176}Hf/^{177}Hf_{(t)}$ from 0.28109 ± 3 to 0.28112 ± 3) corresponding to positive $\varepsilon Hf_{(t)}$ (+0.9 ± 1.1 to +1.9 ± 0.9) (Fig. 7).

Samples from the quartz-monzonite-monzodiorite group show exclusively Paleoproterozoic emplacement ages, distributed in two events (Fig. 7): (i) at ca. 1870–1860 Ma, represented by samples SEN-08a (1869 ± 6 Ma) and KV-25 (1861 ± 5 Ma); and (ii) at ca. 1800 Ma, as indicated by emplacement ages of four samples (KV-03 at 1800 ± 6 Ma; SEN-20 at 1798 ± 5 Ma; SEN-26 at 1797 ± 5 Ma; and SEN-04 at 1790 ± 15 Ma). Zircon of the ca. 1870–1860 Ma samples has identical Hf isotopic composition ($^{176}Hf/^{177}Hf_{(t)}$ of ca. 0.28136) corresponding to negative $\varepsilon Hf_{(t)}$ (ca. −8) (Fig. 7). Contrastingly, zircon

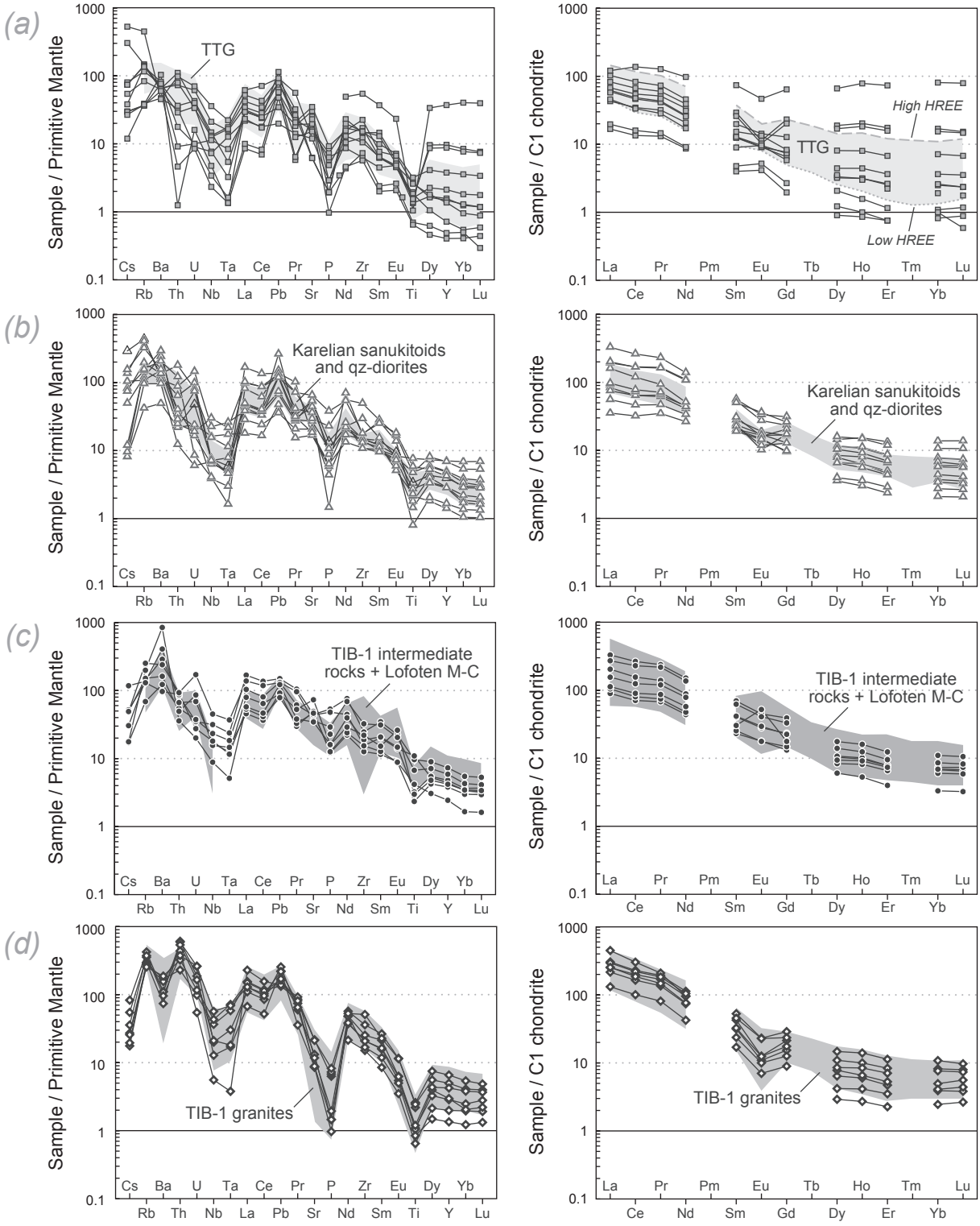

Fig. 5. Trace element compositions of the WTBC granitoids: (a) tonalite-trondhjemite; (b) qz-diorite-granodiorite-granite; (c) qz-monzonite-monzodiorite; (d) monzo-/syenogranite. Symbols are as in Fig. 3. The concentrations are normalized to the primitive mantle (multi-element diagram, left panel) and C1 chondrite (REE pattern, right panel) values from McDonough and Sun (1995). Also shown are data from Archean TTGs worldwide (Moyen, 2011; Moyen and Martin, 2012), Archean sanukitoids and qz-diorites from the Karelian province (Halla et al., 2009; Heilimo et al., 2010; Mikkola et al., 2011), mangerites-charnockites from the Lofoten-Vesterålen AMCG suite (Markl, 2001), and the 1.81–1.76 Ga granitoids from the Transscandinavian Igneous Belt (TIB-1) (Ahl et al., 1999; Andersson, 1997; Claesson and Lundqvist, 1995; Kornfält et al., 1997; Skår, 2002).

from the ca. 1800 Ma samples shows various Hf isotopic compositions: SEN-04 and SEN-20 have identical $^{176}Hf/^{177}Hf_{(t)}$ (0.28145 ± 3 and 0.28141 ± 3, respectively), while KV-03 and SEN-26 have significantly lower ratios (0.28136 ± 3 and 0.28130 ± 2, respectively), all of them corresponding to sub-chondritic $\varepsilon Hf_{(t)}$ ranging from −7 to −12 (Fig. 7). Notably, the ca. 1870–1860 Ma samples commonly contain inherited zircon cores of Archean (ca. 2500–2870 Ma) and early Paleoproterozoic (ca. 1990–2450 Ma) ages (Fig. 7), whereas the ca.

Table 2
Summary of the U-Pb and Lu-Hf isotopic results obtained on zircons from the WTBC granitoids.

Sample ID	Rock type[a]	Island	Unit[b]	Lat. N[c]	Long. E[c]	Group[d]	U–Pb age[e] (Ma)	± 2σ[e]	Type[e]	$N_{U\text{-}Pb}$[f]	Inheritance (Ma)[g]	$^{176}Hf/^{177}Hf_t$ (avg.)[h]	± 2 S.D.	$\varepsilon Hf_{(t\ Int)}$[i]	± 2 S.D.	$T_{DM\ G}$ (Ga)[j]	$T_{DM\ N}$ (Ga)[j]	$N_{Lu\text{-}Hf}$[f]
VN-03	T-T	Vanna	Dåfjord g.	7790553	0444541	1	2865	8	Conc.	*23*		0.281020	0.000025	+2.9	0.9	3.14	2.96	*14*
RG-02	T-T	Ringvassøya	Dåfjord g.	7769359	0435053	3	2840	9	Conc.	*9*	c. 3020	0.281030	0.000040	+2.7	1.4	3.13	2.95	*15*
RG-09	T-T	Ringvassøya	Dåfjord g.	7772928	0425110	1	2866	7	Conc.	*22*		0.281022	0.000032	+3.0	1.1	3.13	2.95	*15*
RG-10	T-T	Ringvassøya	Dåfjord g.	7763051	0418911	2	2920	7	Conc.	*18*		0.280972	0.000025	+2.5	0.9	3.21	3.03	*16*
RG-15	T-T	Ringvassøya	Dåfjord g.	7749261	0434372	1	2831	7	Conc.	*20*		0.281033	0.000027	+2.5	1.0	3.14	2.95	*16*
KV-20	T-T	Kvaløya	Kvalsund g.	7739726	0417628	3	2828	8	Conc.	*7*		0.281018	0.000037	+2.0	1.3	3.17	2.99	*17*
							2681*	*10*	*Conc.*	*10*		*0.280994**	*0.000013**	*−2.4**	*0.4**			
KV-23	T-T	Kvaløya	Kvalsund g.	7748212	0421764	3	2685	8	Conc.	*8*	c. 2750; 2800–2935	0.281031	0.000039	−0.9	1.4	3.24	3.07	*12*
KV-31	T-T	Kvaløya	Gråtind g.	7719465	0405561	2	2835	8	Conc.	*9*	c. 2880; 2915	0.281043	0.000059	+3.0	2.1	3.11	2.93	*13*
KV-08	D-G-G	Kvaløya	Kattefjord g.	7727060	0389352	3	2744	11	Av. 7/6	*5*		0.280990	0.000032	−1.0	1.1	3.29	3.12	*9*
							1702†	*49*	UI	*11*		*0.281375*†	*0.000027*†	*−11.8*†	*1.1*†			
KV-15	D-G-G	Kvaløya	Kattefjord g.	7722433	0383856	2	2957	9	Conc.	*3*		0.280770	0.000041	−3.8	1.5	3.64	3.48	*20*
SEN-01	D-G-G	Senja	SW Senja g.	7688776	0576024	2	2665	8	Conc.	*7*		0.281101	0.000026	+1.1	0.9	3.10	2.92	*17*
SEN-17	D-G-G	Senja	Senja SB	7710732	0591302	2	2678	9	Conc.	*11*		0.281087	0.000031	+0.9	1.1	3.12	2.94	*24*
SEN-22	D-G-G	Senja	Senja SB	7713699	0596825	3	2673	7	Conc.	*8*		0.281118	0.000026	+1.9	0.9	3.05	2.87	*11*
							1781◊	*8*	*LI*	*5*								
KV-03	qM-MD	Kvaløya	Ersfjord p.*	7743642	0404984	1	1800	6	Conc.	*15*	c. 1850	0.281356	0.000034	−10.0	1.2	3.11	2.94	*12*
KV-25	qM-MD	Kvaløya	Bakkan p.*	7733347	0410764	3	1861	5	Conc.	*9*	c. 1990–2090; 2770–2870	0.281364	0.000020	−8.3	0.7	3.06	2.87	*10*
SEN-04	qM-MD	Senja	SW Senja g.	7688810	0576088	2	1790	15	UI	*21*		0.281445	0.000029	−7.0	1.0	2.92	2.73	*11*
SEN-08	qM-MD	Senja	Skrolsvik p.*	7663008	0572204	3	1869	6	Conc.	*8*	c. 2450–2680	0.281357	0.000026	−8.4	0.9	3.07	2.89	*12*
SEN-20	qM-MD	Senja	Senja SB	7719545	0612947	1	1798	5	Conc.	*15*		0.281409	0.000031	−8.1	1.1	3.00	2.81	*13*
SEN-26	qM-MD	Senja	Senja SB	7705374	0591757	1	1797	5	Conc.	*17*		0.281300	0.000017	−12.0	0.6	3.24	3.07	*14*
KV-09	m-sG	Kvaløya	Ersfjord p.*	7726730	0389005	2	1791	6	Conc.	*8*		0.281310	0.000032	−11.8	1.1	3.22	3.05	*17*
SEN-02	m-sG	Senja	SW Senja g.	7688807	0576045	2	1759	27	UI	*10*		0.281383	0.000031	−10.0	1.1	3.08	2.90	*12*
SEN-07	m-sG	Senja	Senja p.	7686426	0594586	3	1784	6	Conc.	*6*	c. 2640; 2780	0.281305	0.000057	−12.1	2.0	3.24	3.07	*12*
SEN-15	m-sG	Senja	Senja SB	7696128	0596078	1	1789	5	Conc.	*13*		0.281305	0.000020	−12.0	0.7	3.24	3.06	*14*

[a] According to the petrographic classification of granitoids presented in this work (see Section 3): T-T = tonalite-trondhjemite; D-G-G = qz-diorite-granodiorite-granite; qM-MD = qz-monzonite-(monzo)diorite; m-sG = monzo-/syenogranite.

[b] Following previous terminology (e.g. Bergh et al., 2010, 2014; Myhre et al., 2013; Zwaan, 1995; Zwaan et al., 1998) except marked names (*) that are revised based on our results (g. = gneiss; p. = pluton; SB = shear belt).

[c] GPS co-ordinates of sample locations in UTM zone 34 W, except for Senja samples (zone 33 W).

[d] Sample subsetting on the basis of zircon textures, U-Pb dates and Lu-Hf isotopic data (see Section 4.2 for details).

[e] Age retained as that of granitoid intrusion (bold font), which is either the concordant U–Pb age ("Conc"); the weighted average of individual $^{207}Pb/^{206}Pb$ ages ("Av. 7/6"); or the upper intercept age ("UI"). The displayed uncertainty includes "raw" uncertainty on the calcualted date and propagated, systematic uncertainties as described in the Electronic Supplementary Material.

[f] Number of individual spots used in the calculation of the U-Pb age or initial Hf isotopc composition.

[g] Approximate ages of inherited zircons (if appropriate).

[h] Average $^{176}Hf/^{177}Hf$ ratio at the time of granitoid intrusion, calculated from cogenetic zircon domains in a given sample (i.e. excluding inherited cores or xenocrysts) and using the retained U-Pb emplacement age of the sample.

[i] Calculated using the parameters of the Chondrite Uniform Reservoir (CHUR) recommended by Bouvier et al. (2008), i.e. present-day values of $^{176}Hf/^{177}Hf = 0.282785$ and $^{176}Lu/^{177}Hf = 0.0336$.

[j] Two-stage Hf model age calculated using the zircon $^{176}Lu/^{177}Lu$ and intrusion age for the first stage; and a $^{176}Lu/^{177}Lu$ of 0.015 for the crustal reservoir. The DM models of Griffin et al. (2002) ($T_{DM\ G}$) and Næraa et al. (2012) ($T_{DM\ N}$) were used.

* Age and corresponding Hf isotopic composition of zircon rims in sample KV-20, interpreted as reflecting a thermal event (migmatization, granite injection).

† Age and corresponding Hf isotopic composition of dark-CL zircons in sample KV-08, interpreted as reflecting neocrystals formed during the intrusion of pegmatites.

◊ Age of zircon recrystallization event in sample SEN-22 ("LI" = lower intercept age).

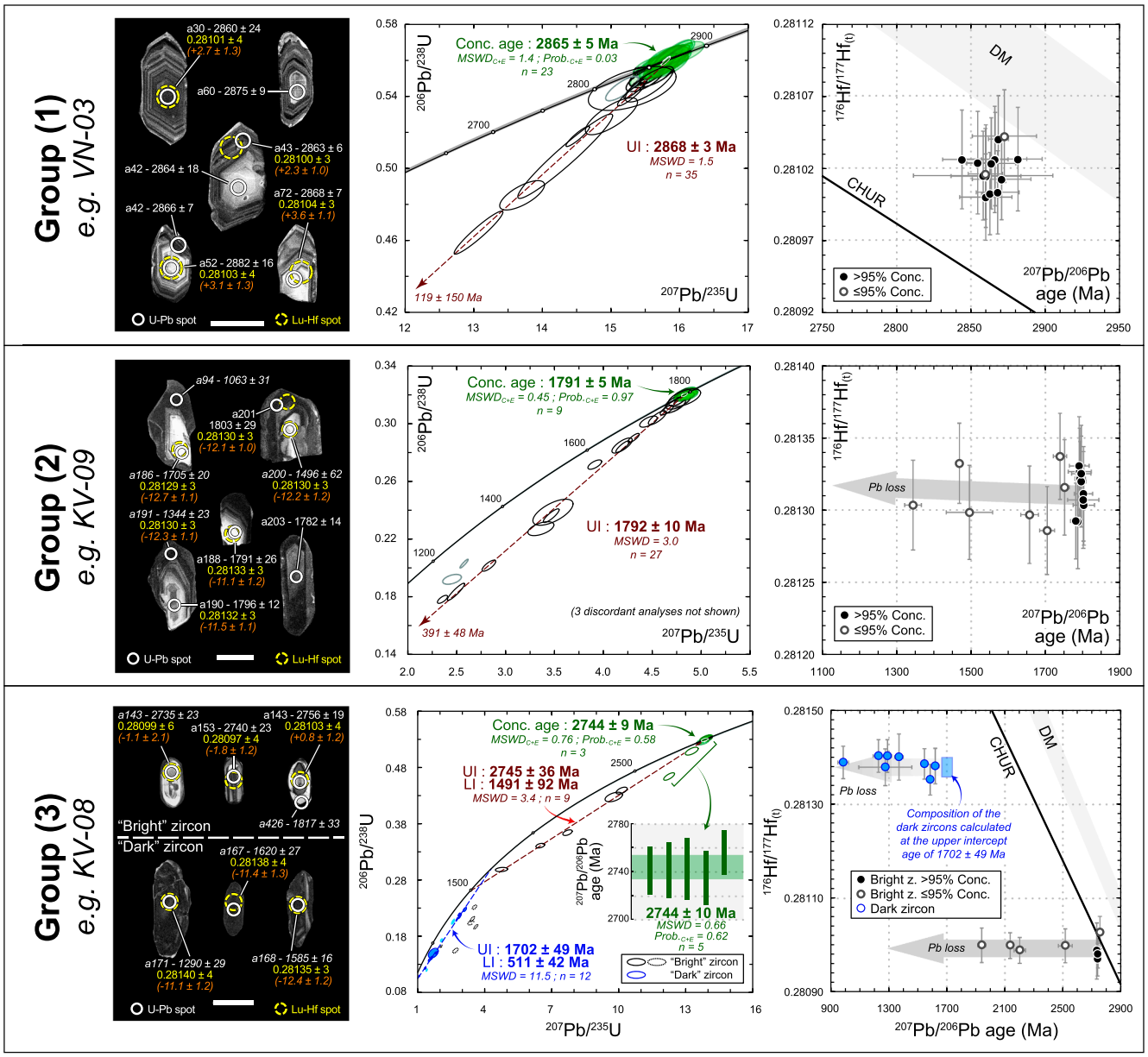

Fig. 6. Representative CL images (left panel), U-Pb Concordia diagrams (central panel) and plots of $^{176}Hf/^{177}Hf_{(t)}$ vs. apparent $^{207}Pb/^{206}Pb$ date (right panel) illustrating the three groups of zircon populations identified in the WTBC granitoid samples. In the left panel, the label indicates the spot number, the corresponding $^{207}Pb/^{206}Pb$ date in white (in Ma), $^{176}Hf/^{177}Hf_{(t)}$ in yellow (uncertainty on the last digit) and the calculated $\varepsilon Hf_{(t)}$ for the intrusion age in orange. Dates indicated in italic font represent analyses with < 95% U-Pb concordance; dates reported in gray font correspond to those from zircons interpreted as inherited or xenocrystic in origin. The scale bar is 100 µm. Error bar, ellipses and quoted uncertainties are all at 95% confidence level. See text for details, and Electronic Supplementary Material for similar documentation of all samples. (For interpretation of the references to color in this figure legend, the reader is referred to the web version of this article.)

1800 Ma samples are almost devoid of inherited zircon.

The combined U-Pb and Lu-Hf zircon data from the monzo-/syenogranite group show a simple pattern. Three samples have overlapping emplacement ages at ca. 1790–1785 Ma (KV-09 at 1791 ± 6 Ma; SEN-15 at 1789 ± 5 Ma and SEN-07 at 1784 ± 6 Ma) and very homogeneous $^{176}Hf/^{177}Hf_{(t)}$ (ca. 0.28131) corresponding to sub-chondritic $\varepsilon Hf_{(t)}$ of ca. −12 (Fig. 7). Sample SEN-02 has a younger (poorly constrained) upper intercept age of 1759 ± 27 Ma, which yet overlaps with those from other samples. However, the $^{176}Hf/^{177}Hf_{(t)}$ ratio in this sample is slightly higher (0.28138 ± 3, corresponding to $\varepsilon Hf_{(t)}$ of −10.0 ± 1.1) (Fig. 7). These granites lack inherited zircon, with the exception of two Archean cores in sample SEN-07.

6. Discussion

6.1. Architecture of the Archean crust in north Norway

The geographic distribution of geochronological and petrographic data on Archean granitoids of the WTBC is shown on the map of Fig. 8, including compilation of published results and our new data. Three distinct domains can be identified:

(1) In Vanna, Ringvassøya and most of Kvaløya (NE of the Mjelde-Skorelvvatn belt, MSB), the basement granitoids (Dåfjord, Kvalsund and Gråtind gneisses) are dominated by Mesoarchean, 2.88 to

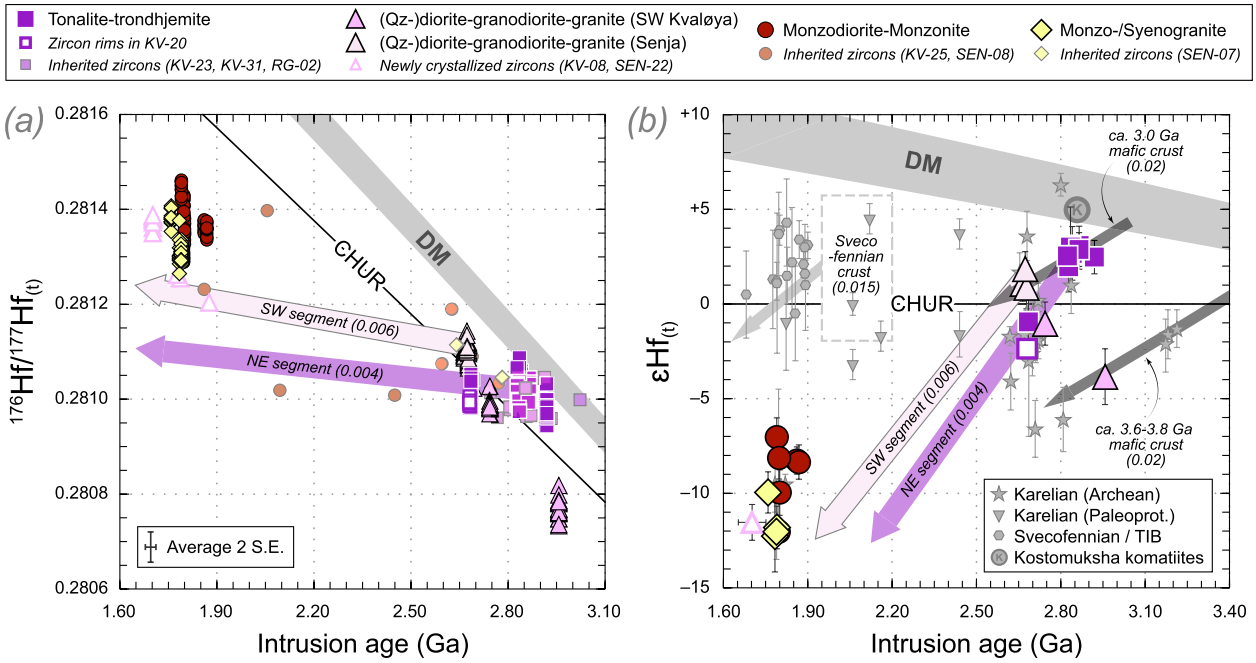

Fig. 7. Summary of combined, LA-(MC-)ICP-MS U-Pb and Lu-Hf isotopic analyses in zircons from the WTBC granitoids: (a) plot of $^{176}Hf/^{177}Hf_{(t)}$ of individual zircon analyses, reported at the intrusion age for igneous zircon and at the individual age for other zircon types; and (b) average $\varepsilon Hf_{(t)}$ calculated on the basis of all igneous zircon analyses at the intrusion age. The compositional range of the depleted mantle (DM) is bound by the Archean DM model of Næraa et al. (2012) (lowermost value), corresponding to the least radiogenic of DM models for Archean times; and the commonly used regression from present-day MORB of Griffin et al. (2002) (uppermost value). The CHUR model is from Bouvier et al. (2008). The colored arrows delineate the isotopic evolution vectors of the crust from the two lithotectonic segments of the WTBC (SE and NW; see Section 6.1), based on the average Lu/Hf ratios of bulk rocks in each segment (numbers in brackets are the corresponding $^{176}Lu/^{177}Hf$ ratios). In (b), data from other granitoids of the Fennoscandian shield (Andersen et al., 2009; Heilimo et al., 2009; Kurhila et al., 2010; Lauri et al., 2011; Patchett et al., 1981) and the Kostomuksha komatiites (Blichert-Toft and Puchtel, 2010) are reported. The composition and evolution of Svecofennian crust are after Andersen et al. (2009). The black arrows correspond to the isotopic evolution of putative ca. 3.0 Ga and ca. 3.6–3.8 Ga mafic crust (see Section 6.3.1) assuming a $^{176}Lu/^{177}Hf$ ratio of 0.02. Error bars indicate uncertainties at 95% confidence level.

2.83 Ga-old tonalites-trondhjemites (9 out of 13 dated samples), with minor 2.92 Ga remnants (RG-10; inherited zircons from KV-31 and sample C01-107 of Myhre et al., 2013) (Fig. 8). A few younger rocks cluster around 2.69 Ga (emplacement of KV-23 trondhjemite; zircon rims in KV-20; zircons from migmatite neosome C01-110 of Myhre et al., 2013) (Fig. 8). These are all located in the vicinity of the Kvalsund Shear Zone, with the exception of the Mikkelvik alkaline stock, located more to the northeast (Zozulya et al., 2009).

(2) In SW Kvaløya, i.e. SW of the MSB, the granitoids are mostly (qz-) diorites, granodiorites and granites (Fig. 8). Besides our 2.96 Ga qz-diorite sample KV-15, all samples (n = 6) define two Neoarchean age groups. (i) A 2.74–2.71 Ga group corresponds to the emplacement of the protoliths of the Kattefjord gneisses (sample KV-08 and inherited zircon in migmatite neosome sample PIM-07-69 of Myhre et al., 2013) and the Bakkejord qz-diorite (sample C-04-35 of Myhre et al., 2013). (ii) A 2.69–2.67 Ga group corresponds to the emplacement of granites (samples KV-02 of Corfu et al., 2003 and PIM-06-67 of Myhre et al., 2013), mafic dykes (sample C-04-31 of Myhre et al., 2013), and migmatization of earlier gneisses (neosome PIM-07-69 of Myhre et al., 2013) (Fig. 8).

(3) On Senja, (quartz-)diorites, granodiorites and granites are also dominant and their ages cluster between 2.71 and 2.67 Ga (5 out of 6 samples) (Fig. 8). Older ages are only represented by scarce 2.83–2.81 Ga inherited zircon cores in the 2.71 Ga-old granodiorite C-04-46 of Myhre et al. (2013). In contrast, the migmatite sample C-04-47 of Myhre et al. (2013) only contains 2.69–2.67 Ga-old inherited zircons, and leucosome crystallization age at ca. 2.61 Ga points to a younger migmatitization event (Fig. 8).

Bergh et al. (2014) proposed that the Kvalsund Shear Zone represents a major Neoarchean suture zone between the 2.92–2.80 Ga Ringvassøya-Vanna domain and the 2.75–2.67 Ga Kvaløya-Senja domain. However, the presence of trondhjemitic gneisses on Kvaløya (KV-20, KV-31), having similar petrography, geochemistry, U-Pb ages and zircon $\varepsilon Hf_{(t)}$ (+2 to +3) as the ca. 2.83 Ga trondhjemites on Ringvassøya (RG-15, RG-02) (Figs. 7 and 8), challenges this interpretation. Instead, our new results comply with the interpretation of Zwaan and Tucker (1996) that Archean rocks of central and NE Kvaløya belong to the same, > 2.8 Ga-old unit as those from Ringvassøya and Vanna. From this perspective, the Kvalsund Shear Zone would only represent a zone of preferential crustal reworking at ca. 2.69 Ga (Fig. 8) within one single 2.88–2.83 Ga-old crustal segment. Consistently, trondhjemites intruded along the Kvalsund Shear Zone at 2.69 Ga (KV-23) contain numerous enclaves of earlier, highly deformed tonalitic-trondhjemitic gneisses; abundant xenocrystic zircons with U-Pb ages of 2.87–2.81 Ga; and igneous zircons showing an $\varepsilon Hf_{(t)}$ of ca. −1 pointing to reworking of > 2.8 Ga crust (Fig. 7).

The Archean gneisses in SW Kvaløya and Senja are characterized by 2.74–2.67 Ga (quartz-)diorites, granodiorites and granites, lacking extensive tonalite-trondhjemite components and ages > 2.8 Ga (Fig. 8). Indeed, out of 11 samples dated at 2.74–2.67 Ga, only one has a few grains with ages > 2.75 Ga (sample C04-46 of Myhre et al., 2013; Fig. 8). Moreover, our three 2.68–2.67 Ga samples from Senja notably show positive zircon $\varepsilon Hf_{(t)}$ (+1 to +2) plotting above the isotopic evolution trend of > 2.8 Ga tonalites-trondhjemites (Fig. 7), and thus inconsistent with reworking of the latter. Altogether, this indicates that there was very little, older felsic crust (if any) in SW Kvaløya and Senja prior to the emplacement of the 2.74–2.67 Ga granitoids. Therefore, the 2.74–2.67 Ga SW Kvaløya and Senja domain in one hand, and the > 2.8 Ga NE Kvaløya, Ringvassøya and Vanna domain on the other hand, certainly represent two distinct crustal segments. This interpretation is supported by gamma-ray spectrometric data showing strikingly

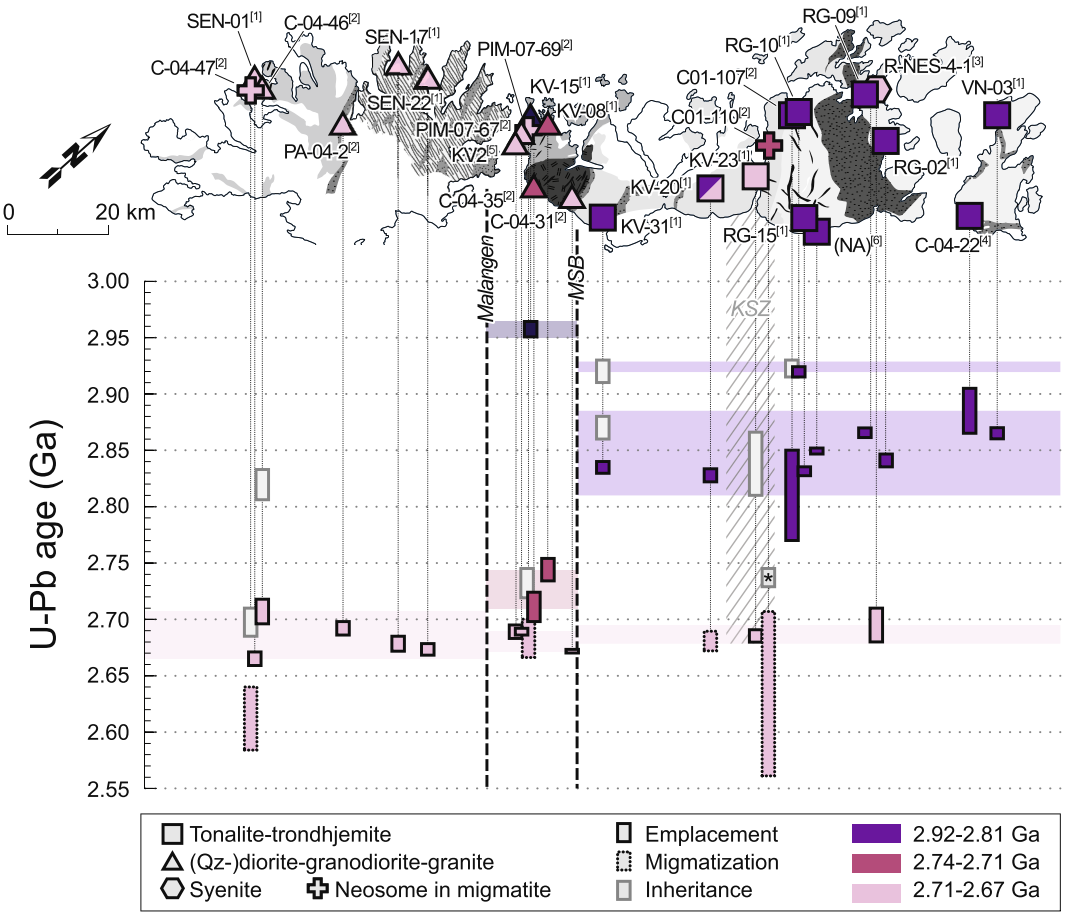

Fig. 8. Compilation of zircon U-Pb ages on Archean granitoid rocks of the WTBC. Top: sketch geological map of the Archean basement of the WTBC (after Fig. 1) showing the position of the dated samples and the corresponding rock type (symbols). Bottom: zircon U-Pb age data for the corresponding samples, plotted as a function of the sample position along the SW–NE transect of the WTBC. MSB = Mjelde-Skorelvvatn greenstone belt. References: [1] this study; [2] Myhre et al., 2013; [3] Zozulya et al., 2009; [4] Bergh et al., 2007; [5] Corfu et al., 2003; [6] Zwaan and Tucker, 1998.

different signatures between Senja and Ringvassøya-Vanna (Nasuti et al., 2015). Furthermore, the Archean rocks in the Lofoten-Vesterålen province lying to the SW of the WTBC are also characterized by emplacement ages in the range 2.74–2.66 Ga and metamorphism at 2.65–2.63 Ga (Corfu, 2007; Griffin et al., 1978), identical to those obtained in SW Kvaløya and Senja. As suggested by Bergh et al. (2014), this hints that the crustal segment represented by the latter continues further SW to the Lofoten-Vesterålen province.

The slight age differences between SW Kvaløya and Senja regarding granitoid emplacement (2.74–2.71 Ga on SW Kvaløya vs. 2.71–2.67 Ga on Senja) and migmatitization (2.69 Ga on SW Kvaløya vs. 2.61 Ga on Senja) may suggest that these represent two separate lithotectonic segments (Fig. 8). The zircon Hf isotopic composition of the 2.74 Ga granitoids of SW Kvaløya (KV-08) is significantly lower ($\varepsilon Hf_{(t)} = -1$) than that of zircons from the Senja samples ($\varepsilon Hf_{(t)} = +1$ to $+2$), also supporting this view. In fact, this Hf isotopic signature could be explained by reworking of the > 2.8 Ga tonalite-trondhjemite gneisses (Fig. 7). It is therefore possible that the SW Kvaløya domain represents the margin of the NE Kvaløya, Ringvassoya and Vanna block reworked at 2.74–2.69 Ga. On the other hand, there is no dated zircon in the age range 2.9–2.8 Ga in SW Kvaløya (Fig. 8). Furthermore, the 2.96 Ga sample KV-15 from SW Kvaløya is very different in zircon Hf isotopic signature ($\varepsilon Hf_{(t)} = -3.8$) from the rocks of closest age on Ringvassøya (e.g. 2.92 Ga trondhjemitic gneisses with zircon $\varepsilon Hf_{(t)} = +2.5$) (Fig. 7). Therefore, we cannot exclude that the SW Kvaløya domain was a third, intervening crustal segment.

From the above discussion, we conclude that the Precambrian basement inliers of north Norway consist of at least two distinct crustal segments (Fig. 9):

(1) A **northeastern Mesoarchean lithotectonic segment** (NE Kvaløya, Ringvassøya and Vanna; hereafter "**NE segment**") dominated by 2.92- to 2.89–2.83 Ga tonalitic-trondhjemitic gneisses;
(2) A **southwestern Neoarchean lithotectonic segment** (Senja and Lofoten-Vesterålen province; hereafter "**SW segment**") largely consisting of 2.71–2.67 Ga (quartz-)dioritic, granodioritic and granitic gneisses.

The SW Kvaløya zone represents either a third, 2.74–2.71 Ga segment, or the reworked margin of the NE segment. In either case, the area between the Malangen strait and the Mjelde-Skorelvvatn greenstone belt hosts at least one, and perhaps two, major tectonic boundaries roughly striking NW-SE (Figs. 8 and 9). Offshore bathymetric data support this interpretation, as they point to the existence of major NW-trending structures along strike of the Malangen strait (Indrevær et al., 2013; Indrevaer and Bergh, 2014). Aeromagnetic data also show that a prominent, sub-linear negative magnetic anomaly strikes roughly NNW-SSE along the proposed suture zone(s) (Nasuti et al., 2015). In a broader context, the inferred suture zone(s) are located along major NNW-SSE- to NW-SE-trending, crustal-scale structures of the Fennoscandian Shield (Bergh et al., 2014) (Fig. 9). These comprises the Bothnian-Senja Shear Zone (Henkel, 1991; Zwaan, 1995) and the Onega-Malangen Lineament (Koistinen et al., 2001) (Fig. 9), two corridors of steeply dipping shear zones that can be traced further SE,

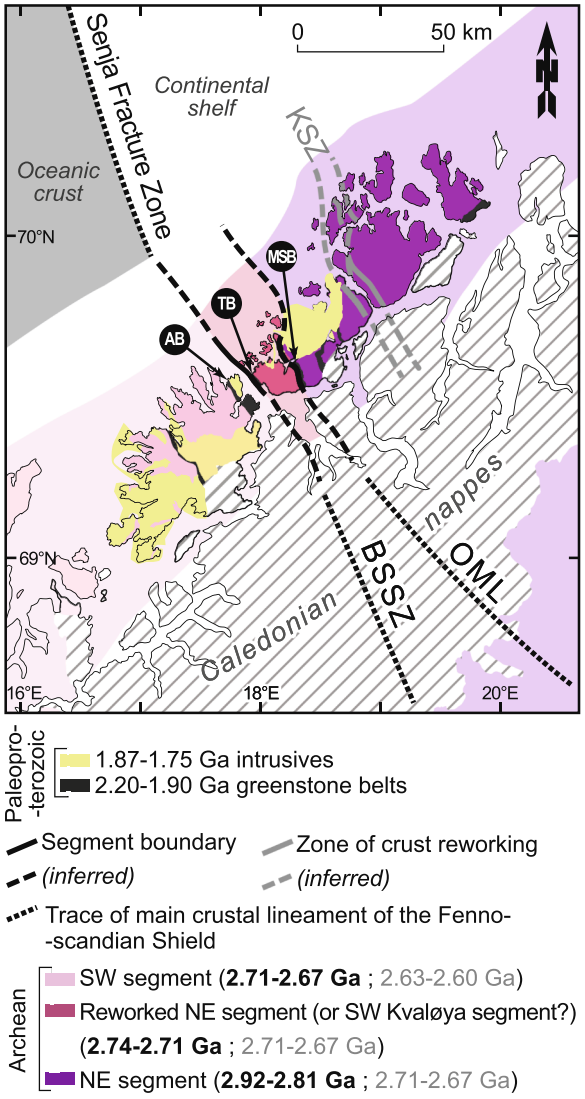

Fig. 9. Sketch map showing the proposed crustal architecture of the WTBC, especially the position of the two inferred Archean lithotectonic segments. In the caption, the ages in bold refer to the periods of crust formation in each segment, and gray font to periods of crust reworking. The approximate positions of the Bothnian-Senja Shear Zone (BSSZ; Henkel, 1991; Zwaan, 1995), the Onega-Malangen Lineament (OML; Koistinen et al., 2001) and the offshore Senja Fracture Zone (Doré et al., 1997; Indrevær et al., 2013) are also reported. The main Paleoproterozoic greenstone belts of the WTBC are also highlighted (AB = Astridal Belt; MSB = Mjelde-Skorelvvatn Belt; TB = Torsnes Belt) (Bergh et al., 2015; Myhre et al., 2011). KSZ = Kvalsund Shear Zone, interpreted as a zone of preferential crust reworking within the NE segment.

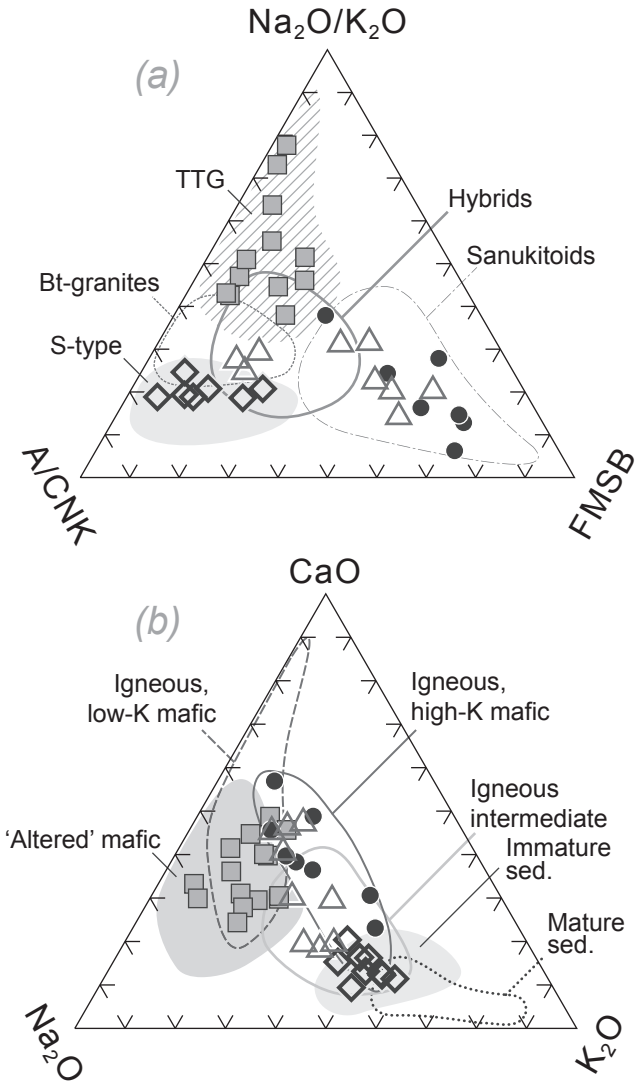

Fig. 10. (a) Ternary A/CNK–Na_2O/K_2O–FMSB ($[FeO_t + MgO]_{wt.\%}$·$[Sr + Ba]_{wt.\%}$) diagram (Laurent et al., 2014) where the compositions of the WTBC granitoids are reported and compared to those of the main types of Archean granitoids (Laurent et al., 2014) and Phanerozoic S-type granites (data from the Variscan French Massif Central; Laurent et al., 2017). (b) Ternary Na_2O–CaO–K_2O diagram comparing the compositions of the WTBC granitoids with those of experimental melts derived from a range of starting materials produced at conditions relevant for crustal melting (0.1–1.2 GPa; 750–1050 °C), including low-K igneous mafic rocks (Beard and Lofgren, 1991; Rapp and Watson, 1995; Wolf and Wyllie, 1994); "altered" (high-Na) igneous mafic rocks (Skjerlie and Johnston, 1996; Zamora, 2000); high-K igneous mafic rocks (Alonso-Perez et al., 2009; Almeev et al., 2013; Blatter et al., 2013; Sisson et al., 2005; Sisson and Grove, 1993); igneous intermediate rocks (Bogaerts et al., 2006; Martel et al., 1999; Singh and Johannes, 1996; Watkins et al., 2007); immature (greywacke) sediments (Montel and Vielzeuf, 1997; Patiño-Douce and Beard, 1996; Stevens, 1995; Vielzeuf and Holloway, 1988) and mature (pelitic) sediments (Patiño-Douce and Johnston, 1991; Patiño-Douce and Harris, 1998; Pickering and Johnston, 1998; Vielzeuf and Holloway, 1988).

respectively to the gulf of Bothnia and across the Karelian Province to eastern Finland. To the NW, the suture extends to the offshore Senja Fracture Zone, a major transfer zone that bounds the western margin of the Barents continental shelf (Fig. 9) and interpreted as a the re-activation of a basement lineament (Doré et al., 1997; Indrevær et al., 2013). We therefore suggest that these structures are primarily inherited from the proposed Archean segment boundary, and that the latter might extend way beyond the limits of the Precambrian basement inliers of north Norway to other parts of the Fennoscandian Shield.

This model is further backed by similarities in the geological record between the WTBC and the basement rocks on the opposite side of the Caledonides, i.e. the Norrbotten Province (Höltta et al., 2008; Lahtinen et al., 2005). Archean rocks in Finnmarkvidda located to the NE of the inferred suture (the Jergul complex) are indeed comparable to those from the NE segment of the WTBC (2.98–2.78 Ga-old, dominantly tonalitic-trondhjemitic gneisses; Bingen et al., 2015). In contrast, in southern Troms and northern Sweden, to the SW of the inferred suture, Archean gneiss protolith ages are rather clustered around 2.7 Ga and Paleoproterozoic magmatism (1.87–1.75 Ga) is much more common (Martinsson et al., 1999; Slagstad et al., 2015), as typically observed in Senja (Figs. 8 and 9), in the Lofoten-Vesterålen province (Corfu 2004, 2007; Griffin et al., 1978) and surrounding basement windows in the

Caledonides (Skår, 2002). Finally, the zircon Hf isotopic compositions of the WTBC granitoids also overlap with those of Archean to Paleoproterozoic granitoids in Fennoscandia (Fig. 7), clearly suggesting a common crustal ancestry.

6.2. Granitoid petrogenesis

6.2.1. Tonalite-trondhjemite

In terms of petrography and geochemistry, the tonalites-trondhjemites from the NE segment are clearly akin to the tonalite-trondhjemite-granodiorite (TTG) group (Figs. 3–5 and 10), i.e. the most widespread granitoids in the Archean (Moyen and Martin, 2012). Although some authors proposed that TTG form by crystallization of calc-alkaline mafic magma (Jagoutz et al., 2013; Kamber et al., 2002; Kleinhanns et al., 2003), the most plausible model (see discussion in Moyen and Laurent, 2018) is that these rocks derive from partial melting of hydrous basaltic material, variously enriched in LILE (Moyen and Martin, 2012; Martin et al., 2014). Consistently, the composition of the WTBC TTGs overlaps with those of experimental liquids derived from melting of low-K, pristine to altered basalts (Fig. 10).

As discussed in earlier studies, the trace element variability of TTGs reflects various melting depths, especially when considering the elements that are preferentially incorporated in garnet (Y, HREE) and plagioclase (Sr, Eu) which have pressure-sensitive stability fields (Halla et al., 2009; Moyen, 2011). In this respect, the TTGs of the WTBC define two groups (Fig. 11):

(1) Samples with high Y (6–42 ppm and up to 160 ppm for the highly fractionated sample KV-31 with 76 wt% SiO_2), low Sr contents (< 350 ppm), conversely low Sr/Y ratios (< 50) and weakly fractionated HREE profiles (low Gd_N/Er_N). Those are akin to the "low-pressure" TTG group (Moyen, 2011);
(2) Samples with low Y (2–7 ppm) and high Sr contents (> 400 ppm), conversely high Sr/Y ratios (> 90) together with fractionated HREE patterns (higher Gd_N/Er_N). These samples straddle the boundaries between the fields of "medium-" and "high-pressure" TTGs of Moyen (2011).

The characteristics of the "low-pressure" group imply the presence of plagioclase and the absence of garnet in the residue (Halla et al., 2009; Moyen, 2011) which constrains maximum melting pressures to ca. 1.0 GPa (Almeida et al., 2011; Johnson et al., 2013; Nagel et al., 2012) (Fig. 11). In contrast, the trace element signature of the "medium-/high-pressure" groups requires formation in equilibrium with residual garnet amphibolite-granulite or rutile-bearing eclogite (Halla et al., 2009; Moyen, 2011), i.e. melting pressures of 1.2–2.0 GPa (Johnson et al., 2013, 2017; Nair and Chacko, 2008). Thermodynamic modelling consistently shows that melting of Archean mafic rocks at 1.4 and 1.8 GPa (Nagel et al., 2012) produces melts with compositions matching those of the "medium-/high-pressure" TTGs of the WTBC (Fig. 11). We therefore consider that the "low-pressure" and "medium-/high-pressure" TTG groups of the WTBC result from melting of hydrous, variably LILE-rich mafic rocks, respectively at pressures of ≤ 1.0 GPa (≤ 30 km depth) and 1.4 to 1.8 GPa (ca. 45–60 km depth).

Importantly, the Sr/Y and Eu_N/Eu^* ratios, both depicting the presence/absence of plagioclase in the melting residue, progressively increase over time in the WTBC TTGs (Fig. 12). The samples older than 2.9 Ga have the lowest Sr/Y and most pronounced negative Eu anomaly; the 2.87–2.89 Ga samples have intermediate Sr/Y and no Eu anomaly; and the 2.83 Ga samples have the highest Sr/Y and a positive Eu anomaly (Fig. 12). This suggests that the pressure of melting gradually increased from ≤1.0 GPa before 2.9 Ga, to 1.0–1.4 GPa at 2.89–2.87 Ga and up to 1.4–1.8 GPa at 2.83 Ga. Notable exceptions to this trend are samples KV-31 and KV-23, akin to the "low-pressure" group yet both showing young ages (2.83 and 2.69 Ga respectively) (Fig. 12). The geodynamic implications are further discussed in Section 6.3.

The zircons from all 2.92–2.83 Ga-old tonalite-trondhjemite samples are characterized by positive $\varepsilon Hf_{(t)}$, i.e. between +2 and +3 (Table 2 and Fig. 7). These TTGs are thus derived from relatively young mafic sources, i.e. extracted from the mantle a maximum of 100–150 Ma before melting (Fig. 7). The only exception is the youngest, trondhjemitic sample KV-23 (2.69 Ga) that shows a negative zircon $\varepsilon Hf_{(t)}$ (ca. −1; Table 1), thus sitting on the reworking trend of the > 2.8 Ga TTGs (Fig. 7). The trondhjemite also contains numerous enclaves of older tonalitic-trondhjemitic gneisses, and zircons showing partly dissolved 2.87–2.81 Ga cores overgrown by ca. 2.69 Ga rims, respectively interpreted as xenocrystic and magmatic in origin (see Electronic Supplementary Material). This would result from reworking and assimilation of the ancient TTGs upon emplacement of the more recent ones, as already described in other Archean cratons (Laurent and Zeh, 2015).

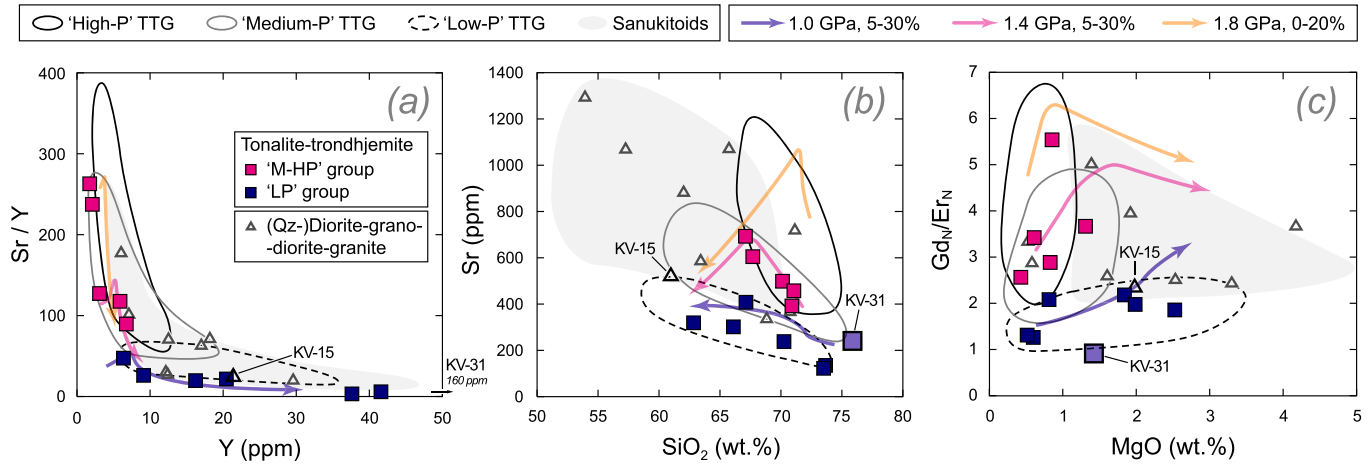

Fig. 11. Composition of the Archean granitoids of the WTBC (tonalite-trondhjemite and qz-diorite-granodiorite-granite) plotted in Sr/Y vs. Y (a), Sr vs. SiO_2 (b) and Gd_N/Er_N vs. MgO (c) diagrams. The tonalite-trondhjemite granitoids of the WTBC are split in two groups formed by melting of mafic rocks respectively at low pressure ('LP', dark blue squares) and medium-high pressure ('M-HP', pink squares) (see text for details). The fields of high-, medium- and low-pressure (P) TTG (Halla et al., 2009; Moyen, 2011) and sanukitoids (Laurent et al., 2014) are reported for comparison. The arrows correspond to the chemical evolution of liquids formed by melting of Archean amphibolite in the range of melt fractions reported in the caption (arrow pointing towards higher melt fraction) and at three different pressures: 1.0 GPa (purple arrow), 1.4 GPa (pink arrow) and 1.8 GPa (orange arrow) (Nagel et al., 2012). (For interpretation of the references to color in this figure legend, the reader is referred to the web version of this article.)

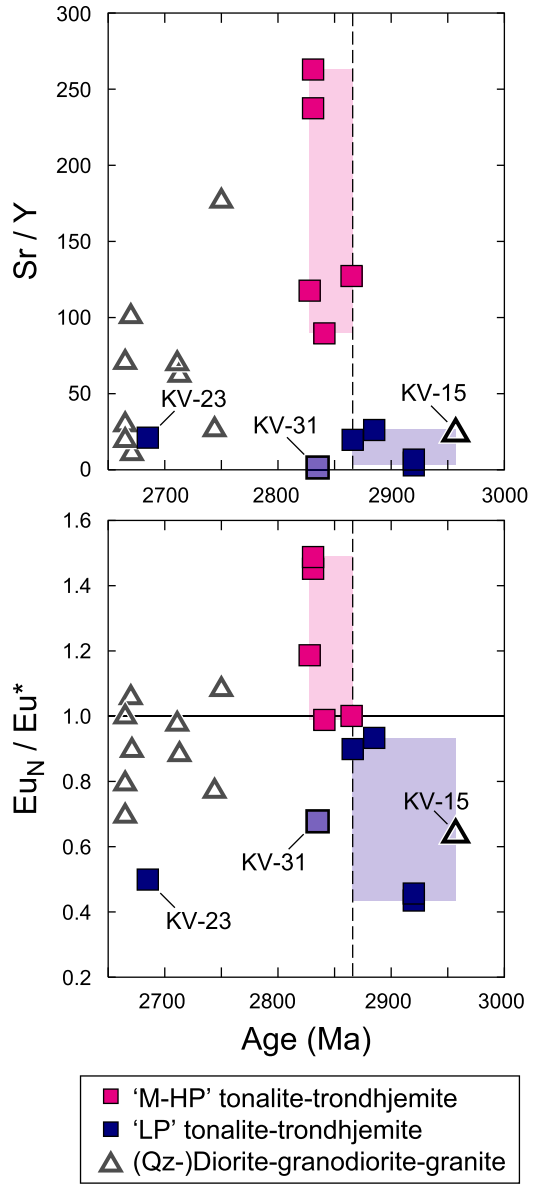

Fig. 12. Sr/Y and EuN/Eu* ratios of the Archean granitoids of the WTBC (tonalite-trondhjemite and qz-diorite-granodiorite-granite) as a function of the emplacement age, based on zircon U-Pb data either directly from the corresponding sample or for the unit to which it belongs. The two colored boxes highlight that the tonalites-trondhjemites of the 'low-pressure' (LP) group are dominantly ≥2.86 Ga-old (except KV-23 and KV-31), while those of the 'medium-/high-pressure' (M-HP) group are dominantly ≤ 2.86 Ga-old.

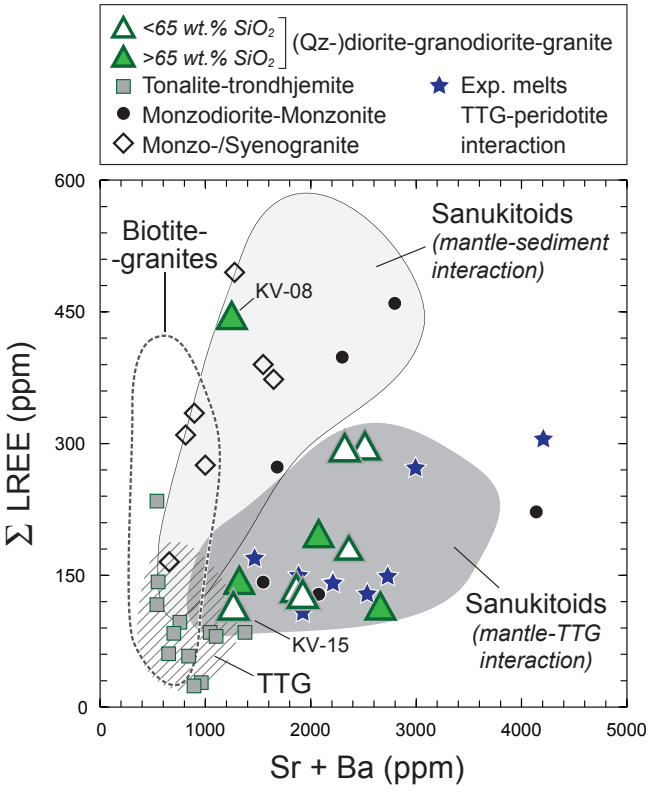

Fig. 13. ΣLREE (La + Ce + Pr + Nd) vs. Sr + Ba concentrations of WTBC granitoids, with emphasis on the qz-diorites-granodiorites-granites, compared to those of typical Archean granitoids: TTG (Moyen, 2011; Moyen and Martin, 2012), biotite-granites (Moyen, 2011; Laurent et al., 2014) and sanukitoids (Laurent et al., 2014). For sanukitoids, the distinction is made between sanukitoids interpreted to derive from interactions between mantle peridotite and TTG melts (dark gray field) or sedimentary material (light gray field) (Laurent et al., 2011, 2014). The stars correspond to the composition of experimental melts resulting from hybridization between TTG melts and peridotite (Rapp et al., 1999, 2010).

6.2.2. Qz-diorite-granodiorite-granite

The 2.75–2.68 Ga (qz-)diorites, granodiorites and granites are richer in K_2O than TTGs and show a wider range of SiO_2, extending from mafic to felsic compositions (Figs. 3 and 4). Those properties are characteristic of sanukitoids (Figs. 3–5 and 10), a suite of mafic to felsic granitoids very common in Neoarchean terranes (Halla et al., 2009; Heilimo et al., 2010, 2011; Laurent et al., 2014; Martin et al., 2005). The qz-diorites show the diagnostic chemical criteria of sanukitoids (Heilimo et al., 2010): high K_2O content (1.8–4.3 wt%) with K_2O/Na_2O > 0.4 (up to 1.1), at low SiO_2 (54–63 wt%) and Mg# ≥0.4–0.5, as well as elevated concentrations in Ba + Sr (> 1800 ppm) and LREE (130–300 ppm) (Fig. 13). Such ambivalent chemical features reflect interactions between mantle peridotite and a component rich in incompatible elements (Laurent et al., 2014). The latter is most often represented by a silicate melt, either TTG in composition (Halla et al., 2009; Heilimo et al., 2010; Martin et al., 2005; Oliveira et al., 2011) or derived from sedimentary material (Halla, 2005; Laurent et al., 2011; Mikkola et al., 2011). The compositions of the WTBC qz-diorites differ from those of the sanukitoids formed by sediment-peridotite interaction, being richer in Ba + Sr and no so rich in LREE (Fig. 13). They are in contrast identical to those of sanukitoids produced by experimental reaction between TTG and peridotite (Rapp et al., 1999, Rapp et al., 2010) (Fig. 13). We therefore conclude that the qz-diorites from the WTBC derive from a two-step process: (i) burial of mafic rocks at mantle levels and their melting to produce TTGs; (ii) interaction of the resulting TTGs with the surrounding mantle en-route to the crust.

One exception is sample KV-15, which has an older age (2.96 Ga), less radiogenic Hf isotopic composition ($\varepsilon Hf_{(t)}$ of ca. −4) (Fig. 7), lower Mg# (0.36) than other qz-diorites and not so high Sr + Ba (1265 ppm) and LREE (116 ppm). In this respect, its composition is closer to those of the WTBC TTGs (Fig. 13), especially the "low-pressure" ones, since it also bears a strong negative Eu anomaly (Eu_N/Eu^* = 0.65) and low Sr/Y ratio (25) (Figs. 11 and 12). Therefore, those properties may rather point to either an origin by low-pressure melting of relatively enriched basalts, as proposed for rocks of comparable composition in other Archean cratons (Hoffmann et al., 2016; Laurent and Zeh, 2015; Reimnik et al., 2014), or very limited interactions between TTG-like melt and the mantle.

At first glance, the granodiorites and granites (SiO_2 > 65 wt%) resemble the potassic biotite-granites (Figs. 3, 4 and 10) that are very common in most Archean cratons as melting products of pre-existing

TTG (Almeida et al., 2013; Dey et al., 2012; Laurent et al., 2014; Moyen et al., 2003). However, they show higher Al_2O_3 (> 15 wt%), Ba + Sr (> 1250 ppm; Fig. 13) and less pronounced negative Eu anomaly (Eu_N/Eu^* = 0.75–0.90) than such biotite-granites (Al_2O_3 < 15 wt%; Ba + Sr < 1000 ppm; Eu_N/Eu^* < 0.70; Laurent et al., 2014). These features preclude an origin by melting of TTGs, because this would entail large amounts of residual plagioclase (Singh and Johannes, 1996; Skjerlie and Johnston, 1994; Watkins et al., 2007) and thus, retention of Al, Eu, Sr and Ba in the source. The WTBC granodiorites-granites also show higher Mg# (0.35–0.45) and ferromagnesian oxides contents (FeO_t + MgO + MnO + TiO_2 = 2–4 wt%) than TTG-derived granites (Mg# = 0.10–0.35 and FeO_t + MgO + MnO + TiO_2 = 1–3 wt%; Laurent et al., 2014) and notably lack inherited zircons. As such, they are similar to the felsic facies of sanukitoid suites, which result from differentiation of the mafic end-member, i.e. the qz-diorites (Heilimo et al., 2010; Laurent et al., 2014). The LREE and Ba + Sr contents of the WTBC granodiorites-granites are comparable to those of the qz-diorites (Fig. 13) but Y–HREE contents are lower (Table 1), as would be expected in the case of amphibole-dominated fractionation, typical for sanukitoids (Laurent et al., 2013; Oliveira et al., 2010). A genetic lineage between the granodiorites-granites and the qz-diorites is further supported by their common association in the field (Fig. 2b) and their similar, positive zircon $\varepsilon Hf_{(t)}$ (Table 2).

Because Hf is an incompatible element, a magma derived from interactions between mantle peridotite and crustal material largely inherits the Hf isotopic composition of the latter (Couzinié et al., 2016). Therefore, the positive $\varepsilon Hf_{(t)}$ of most qz-diorite-granodiorite-granite samples (Fig. 7) points out that the TTG material that interacted with peridotite to form the parent sanukitoids was juvenile. Specifically, it cannot be represented by the > 2.8 TTGs from the NE segment, which already had negative $\varepsilon Hf_{(t)}$ at ca. 2.7 Ga (Fig. 7). One exception is sample KV-08 that has a negative $\varepsilon Hf_{(t)}$ (ca. −1) (Fig. 7), which could be explained by interactions between peridotite and sediments resulting from the erosion of the > 2.8 Ga TTGs. This is furthermore consistent with the much higher LREE contents of KV-08 (ca. 450 ppm) relative to other samples, similar to those of sanukitoids resulting from peridotite-sediment interactions (Fig. 13).

6.2.3. Qz-monzonite-monzodiorite and monzo-/syenogranite

The qz-monzonite-monzodiorite and the monzo-syenogranite plutonic rocks in the WTBC are discussed jointly because their ages and location indicate that they both belong to the Transscandinavian Igneous Belt (TIB), a voluminous and well-described family of Paleoproterozoic plutonic igneous rocks of the Fennoscandian Shield. The TIB forms a roughly N–S trending array of granitoids and minor mafic rocks, stretched over 1400 km from southern Sweden to the Lofoten-Vesterålen province of north Norway (Fig. 1) (Åhäll and Larson, 2000; Högdahl et al., 2004; Nironen, 2005; Patchett et al., 1987; Skår, 2002). They were emplaced during three distinct events: 1.86–1.83 Ga ("TIB-0"), 1.81–1.76 Ga ("TIB-1") and 1.71–1.67 Ga ("TIB-2/3") (Ahl et al., 2001; Andersen et al., 2009; Andersson et al., 2004; Corfu, 2004; Gorbatschev, 2004; Högdahl et al., 2004). In the WTBC, a minority of qz-monzonite and monzodiorite plutons have an age of ca. 1.87 Ga and link to the TIB-0 event. Most Paleoproterozoic granitoids and mafic rocks are however coeval with the TIB-1 event (1.80–1.75 Ga; Table 2), i.e. the dominant episode in the whole belt (Åhäll and Larson, 2000). Moreover, the petrography of the TIB-1 igneous rocks (microcline-rich, amphibole- and biotite-bearing granitoids, with titanite and Fe-Ti oxides as main accessories; Andersen et al., 2009; Andersson et al., 2004; Gorbatschev, 2004; Rutanen and Andersson, 2009; Skår, 2002) and their whole-rock compositions (Figs. 3–5) very well match those of the WTBC qz-monzonites-monzodiorites and monzo-/syenogranites.

Apart from some ca. 1.82 Ga S-type granites formed by melting of Svecofennian metasediments (Claesson and Lundqvist, 1995), the dominant TIB-1 granites from Sweden and north Norway have I- to A-type affinity (Andersson, 1997; Andersson et al., 2004; Gorbatschev, 2004; Skår, 2002), as well as positive zircon $\varepsilon Hf_{(t)}$ (Fig. 7) and whole-rock $\varepsilon Nd_{(t)}$ (Andersen et al., 2009; Claesson and Lundqvist, 1995; Mellqvist et al., 1999). This would result from melting of mafic to intermediate, arc-like crust formed during the Svecofennian accretionary orogeny (ca. 1.9–2.1 Ga) (Andersen et al., 2009), with minor involvement of sediments (Patchett et al., 1987) and/or mantle-derived melts (Skår, 2002). The similar chronological, petrographic and compositional features between these granites and the WTBC monzo-/syenogranites suggest that the latter have a comparable source. Consistently, experimental data show that differentiation of K-rich mafic to intermediate compositions (50–60 wt% SiO_2; 1–3 wt% K_2O) produces granitic liquids similar in composition (69–75 wt% SiO_2; 4–5 wt% K_2O) to the WTBC monzo-/syenogranites (Bogaerts et al., 2006; Sisson et al., 2005) (Fig. 10). However, the latter significantly differ from other TIB-1 granites by their strongly negative zircon $\varepsilon Hf_{(t)}$ ranging from −10 to −12 (Fig. 7).

This apparent discrepancy can be explained if one considers that the monzo-/syenogranites result from melting of a compositionally similar source as the other TIB-1 granites, but one that is much older (Archean). In the WTBC, the Archean qz-diorites from the SW segment, of sanukitoid affinity, would represent a plausible source for the monzo-/syenogranites. In addition to having the appropriate major element composition, their trace element pattern reasonably matches that of the modelled source of the monzo-/syenogranites using phase relationships from experimental data (Fig. 14). Furthermore, the zircon Hf isotopic composition of the monzo-/syenogranites is close to the expected $\varepsilon Hf_{(t)}$ of the SW segment crust at 1.8 Ga (ca. −14; Fig. 7). Alternatively, the coeval qz-monzonites and monzodiorites could also represent possible parental compositions, as indicated by trace element modelling (Fig. 14). The more radiogenic zircon Hf isotopic compositions of the qz-monzonites/monzodiorites ($\varepsilon Hf_{(t)}$ mostly between −7 and −10) relative to the monzo-/syenogranites ($\varepsilon Hf_{(t)}$ beween −10 and −13) (Fig. 7) does not favor this possibility, but it cannot be ruled out because this discrepancy may be explained by assimilation of the local Archean crust upon magma differentiation.

The origin of the intermediate rocks (qz-monzonites and monzodiorites) is faintly constrained at the scale of the whole TIB. They could result from mixing between the granites and coeval mantle-derived melts (Andersson et al., 2004; Skår, 2002), represented by the minor mafic rocks present throughout the TIB (Andersson et al., 2004, 2007; Rutanen and Andersson, 2009). This model has been also proposed to explain the formation of the (compositionally similar and coeval) mangerites and charnockites of the anorthosite-mangerite-charnockite-granite (AMCG) suite in the Lofoten-Vesterålen province (Markl, 2001; Markl and Höhndorf, 2003). However, the mafic and intermediate rocks of the TIB show no correlation whatsoever between differentiation indexes and bulk-rock Sr–Nd isotopic composition (Andersson et al., 2007; Rutanen and Andersson, 2009), as would be expected in the case of extensive contamination/mixing. In fact, even the most primitive TIB mafic rocks (SiO_2 ~ 50 wt%; Mg# ≥0.7) are already isotopically evolved and LILE-, LREE-rich, suggesting that they stem from a lithospheric mantle source enriched in incompatible elements during Svecofennian subduction (Andersson et al., 2007; Rutanen and Andersson, 2009).

The qz-monzonites-monzodiorites of the WTBC (and in the TIB in general) could derive directly from fractionation of these enriched mantle-derived magmas. Consistently, the latter show a nearly continuous liquid line of descent, down to dioritic compositions very similar to those of the qz-monzonites and monzodiorites (ca. 55–60 wt% SiO_2; 2 wt K_2O; Mg# ~0.5) (Rutanen and Andersson, 2009). Experimental data further show that such monzodioritic compositions (56–62 wt% SiO_2; 1.5–4.5 wt% K_2O) can be produced by differentiation of K-rich, broadly basaltic starting compositions (SiO_2 ~ 50 wt%; K_2O ≥ 1 wt%) at temperatures of 950–1050 °C and melt fractions of 30–45% (Alonso-Perez et al., 2009; Sisson et al., 2005; Sisson and

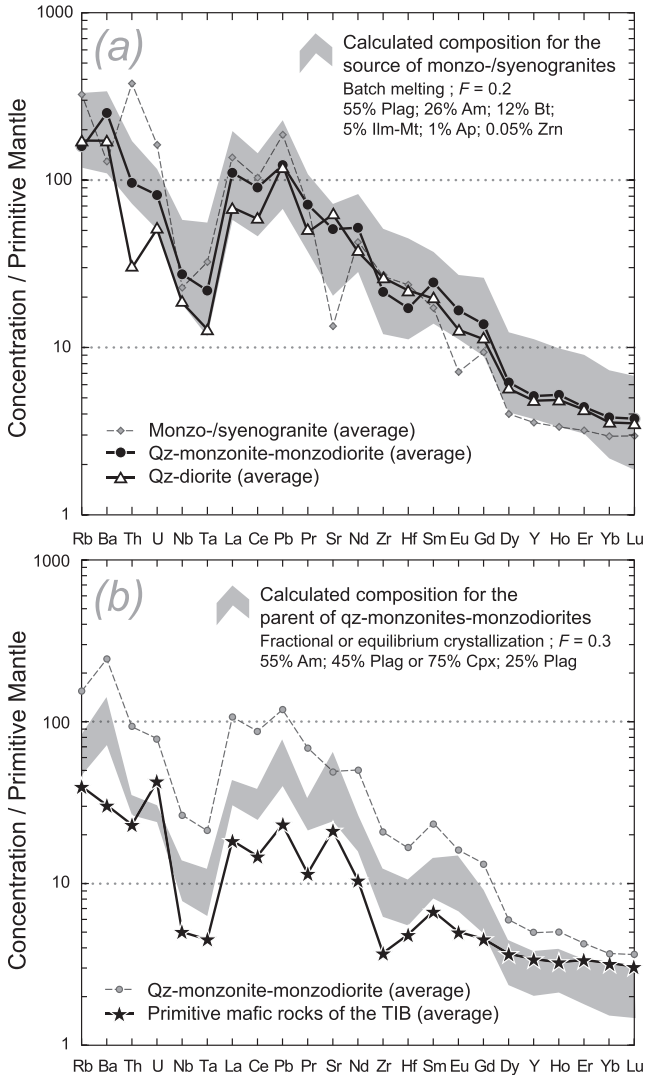

Fig. 14. Multi-element diagrams (concentrations normalized to primitive mantle values; McDonough and Sun, 1995) showing the results of trace element modelling focused on the origin of the WTBC Paleoproterozoic granitoids. (a) Composition of the source of the monzo-/syenogranites (gray field), calculated using the average composition of the monzo-/syenogranites as that of the liquid; liquid and mineral proportions based on the experiments of Sisson et al. (2005) at 800–850 °C; and a range of partition coefficients for felsic to intermediate melts (Laurent et al., 2013). The average compositions of the WTBC qz-monzonites-monzodiorites and qz-diorites are also shown. (b) Composition of the parent magma of the qz-monzonites-monzodiorites (gray field), calculated using the average composition of the qz-monzonites-monzodiorites as that of the liquid; liquid and mineral proportions based either on the experiments of Sisson et al. (2005) at 950–975 °C, or using a mineral assemblage dominated by Cpx as postulated for the liquid line of descent of the TIB mafic rocks (Rutanen and Andersson, 2009); and a range of partition for intermediate to mafic melts (Laurent et al., 2013). The composition of the primitive mafic rocks of the TIB correspond to samples with SiO_2 ~ 50 wt% and Mg# ≥0.7 (Rutanen and Andersson, 2009). For both models, the results obtained using the different sets of parameters used (partition coefficients; mineral assemblage; differentiation process) are pooled together to yield a range of possible source/parental compositions.

Grove, 1993) (Fig. 10). Trace element modelling confirms this hypothesis, since the patterns calculated for the mafic parent are comparable to those of the most primitive mafic rocks of the TIB, albeit being significantly richer in the most incompatible elements (Fig. 14), possibly indicating a more enriched mantle source.

As observed for the monzo-/syenogranites, the qz-monzonites and monzodiorites of the WTBC have strongly negative zircon εHf_t (ca. −7 to −10), whereas their counterparts elsewhere in the TIB are more juvenile (εHf_t of ca. 0 to +6; Andersen et al. 2009) (Fig. 7). This cannot reflect crustal contamination, because assimilation of Archean rocks with $\varepsilon Hf_{(t)}$ of ca. −15 by a mafic magma similar to the TIB mafic rocks ($\varepsilon Hf_{(t)}$ of ca. +3) would require unrealistically high proportions of contamination (60–80%) to explain the composition of the qz-monzonites-monzodiorites. This means that even if contamination played a role, their parental magma had to be much less radiogenic than the mafic rocks elsewhere in the TIB, i.e. characterized by $\varepsilon Hf_{(t)}$ not exceeding −5 to −8 (for max. 20% contamination). To explain such negative zircon $\varepsilon Hf_{(t)}$ signatures at 1.8 Ga, it is necessary either that mantle enrichment took place in the Archean, or, if it happened later, that Archean crustal material(s) represented the main metasomatic agent(s).

6.3. A Tectonic model for continent formation and evolution in the WTBC

6.3.1. Nucleation of felsic crust

Only very few zircon crystals yield ages in excess of 3.0 Ga in the WTBC, whether detrital crystals from clastic sediments in the greenstone belts (3 out of 131 grains; Bergh et al., 2007; Myhre et al., 2011) or xenocrysts in granitoids (1 grain in our dataset and none in that of Myhre et al., 2013). This paucity suggests that no significant felsic crust existed prior to 3 Ga in the area. However, the oldest granitoid rock identified so far in the WTBC, i.e. qz-diorite sample KV-15 (2.96 Ga), has negative zircon $\varepsilon Hf_{(t)}$ (ca. −4; Fig. 7) corresponding to the reworking of a significantly older crust. In fact, it belongs to a group of 3.2–2.7 Ga-old Archean gneisses of the Karelian province that show zircon Hf isotopic compositions consistent with reworking of 3.8 to 3.6 Ga-old mafic crust (Fig. 7) and that consistently contain zircon xenocrysts with crystallization ages up to 3.7 Ga (Lauri et al., 2011). Similar trends pointing to crust extraction ages of 3.7 to 4.5 Ga and slopes corresponding to $^{176}Lu/^{177}Hf$ ratios of mafic rocks (ca. 0.02–0.03) were already documented in several Archean cratons worldwide and interpreted as long-lived, closed-system reworking of a dominantly basaltic protocrust (Kemp et al., 2009, 2010; Næraa et al., 2012; Nebel-Jacobsen et al., 2010; Thomas et al., 2016; Zeh et al., 2014).

The 2.92–2.83 Ga TTGs represent the main event of felsic crust formation in the NE segment of the WTBC (Fig. 8). Those rocks have positive zircon $\varepsilon Hf_{(t)}$ (+2 to +3), unchanged throughout the 90 Ma range of emplacement ages (Table 2; Fig. 7) and partly overlapping, within uncertainties, that of the depleted mantle underneath Fennoscandia as represented by the ca. 2.84 Ga Kostomuksha komatiites ($\varepsilon Hf_{(t)}$ = +4.9; Blichert-Toft and Puchtel, 2010) (Fig. 7). This range requires that a short time (maximum 100–150 Ma) was elapsed between massive extraction of mafic crust from the convective mantle and its transformation into a TTG-dominated, felsic crust. On the other hand, the TTGs show a continuous trend of increasing melting depths from ≤30 km at > 2.9 Ga, to 30–45 km at 2.89–2.87 Ga and up to 45–60 km at 2.86–2.83 Ga (see Section 6.2.1 and Fig. 12). Both lines of evidence entail that the TTGs were formed in response to progressive thickening of a young mafic crust.

This could have taken place through either repeated melting at the base of a thickening mafic plateau, developed above a long-lived mantle upwelling or plume (e.g. Bédard, 2006, 2018; Smithies et al., 2009; van Kranendonk et al., 2015), or tectonic stacking of slivers of recently formed mafic crust (e.g. de Wit, 1998; Hiess et al., 2009; Nutman et al., 2015; Sizova et al., 2010). Both models are not mutually exclusive, since tectonic imbrication is likely to initiate at the margins of a buoyant mafic plateau (Nair and Chacko, 2008). Regardless of the thickening mechanism, phase equilibria modelling indicate that if the thickness of the mafic crust exceeds ca. 45 km, the lowermost part becomes denser than the underlying mantle, hence gravitationally unstable (Johnson et al., 2013). Delamination of the lower crust would

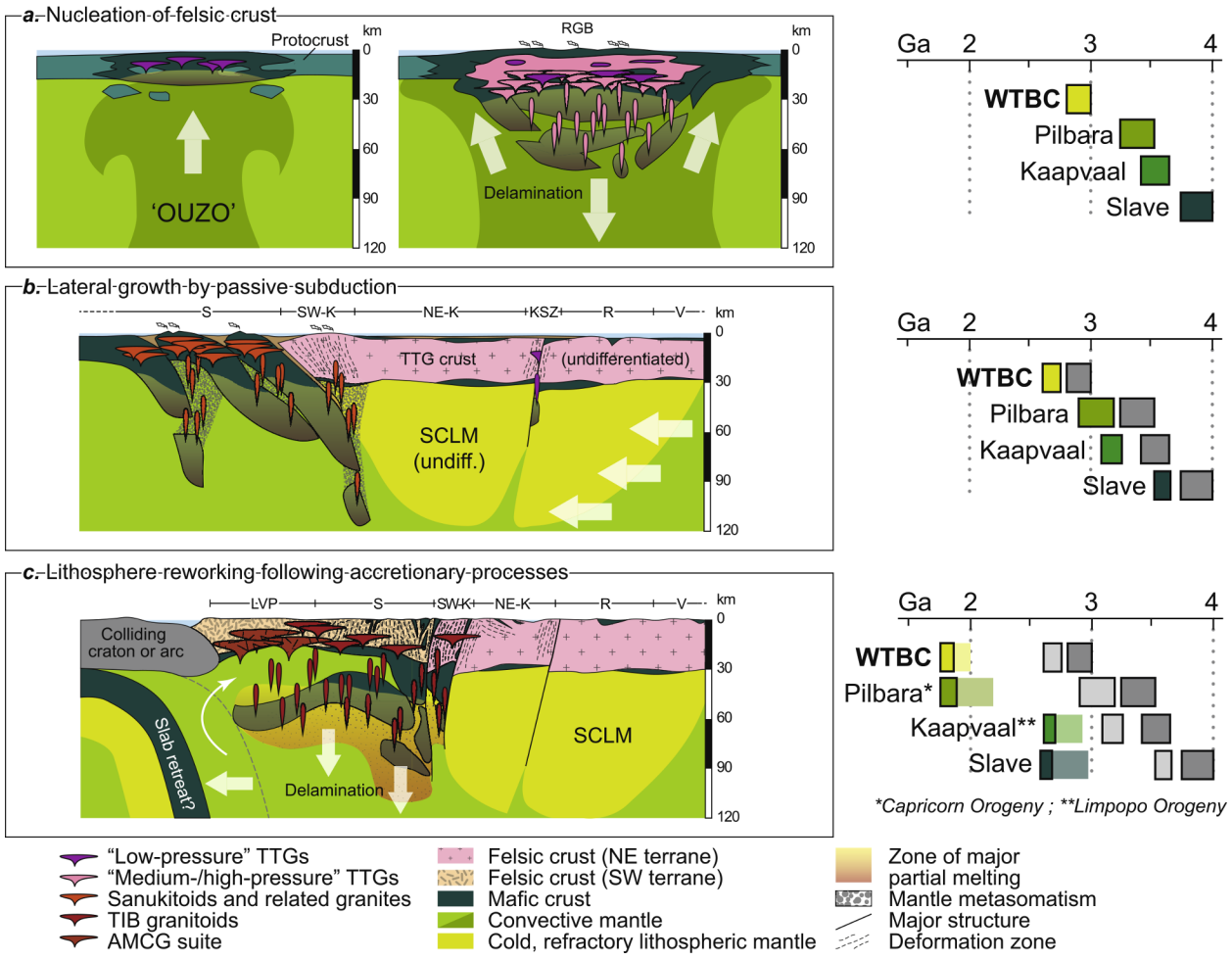

Fig. 15. Geodynamic model. Sketches to the left of the figure are schematic cross sections showing the three main phases of the proposed model of continent formation and stabilization in the WTBC. (a) Phase of felsic crust nucleation in an "intraplate" plateau-like setting forming the TTG-dominated crust of the NE terrane; the left sketch indicates the incipient plateau stage at 3.00–2.92 Ga above a mantle upwelling (OUZO, "overturn upwelling zones" after Bédard, 2018), whereas the right sketch depicts the 2.86–2.83 Ga delamination event following rapid thickening. (b) Phase of lateral growth of the proto-craton at 2.75–2.67 Ga, by lateral drifting of the proto-craton. This induces passive, proto-subduction at its leading edge, forming the sanukitoid-dominated crust of the SW segment; SCLM = sub-continental lithospheric mantle, comprising refractory mantle and mafic residues after the formation of TTGs. (c) Phase of post-collisional, lithospheric reworking responsible for the 1.80–1.75 Ga TIB magmatism, here explained by delamination (and melting) of the mafic-intermediate lower crust and mantle lithosphere, following over-thickening during the previous Svecofennian (2.0–1.8 Ga) accretionary processes. NE-K = northeast Kvaløya; SW-K = southwest Kvaloya; KSZ = Kvalsund Shear Zone; LVP = Lofoten-Vesterålen Province; R = Ringvassoya; S = Senja; V = Vanna. The right part of the figure shows a timeline indicating the age and duration of each stage in selected cratonic domains (not necessarily corresponding to the exact same tectonic situation as in the WTBC, but to the same main continent formation event), including the Pilbara craton (Smithies et al., 2009; van Kranendonk et al., 2007; Wiemer et al., 2018) and adjacent Capricorn Orogeny (Cawood and Tyler, 2004), the Kaapvaal craton (Hoffmann et al., 2016; Kröner et al., 2016; Moyen et al., 2007) and adjacent Limpopo Orogeny (Laurent and Zeh, 2015; Vezinet et al., 2018), and the Slave craton (Davis et al., 2003; Reimnik et al., 2014, 2016). In (c), the shaded color indicates the timing of accretionary processes pre-dating the main, post-collisional magmatic event.

result in extensive melting of mafic material at great depths, explaining the formation of high-pressure TTGs (Bédard, 2006; Zegers and van Keken, 2001). This would adequately explain the flare-up of 2.86–2.83 Ga TTGs formed at ≥45 km in the WTBC, as indicated by the cluster of emplacement ages (Fig. 8) and abundant detrital zircon dates in this timespan (Bergh et al., 2007; Myhre et al., 2011).

We therefore propose that the nucleation of felsic continental crust in the WTBC occurred as a two-step scenario (Fig. 15a).

(1) Between 3.00 and 2.92 Ga, incipient formation of a mafic plateau on ancient mafic protocrust took place above a mantle upwelling. Heat conduction and advection by mantle-derived basalt would trigger shallow melting of both the protocrust, forming qz-dioritic magmas with low-pressure TTG affinities and strongly negative zircon $\varepsilon Hf_{(t)}$, and recently emplaced mafic rocks, forming the earliest, ca. 2.92 Ga low-pressure TTGs with positive zircon $\varepsilon Hf_{(t)}$.

(2) Between 2.92 and 2.83 Ga, the juvenile plateau crust was magmatically and/or tectonically thickened, until reaching a thickness of ca. 45 km (at 2.86–2.83 Ga) that triggered lower crustal delamination, melting and generation of massive volumes of medium-/high-pressure TTGs. Concurrently, continued shallow melting contributed to form minor, low-pressure TTGs (e.g. sample KV-31).

6.3.2. *Lateral growth of the proto-craton*

In the WTBC, the 2.74–2.67 Ga period is marked by (i) a clear shift of magmatic activity from the NE to the SW segment; and (ii) a change from TTG-dominated magmatism to sanukitoid-like magmatism (see Section 6.2.2 and Fig. 8). The peculiar petrogenesis of sanukitoids requires the burial of supracrustal material (basalts, sediments) at sufficient depth to extensively interact with mantle peridotite (Laurent et al., 2014), implying subduction-like processes. The hotter Archean mantle temperature (Herzberg et al., 2010) precludes that "modern"

subduction, i.e. foundering of cold, rigid lithospheric slabs coherent over 100's-1000's of kilometers, was a viable process in the early Earth (Fischer and Gerya, 2016; Gerya, 2014; Sizova et al., 2010; van Hunen and van den Berg, 2008). Nonetheless, intermittent subduction, characterized by frequent breakoff and "dripping" of basaltic rafts into the mantle, would have been possible (Fischer and Gerya, 2016; Moyen and van Hunen, 2012; Sizova et al., 2010). Moreover, slab breakoff represents an adequate trigger for sanukitoid magmatism, gathering the petrological, geometric and thermal constraints required for their formation (Almeida et al., 2011; Halla et al., 2009; Mikkola et al., 2011; Whalen et al., 2004).

The initiation of subduction requires the pre-existence of major lithological and/or hypsometric discontinuities in the lithosphere and one or several driving force(s) (Hall, 2018; Stern and Gerya, in press). In the Archean, subduction could have initiated at the edges of stable proto-continental nuclei, consisting of TTG crust and a thick, refractory mantle keel (Nair and Chacko, 2008; van Kranendonk et al., 2007). However, the unstable nature of Archean subduction would have made slab pull highly inefficient (Bédard, 2018; Sizova et al., 2015), while it is considered as the main driving force for plate tectonics in the modern Earth (Conrad and Lithgow-Bertelloni, 2002; Schellart, 2004; Hall, 2018). To solve this issue, Bédard et al. (2013) proposed that drifting of the proto-cratons, owing to entrainment of their stiff lithospheric mantle keel by mantle convection currents, was responsible for passive tectonic imbrication ("subcretion") at their leading edges.

In the WTBC, such proto-cratonic nucleus would be represented by the > 2.8 Ga-old NE segment, which was already stabilized at the onset of the 2.74–2.67 Ga magmatism (Fig. 15b). Drifting of this segment towards the SW at ca. 2.75 Ga would have initiated subduction of mafic crust along its SW edge. The resulting proto-continental margin was characterized by melting of the buried mafic crust and/or sediments derived from the NE segment, and subsequent reaction of the resulting magmas (mostly TTGs) with the mantle en-route to the crust, forming the 2.74–2.71 Ga sanukitoid rocks in SW Kvaløya (Bakkejord complex and earlier granitoids). Further plate movement propagated the tectonic imbrication to the SW, where no felsic crust existed, resulting in the stacking of mafic, arc-like crustal blocks. Deep melting of the mafic "slabs" and subsequent interactions with the mantle explain the genesis of the juvenile, 2.71–2.67 Ga sanukitoids and related granites in Senja. Interestingly, in the Karelian Province, sanukitoids emplaced mostly in the same timespan as in the WTBC (2.74–2.70 Ga) and are distributed along a rough linear trend (Heilimo et al., 2011; Mikkola et al., 2011). This trend coincides with the Onega-Malangen Lineament, interpreted to be in continuity with the Archean segment boundaries of the WTBC (see Fig. 9 and Section 6.1).

Another possibility would be that the SW segment was formed and evolved as an independent micro-continent and only accreted to the NE segment in the Paleoproterozoic, during the Svecofennian orogeny. This is apparently supported by the presence of 2.0–1.9 Ga greenstone belts (Astridal, Torsnes and Mjelde-Skorelvvatn belts; Armitage and Bergh, 2005; Bergh et al., 2010, 2015; Myhre et al., 2011) along the inferred segment boundary (Fig. 9). However, these belts represent small, epicontinental basins rather than large oceans, given their limited size (Fig. 1) and lithologies (Myhre et al., 2011). The WTBC also lacks the ca. 1.95–1.90 Ga arc complexes associated with Svecofennian accretion observed elsewhere in Fennoscandia (e.g. the Knaften and Savo arcs in Sweden and Finland; Lahtinen et al., 2008). Moreover, the 2.71–2.67 Ga period is characterized by geological activity and magmatism in all domains of the WTBC (Fig. 8). Docking of the Senja arc-like complexes against the NE segment at that time provides an adequate explanation for the deformation, metamorphism and anatexis observed in SW Kvaløya, as well as in other zones of pre-existing lithospheric weakness of the NE segment, such as the Kvalsund Shear Zone (Figs. 8 and 15b). Following Bergh et al. (2014) and Myhre et al. (2013), we therefore favor the hypothesis that the WTBC represented a coherent, single segment by the end of the Archean.

6.3.3. Lithospheric reworking following Paleoproterozoic accretion

The Paleoproterozoic evolution of Fennoscandia is already well documented (see Lahtinen et al., 2005, 2008 and references therein); four main steps can be described.

(1) At ca. 2.5–2.3 Ga, incipient rifting of the continent stabilized by the end of the Archean; the expression of such rifting in the WTBC would be the ca. 2.4 Ga Ringvassøya mafic dyke swarm (Kullerud et al., 2006b).
(2) Rifting of Archean crustal ribbons away from the main cratonic edge at 2.3–2.0 Ga. In the WTBC, the formation of marginal basins, represented by the Paleoproterozoic greenstone belts, witnesses this period (Bergh et al., 2007, 2015; Myhre et al., 2011). These developed along the former Archean terrane boundaries that represent preferential zones of weakness in the lithosphere (see Fig. 9).
(3) Convergence resulting in long-lived, complex accretionary processes along the continental margin of the Archean craton at 1.97–1.81 Ga. This was characterized by the formation of island arcs and their accretion along the craton margin, together with micro-continents and intervening sedimentary basins. In the WTBC, this stage was associated with re-assembly of the two Archean segments, associated with amphibolite-facies metamorphism and polyphased deformation in the SW segment and along the former segment boundary (Armitage and Bergh, 2005; Bergh et al., 2010).
(4) Syn- to post-collisional magmatism. This corresponds to the TIB-0 and TIB-1 plutonism at 1.87–1.75 Ga, followed by anorogenic, intracontinental magmatism at 1.7–1.5 Ga represented by the intrusion of pegmatites in the WTBC (Bergh et al., 2015).

In terms of magmatism, the most prominent expression of this evolution in the WTBC is the emplacement of TIB granitoids (1.87–1.75 Ga). The formation of the TIB granitoids involves melting of enriched lithospheric mantle and mafic-intermediate lower crust of Archean to Svecofennian ancestry, depending on the area (see Section 6.2.3). This complies with delamination of the lower crust and/or lithospheric mantle (Korja et al., 1993), which provided a sustainable heat source (asthenosphere inflow) and the adequate lithologies (delaminated lower crust and mantle lithosphere) in a favorable configuration for melting. Geophysical data reveal that underneath the TIB, the high-velocity lower crust is very thin (Korsman et al., 1999; Mjelde et al., 1993) and the Moho is not as deep (ca. 25–45 km) as in the Archean and Svecofennian domains (45–50 km) (Korja et al., 1993), both being consistent with the removal of the lower crust by delamination. Moreover, gravitational instability of the lower crust and mantle lithosphere would be a natural outcome of the long-lived Svecofennian accretion, especially along former suture zones that are the locus of maximum thickening (Lahtinen et al., 2005) and of major contrasts in the thermo-mechanical structure of colliding lithospheres (Black and Liégeois, 1993). This entails that delamination of the lower crust and mantle lithosphere would have preferably occurred below the SW segment in the WTBC (Fig. 15d), explaining that TIB granitoids are restricted to SW Kvaløya and Senja.

An event of delamination can be reconciled with either of the two tectonic settings commonly proposed to explain the origin of the TIB granitoids. The most popular is an Andean-type margin characterized by eastward subduction below the western paleo-margin of Baltica (e.g. Åhäll and Larson, 2000; Nironen, 1997). The alkali-calcic to alkalic, high-K to shoshonitic affinities of the TIB granitoids (Figs. 4 and 5) preclude that those are classical arc magmas. Nevertheless, thermo-mechanical models of mature convergent zones show that the retreat of the subducting slab following collision could trigger "*retro*-delamination" of the lower crust and mantle lithosphere of the overriding plate (Gray and Pysklywec, 2012). This would adequately explain melting of both Svecofennian and Archean lower crust and mantle lithosphere, as well as the formation of orogen-parallel extension zones in a broader

convergent context, accounting for the nature and spatial distribution of the TIB granitoids (Åhäll and Larson, 2000). Alternatively, the TIB would have formed in an intra-cratonic, post-collisional extensional setting (e.g. Andersson, 1997). One major argument against this model is that there is no significant older crust west of the TIB (Åhäll and Larson, 2000). Instead, geological events and model ages get younger westwards, i.e. from the TIB to the Gothian (1.6–1.5 Ga) and Sveconorwegian (1.2–0.9 Ga) domains (Bingen et al., 2008; Roberts and Slagstad, 2015; Söderlund et al., 2005). However, Lahtinen et al. (2005) proposed that collision with another proto-craton, presumably Amazonia, took place along the northern margin of newly established Fennoscandia at ca. 1.82–1.79 Ga (the "Nordic Orogen"); in this scenario, TIB magmatism would have occured during post-orogenic collapse following collision.

6.4. Implications for Precambrian continent formation

A duality of tectonic regimes, featuring crust formation in "intraplate", plateau-like settings and horizontal tectonics leading to terrane accretion along convergent margins, has long been recognized in the Archean, as highlighted by recent reviews (Bédard, 2018; Moyen and Laurent, 2018; Smithies et al., 2018 and references therein) and results of geodynamic modelling (Gerya, 2014; Sizova et al., 2015). Both processes are well recorded by crustal evolution in the WTBC and, importantly, occur in succession to each other: nucleation of felsic crust in a continuously thickening mafic plateau (Fig. 15a) is followed by lateral growth of this proto-cratonic nucleus, first through "passive" subduction (Fig. 15b) and later by long-lived accretionary processes comparable to modern plate tectonics, leading to a final stage of lithospheric reworking (Fig. 15c).

A similar scenario has been proposed to explain the formation of well-documented Archean cratons worldwide, such as the Slave Craton in Canada (Reimnik et al., 2014, 2016), the Itsaq Gneiss Complex in Greenland (Hoffmann et al., 2014; Næraa et al., 2012), the Kaapvaal Craton in Southern Africa (Laurent and Zeh, 2015; Moyen et al., 2007; Vezinet et al., 2018) and the Pilbara Craton in Australia (Smithies et al., 2009; van Kranendonk et al., 2007, 2015; Wiemer et al., 2018). Importantly, although the succession of geological events and their respective durations are comparable in all areas, their absolute ages vary significantly, by up to > 1 Ga (Fig. 15). While felsic crust formation by reworking of a thick mafic plateau was essentially documented from Eo-/Paleoarchean domains (4.0–3.3 Ga) so far (Hoffmann et al., 2014; Næraa et al., 2012; Reimnik et al., 2014; van Kranendonk et al., 2007; Wiemer et al., 2018), our results on the WTBC suggest that it could occur as late as the Mesoarchean (3.0–2.8 Ga). Likewise, Bédard (2006) proposed that similar processes were responsible for the formation of the 2.9–2.7 Ga Douglas Harbour domain in the Superior Province.

Such intraplate crustal nucleation was therefore taking place while, at the same time, horizontal tectonic processes were already operating along the margins of Eo-/Paleoarchean proto-cratons (Fig. 15). This situation is similar to that predicted by the periodic mantle overturn model of Bédard (2018), in which the formation of new crust above "overturn upwelling zones" (OUZOs) occurs simultaneously to the drifting of earlier-stabilized continental masses. In fact, this style of global-scale convection, entailing the co-existence of the two tectonic regimes at the global scale, might have lasted until the Paleoproterozoic. Intraplate processes were for instance proposed as a possible scenario to explain the formation of juvenile (ca. 2.2–2.1 Ga) domains of the West African Craton (Block et al., 2016), while typical accretionary orogenic events were already operating along the margins of other cratons such as Fennoscandia.

The key conclusion of those observations is that the onset of horizontal, i.e. plate-like tectonics, seems to be controlled by the regional thermo-chemical evolution of the lithosphere, rather than being a globally synchronous event. Specifically, horizontal movements would only start to operate once significant volumes of felsic continental crust and complementary mantle lithosphere were formed and stabilized at a given place, so that subduction-like processes could occur along their margins as they drift. At some point of Earth's history, probably not earlier than the Mesoproterozoic (Ernst, 2009), the increasing efficiency of subduction processes may have stabilized mantle convection and the global balance between heat generation and loss. This prevented further mantle overturns and the formation of new continents above long-lived upwellings, so that crust formation could only take place during collision of pre-existing continental masses or accretion along their margins.

7. Conclusions

Coupled geological and petrographic observations, whole-rock geochemical data and zircon U-Pb/Lu-Hf isotopic data on granitoids of the WTBC lead to the following key conclusions.

(1) The WTBC granitoids belong to four groups: (i) 2.92–2.83 Ga tonalites-trondhjemites of low- to medium-/high pressure TTG affinity; (ii) 2.74–2.67 Ga (qz-)diorites-granodiorites-granites akin to sanukitoid suites; (iii) 1.87–1.86 Ga and 1.80–1.78 Ga qz-monzonites and monzodiorites; (iv) 1.79–1.75 Ga monzo-/syenogranites.

(2) The spatial distribution of granitoid types, ages and zircon Hf isotopic data shows that the WTBC features two Archean lithotectonic segments: (i) a NE segment (Vanna-Ringvassøya-NE Kvaløya) consisting of the 2.92–2.83 Ga TTGs; and (ii) a SW segment (Senja) dominated by the 2.71–2.67 Ga, sanukitoid-like (qz-)diorites-granodiorites-granites. The domain in-between (SW Kvaløya; 2.74–2.69 Ga sanukitoids and granites with minor 2.96 Ga remnants) corresponds either to reworking of the NE segment or a third, intervening micro-segment.

(3) The TTGs of the NE segment formed by melting of young mafic crust (zircon $\varepsilon Hf_{(t)}$ of +2 to +3) at increasing depths with time (< 30 km at 2.92 GPa; 45 km at 2.89–2.86 Ga; up to 45–60 km at 2.85–2.83 Ga), as traced by pressure-sentitive trace element proxies. In contrast, the sanukitoids and granites of the SW segment ultimately result from interactions between mantle peridotite and TTGs. Their positive zircon $\varepsilon Hf_{(t)}$ (+1 to + 2) preclude that the NE segment TTGs played a role in their origin, except in SW Kvaløya ($\varepsilon Hf_{(t)}$ of −1).

(4) The 1.87–1.75 Ga qz-monzonites-monzodiorites and monzo-/syenogranites belong to the Transscandinavian Igneous Belt (TIB). The former derive from fractionation of enriched mantle-derived mafic magmas while the latter stem from mafic-intermediate, lower crustal sources. The strongly negative zircon $\varepsilon Hf_{(t)}$ (−7 to −13) of these rocks hint that both sources involve large proportions of Archean material, in contrast with other (largely juvenile) TIB granitoids.

(5) Our observations are best explained by the following tectonic scenario: (i) stabilization of the NE segment as a 3.0–2.8 Ga proto-cratonic nucleus, by repeated melting of a continuously thickening mafic plateau; (ii) drifting of this proto-craton at 2.75–2.65 Ga, leading to "passive" subduction at its leading edge and formation of the SW segment as a stack of arc-like crustal slivers; (iii) long-lived accretionary processes during the Svecofennian orogeny (1.97–1.81 Ga), leading to over-thickening and eventually delamination of the Archean lower crust and mantle lithosphere to form the 1.87–1.75 Ga granitoids.

(6) A similar evolution from intraplate continental nucleation, to proto-subduction and finally, accretionary processes has been recorded in other cratonic domains worldwide, yet at very different times, the transition from intraplate to horizontal tectonics ranging in age from Paleoarchean to Paleoproterozoic. This shows that the initiation of plate tectonics is strongly dependent on the regional evolution of the lithosphere.

Acknowledgements

This project was funded by the Marie Curie Actions of the European Commission and the University of Liège (Be-IPD-COFUND grant to O.L.). Fieldwork was supported by the Fonds National pour la Recherche Scientifique (FNRS) and the Norges Geologiske Undersøkelse (NGU). We are indebted to N. Delmelle, A. Didier, T. Dipoko, L. Marko and L. Monin for their contributions to sample preparation and analyses. We thank P.I. Myhre for introducing O.L. to the geology of the WTBC at the 5th International Archean Symposium, back in 2010, as well as S. Bergh for sharing his knowledge of the field. We thank the editor G. Zhao and an anonymous reviewer for detailed comments. Geochemical data were plotted using the GCDKit software v.3.15 (Janoušek et al. (2006)).

Appendix A. Supplementary material

Supplementary data to this article can be found online at https://doi.org/10.1016/j.precamres.2018.12.020.

References

Åhäll, K.I., Larson, S.Å., 2000. Growth-related 1.85–1.55 Ga magmatism in the baltic shield: a review addressing the tectonic characteristics of Svecofennian, TIB 1-related, and Gothian events. GFF 122, 193–206.
Ahl, M., Bergman, S., Bergström, U., Eliasson, T., Ripa, M., Weihed, P., 2001. Geochemical classification of plutonic rocks in central and northern Sweden: rapporteroch meddelanden 106. Sver. Geol. Unders. 82.
Ahl, M., Sundblad, K., Schöberg, H., 1999. Geology, geochemistry, age and geotectonic evolution of the dala granitoids, central Sweden. Precambr. Res. 95, 147–166.
Almeev, R.R., Bolte, T., Nash, B.P., Holtz, F., Erdmann, M., Cathey, H.E., 2013. High-temperature, low-H_2O Silicic Magmas of the Yellowstone Hotspot: an Experimental Study of Rhyolite from the Bruneau-Jarbidge Eruptive Center, Central Snake River Plain, USA. J. Petrol. 53 (9), 1837–1866.
Almeida, J.A.C., Dall'Agnol, R., Leite, A.A.S., 2013. Geochemistry and zircon geochronology of the archean granite suites of the Rio Maria granite–greenstone terrane, Carajás Province, Brazil. J. S. Am. Earth Sci. 42, 103–126.
Almeida, J.A.C., Dall'Agnol, R., Oliveira, M.A., Macambira, M.J.B., Pimentel, M.M., Rämö, O.T., Guimarães, F.V., Leite, A.A.S., 2011. Zircon geochronology, geochemistry and origin of the TTG suites of the Rio Maria granite–greenstone terrane: implications for the growth of the Archean crust of the Carajás Province, Brazil. Precambr. Res. 187, 201–221.
Alonso-Perez, R., Müntener, O., Ulmer, P., 2009. Igneous garnet and amphibole fractionation in the roots of island arcs: experimental constraints on andesitic liquids. Contrib. Miner. Petrol. 157, 541–558.
Amelin, Y., Lee, D., Halliday, A.N., Pidgeon, R.T., 1999. Nature of the Earth's earliest crust from hafnium isotopes in single detrital zircons. Nature 399, 252–255.
Andersen, T., Andersson, U.B., Graham, S., Åberg, G., Simonsen, S.L., 2009. Granitic magmatism by melting of juvenile continental crust: new constraints on the source of Palaeoproterozoic granitoids in Fennoscandia from Hf isotopes in zircon. J. Geol. Soc. London 166, 233–247.
Andersson, U.B., 1997. Petrogenesis of some Proterozoic granitoid suites and associated basic rocks in Sweden (geochemistry and isotope geology). Sveriges Geol. Unders., Rapporteroch Meddelanden 91, 1–216.
Andersson, U.B., Eklund, O., Claeson, D.T., 2004. Geochemical character of the mafic-hybrid magmatism in the Småland-Värmland belt. Special Paper 37 In: Högdahl, K., Andersson, U.B., Eklund, O. (Eds.), The Transscandinavian Igneous Belt (TIB) in Sweden: A Review of Its Character and Evolution, Geological Survey of Finland, pp. 47–55.
Andersson, U.B., Rutanen, H., Johansson, Å., Mansfeld, J., Rimša, A., 2007. Characterization of the paleoproterozoic mantle beneath the fennoscandian shield: geochemistry and isotope geology (Nd, Sr) of ~1.8 Ga mafic plutonic rocks from the transscandinavian Igneous Belt in southeast Sweden. Int. Geol. Rev. 49, 587–625.
Armitage, P.E.B., Bergh, S.G., 2005. Structural development of the mjelde-skorelvvatn zone on Kvaløya, Troms: a metasupracrustal shear belt in the Precambrian West Troms basement complex, North Norway. Norw. J. Geol. 85, 117–132.
Arndt, N.T., 2013. The formation and evolution of the continental crust. Geochem. Perspect. 2, 405.
Beard, J.S., Lofgren, G.E., 1991. Dehydrationmelting andwater-saturatedmelting of basaltic and andesitic greenstones and amphibolites at 1, 3 and 6.9 kbar. J. Petrol. 32 (2), 365–401.
Bédard, J., 2006. A catalytic delamination-driven model for coupled genesis of Archaean crust and sub-continental lithospheric mantle. Geochim. Cosmochim. Ac. 70, 1188–1214.
Bédard, J., Harris, L., Thurston, P., 2013. The hunting of the snArc. Precambr. Res. 229, 20–48.
Bédard, J.H., 2013. How many arcs can dance on the head of a plume?: a 'Comment' on: a critical assessment of Neoarchean 'plume only' geodynamics: evidence from the superior province, by Derek Wyman, Precambrian research, 2012. Precambr. Res. 229, 189–197.
Bédard, J.H., 2018. Stagnant lids and mantle overturns: implications for Archaean tectonics, magma genesis, crustal growth, mantle evolution, and the start of plate tectonics. Geosci. Front. 9, 19–49.
Belousova, E.A., Kostitsyn, Y.A., Griffin, W.L., Begg, G.C., O'Reilly, S.Y., Pearson, N.J., 2010. The growth of the continental crust: constraints from zircon Hf-isotope data. Lithos 119, 457–466.
Bergh, S.G., Corfu, F., Myhre, P.I., Kullerud, K., Armitage, P.E.B., Zwaan, C.B., Ravna, E.J.K., Holdsworth, R.H., Chattopadhya, A., 2012. Was the Precambrian basement of western Troms and Lofoten-Vesterålen in northern Norway linked to the Lewisian of Scotland? A comparison of crustal components, tectonic evolu-tion and amalgamation history. Tectonics, In Tech Chapter 11, 283–330. https://doi.org/10.5772/48257.
Bergh, S.G., Corfu, F., Priyatkina, N., Kullerud, K., Myhre, P.I., 2015. Multiple post-Svecofennian 1750–1560 Ma pegmatite dykes in Archaean-Palaeoproterozoic rocks of the West Troms Basement Complex, North Norway: Geological significance and regional implications. Precambr. Res. 266, 425–439.
Bergh, S.G., Eig, K., Kløvjan, O.S., Henningsen, T., Olesen, O., Hansen, J.A., 2007a. The Lofoten-Vesterålen Continental Margin: a multiphase Mesozoic-Palaeogene Rifted Shelf as shown by offshore-onshore Brittle Fault-fracture analysis. Norw. J. Geol. 87, 29–58.
Bergh, S.G., Kullerud, K., Armitage, P.E.B., Zwaan, K.B., Corfu, F., Ravna, E.J.K., Myhre, P.I., 2010. Neoarchaean to Svecofennian tectono-magmatic evolution of the West Troms Basement Complex, North Norway. Norwgian J. Geol. 90, 21–48.
Bergh, S.G., Kullerud, K., Corfu, F., Armitage, P.E.B., Davidsen, B., Johansen, H.W., Pettersen, T., Knudsen, S., 2007b. Low-grade sedimentary rocks on Vanna, North Norway: a new occurrence of a Palaeoproterozoic (2.4–2.2 Ga) cover successionin northern Fennoscandia. Norw. J. Geol. 87, 301–318.
Bergh, S.G., Kullerud, K., Myhre, P.I., Corfu, F., Armitage, P.E.B., Zwaan, K.B., Ravna, E.J.K., 2014. Archaean elements of the basement outliers west of the Scandinavian Caledonides in Northern Norway: architecture, evolution and possible correlation with Fennoscandia. In: In: Dilek, Y., Furnes, H. (Eds.), Evolution of Archean Crust and Early Life, Modern Approaches in Solid Earth Sciences 7. pp. 103–126.
Bingen, B., Andersson, J., Söderlund, U., Möller, C., 2008. The Mesoproterozoic in the Nordic countries. Episodes 31, 29–34.
Bingen, B., Solli, A., Viola, G., Torgersen, E., Sandstad, J.S., Whitehouse, M.J., Skår, Ø., Ganerød, M., Nasuti, A., 2015. Geochronology of the Palaeoproterozoic Kautokeino Greenstone Belt, Finnmark, northern Norway: Tectonic implications in a Fennoscandia context. Norw. J. Geol. 95, 365–396.
Blatter, D.L., Sisson, T.W., Hankins, W.B., 2013. Crystallization of oxidized, moderately hydrous arc basalt at mid- to lower-crustal pressures: implications for andesite genesis. Contrib. Mineral. Petr. 166 (3), 861–886.
Blichert-Toft, J., Puchtel, I.S., 2010. Depleted mantle sources through time: evidence from Lu–Hf and Sm–Nd isotope systematics of Archean komatiites. Earth Planet. Sci. Lett. 297 (3–4), 598–606.
Black, R., Liégeois, J.-P., 1993. Cratons, mobile belts, alkaline rocks and continental lithospheric mantle: the Pan-African testimony. J. Geol. Soc. London 150, 89–98.
Block, S., Baratoux, L., Zeh, A., Laurent, O., Bruguier, O., Jessell, M., Ailleres, L., Sagna, R., Parra-Avila, L., Bosch, D., 2016. Paleoproterozoic juvenile crust formation and stabilisation in the south-eastern West African Craton (Ghana); new insights from U-Pb-Hf zircon data and geochemistry. Precambr. Res. 287, 1–30.
Bogaerts, M., Scaillet, B., Vander Auwera, J., 2006. Phase equilibria of the Lyngdal granodiorite (Norway): implications for the origin of metaluminous ferroan granitoids. J. Petrol. 47 (12), 2405–2431.
Bouilhol, P., Jagoutz, O., Hanchar, J.M., Dudas, F.O., 2013. Dating the India-Eurasia collision through arc magmatic records. Earth Planet. Sci. Lett. 366, 163–175.
Bouvier, A., Vervoort, J.D., Patchett, P.J., 2008. The Lu–Hf and Sm–Nd isotopic composition of CHUR: constraints from unequilibrated chondrites and implications for the bulk composition of terrestrial planets. Earth Planet. Sci. Lett. 273, 48–57.
Cawood, P.A., Tyler, I.M., 2004. Assembling and reactivating the Proterozoic Capricorn Orogen: lithotectonic elements, orogenies, and significance. Precambr. Res. 128, 201–218.
Cawood, P.A., Hawkesworth, C.J., Dhuime, B., 2013. The continental record and the generation of continental crust. GSA Bullet. 125 (1, 2), 14–32.
Cawood, P.A., Kröner, A., Pisarevsky, S., 2006. Precambrian plate tectonics: criteria and evidence GSA. Today 16 (7), 4–11.
Claesson, S., Lundqvist, T., 1995. Origins and ages of Proterozoic granitoids in the Bothnian Basin, central Sweden; isotopic and geochemical constraints. Lithos 36, 115–140.
Condie, K.C., Aster, R.C., 2010. Episodic zircon age spectra of orogenic granitoids: The supercontinent connection and continental growth. Precambr. Res. 180, 227–236.
Condie, K.C., Kröner, A., 2013. The building blocks of continental crust: evidence for a major change in the tectonic setting of continental growth at the end of the Archean. Gondwana Res. 23 (2), 394–402.
Condie, K.C., Bickford, M.E., Aster, R.C., Belousova, E., Scholl, D.W., 2011. Episodic zircon ages, Hf isotopic composition, and the preservation rate of continental crust. Geol. Soc. Am. Bull. 123, 951–957.
Conrad, C.P., Lithgow-Bertelloni, C., 2002. How mantle slabs drive plate tectonics. Science 298 (5591), 207–209.
Corfu, F., 2004. U-Pb Age, setting and tectonic significance of the Anorthosite-Mangerite-Charnockite-Granite Suite, Lofoten-Vesterålen, Norway. J. Petrol. 45, 1799–1819.
Corfu, F., 2007. Multistage metamorphic evolution and nature of the amphibolite–-granulite facies transition in Lofoten-Vesterålen, Norway, revealed by U-Pb in accessory minerals. Chem. Geol. 241 (1–2), 108–128.
Corfu, F., Armitage, P.E.B., Kullerud, K., Bergh, S.G., 2003. Preliminary U-Pb geochronology in the West Troms Basement Complex, North Norway: Archaean and

Palaeoproterozoic events and younger overprints. Bullet. Geol. Survey Norway 441, 61–72.
Couzinié, S., Laurent, O., Zeh, A., Moyen, J.F., Villaros, A., Bouilhol, P., 2016. Post-collisional magmatism: crustal growth not identified by zircon Hf–O isotopes. Earth Planet. Sci. Lett. 456, 182–195.
Davis, W.J., Jones, A.G., Bleeker, W., Grütter, H., 2003. Lithosphere development in the Slave craton: a linked crustal and mantle perspective. Lithos 71, 575–589.
Dey, S., Pandey, U.K., Rai, A.K., Chaki, A., 2012. Geochemical and Nd isotope constraints on petrogenesis of granitoids fromNWpart of the eastern Dharwar craton: possible implications for late Archaean crustal accretion. J. Asian Earth Sci. 45, 40–56.
de Wit, M.J., 1998. On Archaean granites, greenstones, cratons and tectonics: does the evidence demand a verdict? Precambr. Res. 91, 181–226.
Dhuime, B., Hawkesworth, C.J., Cawood, P.A., Storey, C.D., 2012. A change in the geodynamics of continental growth 3 billion years ago. Science 335, 1334–1336.
Dhuime, B., Hawkesworth, C.J., Delavault, H., Cawood, P.A., 2017. Continental growth seen through the sedimentary record. Sed. Geol. 357, 16–32.
Doré, A.G., Lundin, E.R., Fichler, C., Olesen, O., 1997. Patterns of basement structure and reactivation along the NE Atlantic margin. J. Geol. Soc., London 157, 85–92.
Ernst, W.G., 2009. Archean plate tectonics, rise of Proterozoic supercontinentality and onset of regional, episodic stagnant-lid behavior. Gondwana Res. 15, 243–253.
Fischer, R., Gerya, T., 2016. Regimes of subduction and lithospheric dynamics in the Precambrian: 3D thermomechanical modelling. Gondwana Res. 37, 53–70.
Frost, B.R., Barnes, C.G., Collins, W.J., Arculus, R.J., Ellis, D.J., Frost, C.D., 2001. A geochemical classification for granitic rocks. J. Petrol. 42, 2033–2048.
Gaál, G., Gorbatschev, R., 1987. An outline of the Precambrian evolution of the Baltic Shield. Precambr. Res. 35, 15–52.
Gorbatschev, R., 1985. Precambrian Basement of the Scandinavian Caledonides. In: Gee, D.G., Sturt, B.A. (Eds.), The Caledonide Orogen—Scandinavia and Related Areas. Wiley, Chichester, pp. 197–212.
Gorbatschev, R., 2004. The Transscandinavian Igneous Belt—Introduction and background. Special Paper 37 In: Högdahl, K., Andersson, U.B., Eklund, O. (Eds.), The Transscandinavian Igneous Belt (TIB) in Sweden; a Review of its Character and Evolution. Geological Survey of Finland, pp. 9–15.
Gerdes, A., Zeh, A., 2009. Zircon formation versus zircon alteration – new insights from combined U-Pb and Lu–Hf in-situ LA–ICP–MS analyses, and consequences for the interpretation of Archean zircon from the Central Zone of the Limpopo Belt. Chem. Geol. 261, 230–243.
Gerya, T., 2014. Precambrian geodynamics: concepts and models. Gondwana Res. 25 (2), 442–463.
Gray, R., Pysklywec, R.N., 2012. Geodynamic models of mature continental collision: evolution of an orogen from lithospheric subduction to continental retreat/delamination. J. Geophys. Res. 117 (B3), B03408.
Griffin, W.L., Taylor, P.N., Hakkinen, J.W., Heier, K.S., Iden, I.K., Krogh, E.J., Malm, O., Olsen, K.I., Ormaasen, D.E., Tveten, E., 1978. Archaean and Proterozoic crustal evolution in Lofoten-Vesterålen, N Norway. J. Geol. Soc. London 135, 629–647.
Griffin, W.L., Wang, X., Jackson, S.E., Pearson, N.J., O'Reilly, S.Y., Xu, X., Zhou, X., 2002. Zircon chemistry and magma mixing, SE China: in-situ analysis of Hf isotopes, Tonglu and Pingtan igneous complexes. Lithos 61, 237–269.
Guitreau, M., Blichert-Toft, J., Martin, H., Mojzsis, S., Albarède, F., 2012. Hafnium isotope evidence from Archean granitic rocks for deep-mantle origin of continental crust. Earth Planet. Sci. Lett. 337–338, 211–223.
Hall, R., 2018. The subduction initiation stage of the Wilson cycle. In: Wilson, R.W., Houseman, G.A., McCaffrey, K.J.W., Doré, A.G., Buiter, S.J.H. (Eds.), Fifty Years of the Wilson Cycle Concept in Plate Tectonics. Geological Society. Special Publications, London, pp. 470. https://doi.org/10.1144/SP470.3.
Halla, J., 2005. Late Archean high-Mg granitoids (sanukitoids) in the southern Karelian domain, eastern Finland: Pb and Nd isotopic constraints on crust–mantle interactions. Lithos 79 (1–2), 161–178.
Halla, J., van Hunen, J., Heilimo, E., Hölttä, P., 2009. Geochemical and numerical constraints on Neoarchaean plate tectonics. Precambr. Res. 174, 155–162.
Hawkesworth, C.J., Kemp, A.I.S., 2006. Using hafnium and oxygen isotopes in zircons to unravel the record of crustal evolution. Chem. Geol. 226, 144–162.
Hawkesworth, C.J., Dhuime, B., Pietranik, A.B., Cawood, P.A., Kemp, A.I.S., Storey, C.D., 2010. The generation and evolution of the continental crust. J. Geol. Soc. (London) 167, 229–248.
Heilimo, E., Halla, J., Hölttä, P., 2010. Discrimination and origin of the sanukitoid series: geochemical constraints from the Neoarchean western Karelian Province (Finland). Lithos 115, 27–39.
Heilimo, E., Halla, J., Huhma, H., 2011. Single-grain zircon U-Pb age constraints of the western and eastern sanukitoid zones in the Finnish part of the Karelian Province. Lithos 121, 87–99.
Heilimo, E., Halla, J., Lauri, L.S., Rämö, O.T., Huhma, H., Kurhila, M.I., Front, K., 2009. The Paleoproterozoic Nattanen-type granites in northern Finland and vicinity – a postcollisional oxidized A-type suite. Bullet. Geol. Soc. Finland 81, 7–36.
Henkel, H., 1991. Magnetic crustal structures in Northern Fennoscandia. Tectonophysics 192, 57–79.
Herzberg, C., Condie, K.C., Korenaga, J., 2010. Thermal history of the earth and its petrological expression. Earth Planet. Sci. Lett. 292, 79–88.
Hiess, J., Bennett, V.C., Nutman, A.P., Williams, I.S., 2009. In situ U-Pb, O and Hf isotopic compositions of zircon and olivine from Eoarchaean rocks, West Greenland: New insights to making old crust. Geochim. Cosmochim. Acta 73, 4489–4516.
Hoffmann, J.E., Kröner, A., Hegner, E., Viehmann, S., Xie, H., Iaccheri, L.M., Schneider, K.P., Hofmann, A., Wong, J., Geng, H., Yang, J., 2016. Source composition, fractional crystallization and magma mixing processes in the 3.48–3.43 Ga Tsawela tonalite suite (Ancient Gneiss Complex, Swaziland) – Implications for Palaeoarchaean geodynamics. Precambr. Res. 276, 43–66.
Hoffmann, J.E., Nagel, T.J., Münker, C., Næraa, T., Rosing, M.T., 2014. Constraining the process of Eoarchean TTG formation in the Itsaq Gneiss Complex, southern West Greenland. Earth Planet. Sci. Lett. 388, 374–386.
Högdahl, K., Andersson, U.B., Eklund, O., 2004. The transscandinavian igneous belt (TIB) in Sweden: A review of its character and evolution. Geol. Surv. Finland Spec. Pap. 37, 125 p.
Höltta, P., Balagansky, V.V., Garde, A.A., Mertanen, S., Peltonen, P., Slabunov, A.I., Sorjonen-Ward, P., Whitehouse, M.J., 2008. Archean of Greenland and Fennoscandia. Episodes 31, 13–19.
Iizuka, T., Campbell, I.H., Allen, C.M., Gill, J.B., Maruyama, S., Makoka, F., 2013. Evolution of the African continental crust as recorded by U-Pb, Lu–Hf and O isotopes in detrital zircons from modern rivers. Geochim. Cosmochim. Acta 107, 96–120.
Indrevær, K., Bergh, S.G., Koehl, J.B., Hansen, J.A., Schermer, E.R., Ingebrigtsen, A., 2013. Post-Caledonian brittle fault zones on the hyperextended SW Barents Sea Margin: new insights into onshore and offshore margin architecture. Norw. J. Geol. 93, 167–188.
Indrevær, K., Bergh, S.G., 2014. Linking onshore-offshore basement rock architecture and brittle faults on the submerged strandflat along the SW Barents Sea margin, using high-resolution (5 x 5 m) bathymetry data. Norw. J. Geol. 94, 1–34.
Jagoutz, O., Kelemen, P.B., 2015. Role of arc processes in the formation of continental crust. Annu. Rev. Earth Planet. Sci. 43, 363–404.
Jagoutz, O., Schmidt, M.W., Enggist, A., Burg, J.P., Hamid, D., Hussain, S., 2013. TTG-type plutonic rocks formed in a modern arc batholith by hydrous fractionation in the lower arc crust. Contrib. Miner. Petrol. 166 (4), 1099–1118.
Janoušek, V., Farrow, C.M., Erban, V., 2006. Interpretation of whole-rock geochemical data in igneous geochemistry: introducing geochemical data toolkit (GCDkit). J. Petrol. 47, 1255–1259.
Johnson, T.E., Brown, M., Gardiner, N.J., Kirkland, C.L., Smithies, R.H., 2017. Earth's first stable continents did not form by subduction. Nature 543, 239–243.
Johnson, T.E., Brown, M., Kaus, B.J., VanTongeren, J.A., 2013. Delamination and recycling of Archaean crust caused by gravitational instabilities. Nat. Geosci. 7, 47–52.
Kamber, B., Ewart, A., Collerson, K.D., Bruce, M.C., McDonald, G.D., 2002. Fluid-mobile trace elements constraints on the role of slab melting and implications for Archaean crustal growth models. Contrib. Miner. Petrol. 144, 38–56.
Kemp, A.I.S., Foster, G.L., Schersten, A., Whitehouse, M.J., Darling, J., Storey, C., 2009. Concurrent Pb–Hf isotope analysis of zircon by laser ablation multi-collector ICP–MS, with implications for the crustal evolution of Greenland and the Himalayas. Chem. Geol. 261, 244–260.
Kemp, A.I.S., Wilde, S.A., Hawkesworth, C.J., Coath, C.D., Nemchin, A., Pidgeon, R.T., Vervoort, J.D., DuFrane, S.A., 2010. Hadean crustal evolution revisited: new constraints from Pb–Hf isotope systematics of the Jack Hills zircons. Earth Planet. Sci. Lett. 296, 45–56.
Kleinhanns, I.C., Kramers, J.D., Kamber, B.S., 2003. Importance of water for Archaean granitoid petrology: a comparative study of TTG and potassic granitoids from Barberton Mountain Land, South Africa. Contrib. Miner. Petrol. 145, 377–389.
Koistinen, T., Stephens, M.B., Bogatchev, V., Nordgulen, Ø., Wennerström, M., Korhonen, J., 2001. Geological survey finland; geological survey Norway, geological survey Sweden; ministry of natural resources of Russia. Geological Map of the Fennoscandian Shield, Scale 1:2, 000.
Korja, A., Korja, T., Luosto, U., Heikkinen, P., 1993. Seismic and geoelectric evidence for collisional and extensional events in the Fennoscandian shield – implications for Precambrian crustal evolution. Tectonophysics 219, 129–152.
Kornfält, K.A., Persson, P.O., Wikman, H., 1997. Granitoids from the Äspö area, southeastern Sweden - geochemical and geochronological data. GFF 119, 109–114.
Korsman, K., Korja, T., Pajunen, M., Virransalo, P., GGT/SVEKA Working Group, 1999. The GGT/SVEKA transect: structure and evolution of the continental crust in the Paleoproterozoic svecofennian orogen in Finland. Int. Geol. Rev. 41 (4), 287–333.
Krill, A.G., Fareth, E., 1984. Rb-Sr whole-rock dates from Senja, North Norway. Nor. Geol. Tidsskr. 64, 171–172.
Kröner, A., Anhaeusser, C.R., Hoffmann, J.E., Wong, J., Geng, H., Hegner, E., Xie, H., Yang, J., Liu, D., 2016. Chronology of the oldest supracrustal sequences in the Palaeoarchaean Barberton Greenstone Belt, South Africa and Swaziland. Precambr. Res. 279, 123–143.
Kullerud, K., Corfu, F., Bergh, S.G., Davidsen, B., Ravna, E.K., 2006a. U-Pb constraints on the Archaean and Early Proterozoic evolution of the West Troms Basement Complex, North Norway (Abstract). Bullet. Geol. Soc. Finland Special Issue I, 79.
Kullerud, K., Skjerlie, K.P., Corfu, F., de la Rosa, J.D., 2006b. The 2.40 Ga Ringvassøy mafic dykes, West Troms basement complex, Norway: the concluding act of early Palaeoproterozoic continental breakup. Precambr. Res. 150, 183–200.
Kurhila, M., Andersen, T., Rämö, O.T., 2010. Diverse sources of crustal granitic magma: Lu–Hf isotope data on zircon in three Paleoproterozoic leucogranites of southern Finland. Lithos 115 (1–4), 263–271.
Lahtinen, R., Garde, A.A., Melezhik, V.A., 2008. Paleoproterozoic evolution of Fennoscandia and Greenland. Episodes 31 (1), 1–9.
Lahtinen, R., Korja, A., Nironen, M., 2005. Palaeoproterozoic tectonic evolution of the Fennoscandian Shield. In: Lehtinen, M., Nurmi, P., Rämö, T. (Eds.), The Precambrian Bedrock of Finland - Key to the evolution of the Fennoscandian Shield. Elsevier Science B.V, pp. 418–532.
Lancaster, P., Storey, C.D., Hawkesworth, C.J., Dhuime, B., 2011. Understanding the roles of crustal growth and preservation in the detrital zircon record. Earth Planet. Sci. Lett. 305 (3–4), 405–412.
Laurent, O., Couzinié, S., Zeh, A., Vanderhaeghe, O., Moyen, J.F., Villaros, A., Gardien, V., Chelle-Michou, C., 2017. Protracted, coeval crust and mantle melting during Variscan late-orogenic evolution: U-Pb dating in the eastern French Massif Central. Int. J. Earth Sci. 106 (2), 421–451.
Laurent, O., Doucelance, R., Martin, H., Moyen, J.-F., 2013. Differentiation of the late-

Archaean sanukitoid series and some implications for crustal growth: insights from geochemical modelling on the Bulai pluton, Central Limpopo Belt South Africa. Precambrian Res. 227, 186–203.
Laurent, O., Martin, H., Doucelance, R., Moyen, J.F., Paquette, J.L., 2011. Geochem-istry and petrogenesis of high-K “sanukitoids” from the Bulai pluton, Cen-ral Limpopo Belt, South Africa: implications for geodynamic changes at the Archaean-Proterozoic boundary. Lithos 123, 73–91.
Laurent, O., Martin, H., Moyen, J.F., Doucelance, R., 2014. The diversity and evolu-tion of late-Archean granitoids: evidence for the onset of “modern-style” plate tectonics between 3.0 and 2.5 Ga. Lithos 205, 208–235.
Laurent, O., Zeh, A., 2015. A linear Hf isotope-age array despite different granitoid sources and complex Archean geodynamics: example from the Pietersburg block (South Africa). Earth Planet. Sci. Lett. 430, 326–338.
Lauri, L.S., Andersen, T., Hölttä, P., Huhma, H., Graham, S., 2011. Evolution of the Archaean Karelian Province in the Fennoscandian shield in the light of U-Pb zircon ages and Sm–Nd and Lu–Hf isotope systematics. J. Geol. Soc. 168, 201–218.
Malm, O., Ormaasen, D.E., 1978. Mangerite–charnockite intrusives in the Lofoten-Vesterålen area, North Norway: petrography, chemistry and petrology. Nor. Geol. Unders. 338, 83–114.
Markl, G., 2001. REE constraints on fractionation processes of massive-type anorthosites on the Lofoten Islands, Norway. Mineral. Petrol. 72, 325–351.
Markl, G., Höhndorf, A., 2003. Isotopic constraints on the origin of AMCG-suite rocks on the Lofoten Islands, N Norway. Mineral. Petrol. 78, 149–171.
Martel, C., Pichavant, M., Holtz, F., Scaillet, B., Bourdier, J.L., Traineau, H., 1999. Effects of f_{O2} and H_2O on andesite phase relations between 2 and 4 kbar. J. Geophys. Res. Solid Earth 104 (B12), 29453–29470.
Martin, H., Moyen, J.-F., Guitreau, M., Blichert-Toft, J., Le Pennec, J.-L., 2014. Why Archaean TTG cannot be generated by MORB melting in subduction zones. Lithos 198–199, 1–13.
Martin, H., Smithies, R., Rapp, R.P., Moyen, J.F., Champion, D., 2005. An overview of adakite, TTG, and sanukitoid: relationships and some implications for crustal evolution. Lithos 79 (1–2), 1–24.
Martinsson, O., Vaasjoki, M., Persson, P.O., 1999. U–Pb ages of Archaean to Palaeoproterozoic granitoids in the Torneträsk-Råstojaure area, northern Sweden. In: Bergman, S. (Ed.), Radiometric dating results 4, Sveriges Geologiska Undersökning C831, pp. 70–90.
McDonough, W.F., Sun, S.S., 1995. The composition of the Earth. Chem. Geol. 120 (3–4), 223–253.
Mellqvist, C., Öhlander, B., Skiöld, T., Wikström, A., 1999. The Archaean-Proterozoic Palaeoboundary in the Luleå area, northern Sweden: field and isotope geochemical evidence for a sharp terrane boundary. Lithos 96 (3–4), 225–243.
Mikkola, P., Huhma, H., Heilimo, E., Whitehouse, M., 2011Meqsd. Archean crustal evolution of the Suomussalmi district as part of the Kianta Complex, Karelia: constraints from geochemistry and isotopes of granitoids. Lithos 125, 287–307.
Mjelde, R., Sellevoll, M.A., Shimamura, H., Iwasaki, T., Kanazawa, T., 1993. Crustal structure beneath Lofoten, N. Norway, from vertical incidence and wide-angle seismic data. Geophys. J. Int. 114, 116–126.
Montel, J.M., Vielzeuf, D., 1997. Partial melting of metagreywackes, part II. Compositions of minerals and melts. Contrib. Miner. Petrol. 128, 176–196.
Motuza, G., Motuza, V., Beliatsky, B., Savva, E., 2001a. Volcanic rocks of the Ringvassøya greenstone belt (North Norway): Implication for the stratigraphy and tectonic Setting. J. Confr. (Abstract). EUG XI 6 (1), 578.
Motuza, G., Motuza, V., Beliatsky, B., Savva, E., 2001b. The Ringvassøya greenstone belt (Tromsø, North Norway): implications for a Mesoarchaean subduction zone. EUROPROBE time-slice symposium “Archaean and Proterozoic Plate Tectonics: Geological and Geophysical Records”. St Petersburg, Russia 2001, 43–44.
Moyen, J.F., 2011. The composite Archaean grey gneisses: petrological significance, and evidence for a non-unique tectonic setting for Archaean crustal growth. Lithos 123, 21–36.
Moyen, J.F., Laurent, O., 2018. Archaean tectonic systems: a view from igneous rocks. Lithos 302–303, 99–125.
Moyen, J.F., Martin, H., 2012. Forty years of TTG research. Lithos 148, 312–336.
Moyen, J.F., van Hunen, J., 2012. Short term episodicity of Archaean subduction. Geology 40 (5), 451–454.
Moyen, J.F., Laurent, O., Chelle-Michou, C., Couzinié, S., Vanderhaeghe, O., Zeh, A., Villaros, A., Gardien, V., 2017. Collision vs. subduction-related magmatism: two contrasting ways of granite formation and implications for crustal growth. Lithos 277, 154–177.
Moyen, J.F., Martin, H., Jayananda, M., Auvray, B., 2003. Late Archaean granites: a typology based on the Dharwar Craton (India). Precambr. Res. 127, 103–123.
Moyen, J.-F., Stevens, G., Kisters, A.F.M., Belcher, R.W., 2007. TTG plutons of the Barberton granitoid-greenstone terrain, South Africa. In: Van Kranendonk, M.J., Smithies, R.H., Bennett, V. (Eds.), Earth's Oldest Rocks. Elsevier, pp. 606–668.
Myhre, P.I., Corfu, F., Bergh, S.G., 2011. Palaeoproterozoic (2.0–1.95 Ga) pre-orogenic supracrustal sequences in the West Troms basement complex North Norway. Precambr. Res. 186, 89–100.
Myhre, P.I., Corfu, F., Bergh, S.G., Kullerud, K., 2013. U-Pb geochronology along an Archaean geotransect in the West Troms basement complex, North Norway. Norw. J. Geol. 93, 1–24.
Næraa, T., Scherstén, A., Rosing, M.T., Kemp, A.I.S., Hoffmann, J.E., Kokfelt, T.F., Whitehouse, M.J., 2012. Hafnium isotope evidence for a transition in the dynamics of continental growth 3.2 Gyr ago. Nature 485, 627–630.
Nagel, T.J., Hoffmann, J.E., Münker, C., 2012. Generation of Eoarchean tonalite–-trondhjemite–granodiorite series from thickened mafic arc crust. Geology 40, 375–378.
Nair, R., Chacko, T., 2008. Role of oceanic plateaus in the initiation of subduction and origin of continental crust. Geology 36, 583–586.
Nasuti, A., Roberts, D., Dumais, M.A., Ofstad, F., Hyvönen, E., Stampolidis, A., Rodionov, A., 2015. New high-resolution aeromagnetic and radiometric surveys in Finnmark and North Troms: linking anomaly patterns to bedrock geology and structure. Norw. J. Geol. 95 (3–4), 217–243.
Nebel, O., Nebel-Jacobsen, Y., Mezger, K., Berndt, J., 2007. Initial Hf isotope compositions in magmatic zircon from early Proterozoic rocks from the Gawler Craton, Australia: a test for zircon model ages. Chem. Geol. 241 (1–2), 23–37.
Nebel, O., Vroon, P.Z., van Westrenen, W., Iizuka, T., Davies, G.R., 2011. The effect of sediment recycling in subduction zones on the Hf isotope character of new arc crust, Banda arc Indonesia. Earth Planet Sci. Lett. 303, 240–250.
Nebel-Jacobsen, Y., Münker, C., Nebel, O., Gerdes, A., Mezger, K., Nelson, D.R., 2010. Reworking of Earth’s first crust: constraints from Hf isotopes in Archean zircons from Mt, Narryer Australia. Precambr. Res. 182, 175–186.
Nironen, M., 1997. The Svecofennian Orogen: a tectonic model. Precambr. Res. 86, 21–44.
Nironen, M., 2005. Proterozoic orogenic granitoid rocks. In: Lehtinen, M., Nurmi, P.A., Rämö, O.T. (Eds.), Precambrian Geology of Finland Key to the Evolution of the Fennoscandian Shield. Elsevier, Amsterdam, pp. 443–479.
Niu, Y., et al., 2013. Continental collision zones are primary sites for net continental crust growth — A testable hypothesis. Earth-Sci. Rev. 127, 96–110.
Nutman, A.P., Bennett, V.C., Friend, C.R.L., 2015. The emergence of the Eoarchaean proto-arc: evolution of a c. 3700 Ma convergent plate boundary at Isua, southern West Greenland. Geol. Soc., London 389, 113–133.
Olesen, O., Torsvik, T.H., Tveten, E., Zwaan, K.B., Løseth, H., Henningsen, T., 1997. Basement structure of the continental margin in the Lofoten-Lopphavet area, northern Norway: constraints from potential field data, on land structural map-ping and palaeomagnetic data. Nor. Geol. Tidsskr. 77, 15–30.
Oliveira, M.A., Dall'Agnol, R., Almeida, J.A.C., 2011. Petrology of the Mesoarchean Rio Maria suite and the discrimination of sanukitoid series. Lithos 127, 192–209.
Oliveira, M.A., Dall'Agnol, R., Scaillet, B., 2010. Petrological constraints on crystallization conditions of MesoArchean Sanukitoid Rocks, southeastern Amazonian craton, Brazil. J. Petrol. 51, 2121–2148.
Opheim, J.A., Andresen, A., 1989. Basement-cover relationships on northern Vanna, Troms, Norway. Nor. Geol. Tidsskr. 69, 67–81.
Patchett, P.J., Gorbatschev, R., Todt, W., 1987. Origin of continental crust of 1.9–1.7 Ga age. Nd isotopes in the Svecofennian orogenic terrains of Sweden. Precambr. Res. 35, 145–160.
Patchett, P.J., Kouvo, O., Hedge, C.E., Tatsumoto, M., 1981. Evolution of continental crust and mantle heterogeneity: evidence from Hf isotopes. Contrib. Miner. Petrol. 78, 279–297.
Patiño-Douce, A.E., Beard, J.S., 1996. Effects on P, $f(O_2)$ and Mg/Fe ratio on dehydration melting of model metagreywackes. J. Petrol. 37 (5), 999–1024.
Patiño-Douce, A.E., Harris, N., 1998. Experimental constraints on Himalayan anatexis. J. Petrol. 39 (4), 689–710.
Patiño-Douce, A.E., Johnston, D., 1991. Phase equilibria and melt productivity in the politic system: implications for the origin of peraluminous granitoids and aluminous granulites. Contrib. Miner. Petrol. 107, 202–218.
Payne, J.L., McInerney, D.J., Barovich, K.M., Kirkland, C.L., Pearson, N.J., Hand, M., 2016. Strengths and limitations of zircon Lu–Hf and O isotopes in modelling crustal growth. Lithos 248–251, 175–192.
Peccerillo, A., Taylor, S.R., 1976. Geochemistry of Eocene calc-alkaline volcanic rocks from the Kastamonu area, Northern Turkey. Contrib. Miner. Petrol. 58 (1), 63–81.
Pickering, J.M., Johnston, D.A., 1998. Fluid-absent melting behavior of a two-mica metapelite: experimental constraints on the origin of black hills granite. J. Petrol. 39 (10), 1787–1804.
Polat, A., 2012. Growth of Archean continental crust in oceanic island arcs. Geology 40 (4), 383–384.
Rapp, R.P., Watson, E.B., 1995. Dehydration melting of metabasalt at 8–32 kbar: implications for continental growth and crust–mantle recycling. J. Petrol. 36 (4), 891–931.
Rapp, R.P., Norman, M., Laporte, D., Yaxley, G., Martin, H., Foley, S., 2010. Continent formation in the Archean and chemical evolution of the Cratonic lithosphere: melt–rock reaction experiments at 3–4 GPa and Petrogenesis of Archean Mg-diorites (Sanukitoids). J. Petrol. 51, 1237–1266.
Rapp, R.P., Shimizu, N., Norman, M.D., Applegate, G.S., 1999. Reaction between slab-derived melts and peridotite in the mantle wedge: experimental constraints at 3.8 GPa. Chem. Geol. 160, 335–356.
Reimink, J.R., Chacko, T., Stern, R.A., Heaman, L.M., 2014. Earth’s earliest evolved crust generated in an Iceland-like setting. Nat. Geosci. 7, 529–533.
Reimink, J.R., Chacko, T., Stern, R.A., Heaman, L.M., 2016. The birth of a cratonic nucleus: Lithogeochemical evolution of the 4.02–2.94 Ga Acasta Gneiss Complex. Precambr. Res. 281, 453–472.
Roberts, D., Lippard, S.J., 2005. Inferred Mesozoic faulting in Finnmark: current status and offshore links. Bullet. Geol. Survey Norway 55, 60.
Roberts, N.M.W., Slagstad, T., Parrish, R.R., Norry, M.J., Marker, M., Horstwood, M.S.A., 2012. Sedimentary recycling in arc magmas: geochemical and U-Pb–Hf–O constraints on the Mesoproterozoic Suldal Arc, SW Norway. Contrib. Miner. Petrol. 165, 507–523.
Roberts, N.M.W., Slagstad, T., 2015. Continental growth and reworking on the edge of the Columbia and Rodinia supercontinents; 1.86–0.9 Ga accretionary orogeny in southwest Fennoscandia. Int. Geol. Rev. 57 (11–12), 1582–1606.
Roberts, N.M.W., Spencer, C.J., 2015. The Zircon Archive of Continent Formation through Time. London Geological Society 389, 197–225.
Rutanen, H., Andersson, U.B., 2009. Mafic plutonic rocks in a continental-arc setting: geochemistry of 1.87–1.78 Ga rocks from south-central Sweden and models of their

palaeotectonic setting. Geol. J. 44, 241–279.
Schellart, W.P., 2004. Quantifying the net slab pull force as a driving mechanism for plate tectonics. Geophys. Res. Lett. 31, L07611.
Shand, S.J., 1943. Eruptive Rocks. Their Genesis, Composition, Classification, and Their Relation to Ore-Deposits with a Chapter on Meteorite. John Wiley & Sons, New-York.
Singh, J., Johannes, W., 1996. Dehydration melting of tonalites. 2. Compositions of melts and solids. Contrib. Miner. Petrol. 125, 26–44.
Sisson, T.W., Grove, T.L., 1993. Experimental investigations of the role of H_2O in calc-alkaline differentiation and subduction zone magmatism. Contrib. Miner. Petrol. 113, 143–166.
Sisson, T.W., Ratajeski, K., Hankins, W.B., Glazner, A.F., 2005. Voluminous granitic magmas from common basaltic sources. Contrib. Miner. Petrol. 148, 635–661.
Sizova, E., Gerya, T., Brown, M., Perchuk, L.L., 2010. Subduction styles in the Precambrian: insight from numerical experiments. Lithos 116, 209–229.
Sizova, E., Gerya, T., Stüwe, K., Brown, M., 2015. Generation of felsic crust in the Archean: a geodynamic modeling perspective. Precambr. Res. 271, 198–224.
Skår, Ø., 2002. U-Pb geochronology and geochemistry of early Proterozoic rocksof the tectonic basement windows in central Nordland, Caledonides of north-central Norway. Precambr. Res. 116, 265–283.
Skjerlie, K.P., Johnston, A.D., 1994. Vapor-absent melting at 10 kbar of a biotite- and amphibole-bearing tonalitic gneiss: implications for the generation of A-type granites. Geology 20, 263–266.
Skjerlie, K.P., Johnston, A.D., 1996. Vapour-absentmelting from 10 to 20 kbar of crustal rocks that containmultiple hydrous phases: implications for anatexis in the deep to very deep continental crust and active continental margins. J. Petrol. 37, 661–691.
Slagstad, T., Willemoes-Wissing, B., Coint, N., Stampolidis, A., Ganerød, M., Ofstad, F., 2015. Geology and metallogenic potential of the northwesternmost Norrbotten Province around Altevatn in Troms, northern Norway. Norw. J. Geol. 95 (3–4), 1–22.
Smithies, R.H., Champion, D.C., van Kranendonk, M.J., 2009. Formation of Paleoarchean continental crust through infracrustal melting of enriched basalt. Earth Planet. Sci. Lett. 281, 298–306.
Smithies, R.H., Ivanic, T.J., Lowrey, J.R., Morris, P.A., Barnes, S.J., Wyche, S., Lu, Y.J., 2018. Two distinct origins for Archean greenstone belts. Earth Planet. Sci. Lett. 487, 106–116.
Söderlund, U., Isachsen, C.E., Bylund, G., Heaman, L.M., Patchett, P.J., Vervoort, J.D., Andersson, U.B., 2005. U-Pb baddeleyite ages and Hf, Nd isotope chemistry constraining repeated magmatism in the Fennoscandian Shield. Contrib. Miner. Petrol. 150, 174–194.
Stephens, M.B., Gustavson, M., Ramberg, I.B., Zachrisson, E., 1985. The Caledonides of central-north Scandinavia—a tectonostratigraphic overview. In: Gee, D.G., Sturt, B.A. (Eds.), The Caledonide Orogen—Scandinavia and Related Areas. Wiley, Chichester, pp. 135–162.
Stern, R., Gerya, T., 2018Stern and Gerya, in press. Subduction initiation in nature and models: a review. Tectonophysics. https://doi.org/10.1016/j.tecto.2017.10.014.
Stevens, G., 1995. Compositional controls on partial melting inhigh-grade metapelites; a petrological and experimental study. unpublished Ph.D. thesis. University of Manchester.
Thomas, R.J., Spencer, C., Bushi, A.M., Baglow, N., Boniface, N., de Kock, G., Horstwood, M.S.A., Hollick, L., Jacobs, J., Kajara, S., Kamihanda, G., Key, R.M., Maganga, Z., Mbawala, F., McCourt, W., Momburi, P., Moses, F., Mruma, A., Myambilwa, Y., Roberts, N.M.W., Saidi, H., Nyanda, P., Nyoka, K., Millar, I., 2016. Geochronology of the central Tanzania Craton and its southern and eastern orogenic margins. Precambr. Res. 277, 47–67.
van Hunen, J., van den Berg, A.P., 2008. Plate tectonics on the early earth: limitations imposed by strength and buoyancy of subducted lithosphere. Lithos 103, 217–235.
van Kranendonk, M.J., 2010. Two types of Archean continental crust: Plume and plate tectonics on early Earth. Am. J. Sci. 310 (10), 1187–1209.
van Kranendonk, M.J., Hickman, A.H., Smithies, R.H., Champion, D.C., 2007. Paleoarchean development of a continental nucleus: the East Pilbara terrane of the Pilbara craton, Western Australia. In: Van Kranendonk, M.J., Smithies, R.H., Bennet, V. (Eds.), Earth's Oldest Rocks. Elsevier, pp. 307–337.
van Kranendonk, M.J., Smithes, R.H., Griffin, W.L., Huston, D.L., Hickman, A.H., Champion, D.C., Anhaeusser, C.R., Pirajno, F., 2015. Making it thick: a volcanic plateau origin of Palaeoarchean continental lithosphere of the Pilbara and Kaapvaal cratons. Geol. Soc. London 389, 83–111.
Vervoort, J.D., Kemp, A.I.S., 2016. Clarifying the zircon Hf isotope record of crust–mantle evolution. Chem. Geol. 425, 65–75.
Vezinet, A., Moyen, J.F., Stevens, G., Nicoli, G., Laurent, O., Couzinié, S., Frei, D., 2018. A record of 0.5 Ga of evolution of the continental crust along the northern edge of the Kaapvaal Craton, South Africa: consequences for the understanding of Archean geodynamic processes. Precambr. Res. 305, 310–326.
Vielzeuf, D., Holloway, J.R., 1988. Experimental determination of the fluid-absent melting relations in the pelitic system. Consequences for crustal differentiation. Contrib. Miner. Petrol. 98, 257–276.
Watkins, J.M., Clemens, J.D., Treloar, P.J., 2007. Archaean TTGs as sources of younger granitic magmas: melting of sodic metatonalites at 0.6–1.2 GPa. Contrib. Miner. Petrol. 154, 91–110.
Whalen, J.B., Percival, J.A., McNicoll, V.J., Longstaffe, F.J., 2004. Geochemical and isotopic (Nd–O) evidence bearing on the origin of late- to post-orogenic high-K granitoid rocks in the western superior province: implications for late-Archaean tectonomagmatic processes. Precambr. Res. 132, 303–326.
Whitney, D.L., Evans, B.W., 2010. Abbreviations for names of rock-forming minerals. Am. Mineral. 95, 185–187.
Wiemer, D., Schrank, C.E., Murphy, D.T., Wenham, L., Allen, C.M., 2018. Earth's oldest stable crust in the Pilbara Craton formed by cyclic gravitational overturns. Nat. Geosci. 11, 357–361.
Wolf, M.B., Wyllie, P.J., 1994. Dehydration-melting of amphibolite at 10 kbar: the effects of temperature and time. Contrib. Miner. Petrol. 115, 369–383.
Wyman, D., 2013. A critical assessment of Neoarchean “plume only” geodynamics: evidence from the Superior Province. Precambr. Res. 229, 3–19.
Zamora, D., 2000. Fusion de la croûte océanique subductée: approche expérimentale et géochimique. Ph.D. thesis. Université Blaise-Pascal, Clermont-Ferrand, France, pp. 314.
Zegers, T.E., van Keken, P.E., 2001. Middle Archean continent formation by crustal delamination. Geology 29 (12), 1083–1086.
Zeh, A., Gerdes, A., Barton Jr., J.M., 2009. Archean accretion and crustal evolution of the Kalahari Craton – the zircon age and Hf isotope record of granitic rocks from Barberton/Swaziland to the Francistown Arc. J. Petrol. 50, 933–966.
Zeh, A., Stern, R.A., Gerdes, A., 2014. The oldest zircons of Africa—Their U-Pb–Hf–O isotope and trace element systematics, and implications for Hadean to Archean crust–mantle evolution. Precambr. Res. 241, 203–230.
Zozulya, D., Kullerud, K., Ravna, E., Corfu, F., Savchenko, Y., 2009. Geology, age and geochemical constraints on the origin of the Late Archean Mikkelvik alkaline massif, West Troms Basement Complex in Northern Norway. Norwgian J. Geol. 89, 327–340.
Zwaan, K.B., 1995. Geology of the Precambrian West Troms Basement Complex, northern Norway, with special emphasis on the Senja Shear Belt: a preliminaryaccount. Bullet. Geol. Survey Norway 427, 33–36.
Zwaan, K.B., Tucker, R.D., 1996. Absolute and relative age relationships in the Precambrian West Troms Basement Complex, northern Norway (abstract). In: 22nd Nordic Geological Winter Meeting, Åbo, Finland, pp. 237.
Zwaan, K.B., Fareth, E., Grogan, P.W., 1998. Bedrock map Tromsø, scale. Geol. Survey Norway 1, 250.